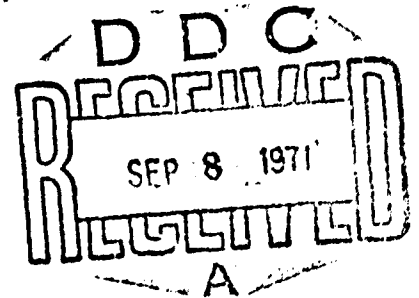AD726238

AEROBALLISTIC EVALUATION AND COMPUTER
STABILITY ANALYSIS OF THE U.S. NAVY
20-MILLIMETER GENERAL PURPOSE
PROJECTILE

By
Frank J. Regan
Virginia L. Scheimerhorn

1 JUNE 1971

D D C
RECEIVED
SEP 8 1971
A

NOL

NAVAL ORDNANCE LABORATORY, WHITE OAK, SILVER SPRING, MARYLAND

DOCUMENT CONTROL DATA - R & D

Security classification of title, body of abstract and indexing annotation must be entered when the overall report is classified)

1. ORIGINATING ACTIVITY (Corporate author)	2a. REPORT SECURITY CLASSIFICATION
NAVAL ORDNANCE LABORATORY Silver Spring, Maryland 20910	UNCLASSIFIED
	2b. GROUP

3. REPORT TITLE

Aeroballistic Evaluation and Computer Stability Analysis of the U. S. Navy 20-Millimeter General Purpose Projectile

4. DESCRIPTIVE NOTES (Type of report and inclusive dates)

5. AUTHOR(S) (First name, middle initial, last name)

Frank J. Regan
Virginia L. Schermerhorn

6. REPORT DATE	7a. TOTAL NO. OF PAGES	7b. NO. OF REFS
1 June 1971	94	8
8a. CONTRACT OR GRANT NO.	9a. ORIGINATOR'S REPORT NUMBER(S)	
b. PROJECT NO. NOL-483/NWC-005-31	NOL TR 71-95	
c.	9b. OTHER REPORT NO(S) (Any other numbers that may be assigned this report)	
d.		

10. DISTRIBUTION STATEMENT

Approved for public release; distribution unlimited.

11. SUPPLEMENTARY NOTES	12. SPONSORING MILITARY ACTIVITY
	Naval Weapons Center China Lake, California 93555

13. ABSTRACT

This report presents the results of ballistics range and wind-tunnel measurements of the static force and moment and the pitch-damping, roll-damping and Magnus moments for a General Purpose 20-Millimeter Projectile. Data are presented for a Smooth and Basic configuration. These aerodynamic data are used in a special digital computer program to rapidly assess the stability of the projectiles over various mission profiles. The normal-force and pitching-moment derivatives are evaluated, theoretically, by Wood's method and compared with the measurements.

DD FORM 1473 (PAGE 1)
1 NOV 65

S/N 0101-807-6801

14 KEY WORDS	LINK A		LINK B		LINK C	
	ROLE	WT	ROLE	WT	ROLE	WT
projectiles						
ballistics range						
wind tunnel						
Magnus						

DD FORM 1473 (BACK)
1 NOV 65
(PAGE 2)

AEROBALLISTIC EVALUATION AND COMPUTER STABILITY ANALYSIS OF
THE U. S. NAVY 20-MILLIMETER GENERAL PURPOSE PROJECTILE

Prepared by:
Frank J. Regan
Virginia L. Schermerhorn

ABSTRACT: This report presents the results of ballistics range and
wind-tunnel measurements of the static force and moment and the pitch-
damping, roll-damping and Magnus moments for a General Purpose
20-Millimeter Projectile. Data are presented for a Smooth and Basic
configuration. These aerodynamic data are used in a special digital
computer program to rapidly assess the stability of the projectiles
over various mission profiles. The normal-force and pitching-moment
derivatives are evaluated, theoretically, by Wood's method and
compared with the measurements.

/

NAVAL ORDNANCE LABORATORY
WHITE OAK, MARYLAND

i

NOLTR 71-95   1 June 1971.

AEROBALLISTIC EVALUATION AND COMPUTER STABILITY ANALYSIS OF THE
U. S. NAVY 20-MILLIMETER GENERAL PURPOSE PROJECTILE

The purpose of this report is to present aerodynamic data from
wind tunnel and ballistics range, together with a stability analysis
based upon these data. This work was sponsored by the Naval Weapons
Center, China Lake, California under Task Number NOL-483/NWC-005-31.

                                ROBERT ENNIS
                                Captain, USN
                                Commander

                                LEON H. SCHINDEL
                                By direction

CONTENTS

TABLES

ILLUSTRATIONS

ILLUSTRATIONS (Cont'd)

ILLUSTRATIONS (Cont'd)

INTRODUCTION

The purpose of this report is twofold: first, aerodynamic static and dynamic measurements are presented for the Basic 20mm general purpose projectile and for configurations which are simple modifications of this basic shape; secondly, these aerodynamic data are used in a specially developed computer program for the rapid evaluation of projectile stability. Details of this program are presented in this report.

This investigation program was carried out in several phases. Initially, a number of configurations were selected from simple modifications of the basic shape. A simple modification is defined as a single change in an important feature of the shape, such as smoothness, length, base geometry, etc. The change of two or more of these salient configuration features would be considered a compound modification. In this early phase these modifications consisted of a 0.6- and 0.3-caliber length extension, a seven-degree 0.5-caliber-long boattail and, finally a smooth body. This last shape was formed from the Basic body by omitting the rotating band and filling in the crimping and fuze grooves. The Basic configuration, which will be discussed in more detail in the next section, is a 4.9-caliber-long 20mm projectile intended for general use within the U. S. Navy.

As a result of this initial investigation it was decided, for various reasons, to retain the Basic configuration as originally formulated. However, it was felt that it would be of value to obtain a fairly detailed set of aerodynamic data on the smooth body. If removable, or consumable, rotating bands have wide use and if improved projectile case bonding eliminates the crimping groove, the low-drag advantages of the smooth configuration might be approached.

These tests were carried out in the Naval Ordnance Laboratory's Supersonic Tunnel No. 1 and Pressurized Ballistics Range. The wind tunnel was used to obtain nonlinear variations of the normal-force and pitching-moment coefficients and the Magnus force and moment coefficients with angle of attack. The ballistics range tests were intended to obtain the damping-in-roll and the damping-in-pitch derivatives which were not available from the wind-tunnel measurements. The ballistics range also furnished the normal-force, pitching-moment and Magnus derivatives, providing a common ground for comparison between the wind tunnel and ballistics range.

In addition to the aerodynamic data, this technical report presents a digital computer program assessment of the stability of the configuration under a variety of conditions. The program is presented in detail in one of the sections. Finally, a comparison is made between the wind-tunnel-ballistics range measurements of the normal-force and pitching-moment derivative with an analytic evaluation of these derivatives based upon a seimempirical method due to Wood. A computer program formulation of Wood's method is presented.

1

SYMBOLS

C_D drag coefficient, D/QS

C_N normal-force coefficient, $-F_z/QS$

C_{N_α} normal-force derivative, $\partial C_N/\partial \alpha$

C_m pitching-moment coefficient, M_y/QSd

C_{m_α} pitching-moment derivative, $\partial C_m/\partial \alpha$

$C_{m_q} + C_{m_{\dot{\alpha}}}$ damping-in-pitch derivative, $\partial C_m/\partial (qd/2V) + \partial C_m/\partial (\dot{\alpha}d/2V)$

C_ℓ rolling-moment coefficient, M_x/QSd

C_{ℓ_p} damping-in-roll derivative, $\partial C_\ell/\partial (pd/2V)$

C_n yawing-moment coefficient, M_z/QSd

C_{n_p} Magnus moment coefficient, $\partial C_n/\partial (pd/2V)$

$C_{n_{p\alpha}}$ Magnus moment derivative, $\partial^2 C_n/\partial (pd/2V)\partial \alpha$

C_y side-force coefficient, F_y/QS

C_{y_p} Magnus force coefficient, $\partial C_y/\partial (pd/2V)$

$C_{y_{p\alpha}}$ Magnus force derivative, $\partial^2 C_y/\partial (pd/2V)\partial \alpha$

d reference length

D drag force

F_y force along the Y axis

F_z force along the Z axis

I_{xx} moment of inertia about the X axis, axial moment of inertia

I_{yy} moment of inertia about the Y axis, transverse moment of inertia

K_x	nondimensional axial radius of gyration, $\sqrt{I_{xx}/md^2}$
K_y	nondimensional transverse radius of gyration, $\sqrt{I_{yy}/md^2}$
M_x	rolling moment
M_y	pitching moment
M_z	yawing moment
m	body mass
p	spin rate (rad/sec)
$pd/2V$, $\tilde{p}$	reduced spin rate
Q	dynamic pressure, $(1/2)\rho V^2$
S	reference area
$1/Sg$	reciprocal of the gyroscopic stability factor
S_d	damping stability factor
V	airspeed
v	vehicle velocity along Y axis
w	vehicle velocity along Z axis
X,Y,Z	conventional aeroballistic body axes
x	horizontal coordinate axis, range
y	vertical coordinate axis, altitude
α	angle of attack, $\tan^{-1} w/V$
α_R	total angle of attack, $\sqrt{\alpha^2 + \beta^2}$
β	angle of side slip, $\tan^{-1} v/V$
δ_R	yaw angle of repose
θ	flight path angle

TEST FACILITIES

All aerodynamic data presented in this report were measured in the Naval Ordnance Laboratory Pressurized Ballistics Range No. 3 and Supersonic Tunnel No. 1. The Pressurized Ballistics Range is a three-foot-diameter 170-foot-long steel tube that can be evacuated to a pressure of 3mm Hg. There are 27 divergent light spark shadowgraph stations along the range tube spaced alternately five and eight feet apart. At these stations, high-quality shadowgraph photographs are obtained in both the vertical and horizontal planes. A complete projectile trajectory is determined from this photographic information. These shadowgraphs are very useful for flow phenomena studies also, although no flow visualization was used in the present work.

Model launchers available for use in this facility include a variety of powder guns, both rifled and smooth bore, as well as a two-stage light-gas gun with a smooth-bore launch tube of 20mm diameter and a smooth-bore launch tube of 1.25-inch diameter. In these tests of the 20mm projectile a rifled powder gun was used. For the smooth projectile tests, a driver plug was used to engage the gun rifling, with the plug in turn keyed to the projectile's base.

The wind-tunnel measurements were carried out, as mentioned, in the NOL Supersonic Tunnel No. 1. This is a blowdown facility, having a 16- by 16-inch test section. Stagnation conditions are essentially atmospheric. The Pressurized Ballistics Range No. 3 and Supersonic Tunnel No. 1, as well as other NOL Aero- and Hydroballistics Facilities, are described and illustrated in Reference (1).

CONFIGURATIONS

All aerodynamic data presented in this report are centered around the Basic 20mm General Purpose Projectile or configurations formed from simple configurational modifications of this basic shape. The Basic configuration is illustrated in Figure 1. It will be noted immediately that this projectile has a number of surface irregularities due to nose fuze, rotating band and crimping groove. While all these contour undulations are necessary on the operational projectile, it was decided to construct a Smooth configuration as a datum to assess the effect of such irregularities on projectile performance. Thus, the Smooth configuration was constructed from the Basic shape by removing the irregularities. This Smooth configuration is illustrated in Figure 2. Most of the data, and all of the analysis, in this report are concerned with these two configurations.

In the initial phases of this program other configurations were studied. Two overlong shapes were formed by adding 0.3- and 0.6-caliber cylindrical afterbody extensions to the Basic shape. Both of these shapes had satisfactory aerodynamic performance, as will be pointed out subsequently. A 0.5-caliber long, seven-degree boattail was also investigated.

Some of the relevant physical properties of the Basic configuration of the 20mm general purpose projectle are given below:

Length: 4.9 calibers
Maximum diameter: 20 millimeters or 0.786 inch
Center of gravity: 2.21 calibers from base
Mass: 1.00578×10^{-2} slugs
Axial moment of inertia: 5.283×10^{-4} slug-ft^2
Transverse moment of inertia: 6.0133×10^{-3} slug-ft^2

The geometric details of the Basic configuration are given in Figure 3.

DATA ACQUISITION

In the Pressurized Ballistics Range, spark shadowgraphic photographs are taken of the model as it passes each station. These photographs are etched on glass to provide a permanent record. Model attitude and down-range position are read on an optical analyzer. Drag and aerodynamic derivatives are then reduced from these measurements by the methods outlined in Reference (2).

In the wind-tunnel tests the model is mounted on a four-component strain-gage balance. Since a Magnus test requires that load measurements be made with the model spinning, it is necessary to provide means for supporting the model in spin to keep vibratory interaction with the load-sensing gages to a minimum. In addition, there must be some source of torque to drive the model in spin.

5

Figure 4 illustrates the essentials of the Magnus balance. In this figure a representative Magnus model is shown mounted on a Magnus balance. It will be noted that the model makes contact with the balance via fore and aft ball bearings. Torque is generated by means of a two-stage air turbine with air entering through the sting and exiting from the model base. The operational procedure is something like the following: Air is admitted to the air turbine at about 400 psi. Once the model has attained a spin rate of about 500 revolutions per second, the air to the turbine is terminated. The strain gages are sampled about 80 times per second as the model undergoes spin decay. A magnetic tachometer, located in the model as shown in Figure 4, provides a nearly continuous record of spin rate. If gage readings are converted to aerodynamic coefficients by means of the balance calibration and a knowledge of the flow properties, it is easy to conceive of a graphical record of force or moment coefficient versus spin. Actually, such a record is essential to wind-tunnel Magnus data reduction.

The view indicated in Figure 4 is such that the plane of the paper is the yaw plane. The component indicated as the Magnus flexure lies at the heart of the Magnus balance. A set of these Magnus flexures is illustrated in Figure 5. It will be noted that the flexure is essentially a miniature beam mounted such that it will be loaded eccentrically by the main beam or balance as the balance is subject to bending by the aerodynamic loads on the model. For example, as the balance is subjected to yaw loads the flexure is eccentrically end loaded. This induced secondary bending results in the flexure acting as a mechanical amplifier. This secondary bending is illustrated, although with considerable exaggeration, in Figure 6. Because the Magnus flexures are used only in the yaw plane, the sensitivity of the balance in yaw is about nine times that of the balance in pitch.

DATA REDUCTION

No discussion will be given herein of the methods used in reducing ballistics range measurements. An outline of the mathematical foundations is given in Reference (2). Several formulations of ballistics range data-reduction methods have been made for application to the technique of wind-tunnel free-flight. One such report is Reference (3).

In the wind tunnel, force and moment data were obtained using the Magnus balance in a rotating sector arm. The model-balance combination is brought to a desired angle of attack, the model then spun to the desired spin rate and the drive air terminated after the flow conditions are established. After tunnel flow has been established, the tachometer and the strain gages are sampled at about 80 times per second. These signals are digitized and recorded on magnetic tape. This record, together with the balance calibration and flow characteristics, produces plots of the force and moment coefficients as a function of reduced spin rate at a specific value of Mach number and angle of attack. The variation

6

of normal force and pitching moment with spin is usually small and
considered negligible in this presentation. However, the side-force
and yawing-moment coefficient indicate a nearly linear variation
with spin rate. A representative plot of side-force and yawing-
moment coefficients versus reduced spin rate is given in Figure 7.
It will be noted that even at this rather large angle of attack
these force and moment coefficients are linear with reduced spin
rate. In order to discuss the Magnus data-reduction methods as
used in wind tunnels, it is necessary to consider the analytic
formulation of the Magnus effect.

The Magnus force, $\vec{F}$, will be defined as a force depending upon
body spin rate and angle of attack, and acting normal to the plane
established by the spin vector, $\vec{p}$, and the free-stream velocity
vector, $\vec{V}_\infty$. Mathematically this force, $\vec{F}$, and its corresponding

moment, $\vec{M}$, can be expressed as

$$\vec{F} = \kappa \left(\vec{p} \times \frac{\vec{V}_\infty}{V_\infty} \right) \tag{1}$$

and

$$\vec{M} = \kappa \left[\vec{r} \times \frac{\vec{p} \times \vec{V}_\infty}{V_\infty} \right] \tag{2}$$

where k is a scalar constant for a given set of flow conditions;
r is the vector distance from the center of gravity to the Magnus
center of pressure, along the body's axis of symmetry; and, $\vec{p}$ is
the spin-rate vector defined along the axis of symmetry.

All forces and moments are referred to the conventional aero-
ballistic body axis system, an axis system which is fixed to the body
and shows all its rotational and translational motion, except spin.
In the axis system, the x axis is forward along the axis of symmetry;
the y axis is to the right when the store is viewed along the
positive x axis; the z axis completes a right-handed triad. The
origin of this axis system is at the moment reference center taken,
in this case, to be the center of gravity. Unit vectors along the
x, y, z axes will be defined as $\vec{1}_x$, $\vec{1}_y$, $\vec{1}_z$. The wind-tunnel

constraints are such that the x, z plane is vertical; and, that
this plane contains the flow velocity vector.

Since $\vec{p} = p \vec{1}_x$, $\vec{V}_\infty = (V_\infty \cos\alpha)\vec{1}_x + (V_\infty \sin\alpha)\vec{1}_z$, Equation

may be rewritten as

$$\vec{F} = -\kappa \left[p \sin\alpha \right]\vec{1}_y = F_Y \vec{1}_y \tag{3}$$

7

where the side force, F_y, is equal to $-kpV_\infty \sin\alpha$. This relationship demonstrates that the Magnus force is an odd function of the angle of attack with spin rate. The Magnus moment equation also may be rewritten using the components of the spin-rate and free-stream velocity vectors. That is,

$$\vec{M} = -\kappa \left[pr \sin\alpha \right] \vec{l}_{\mathcal{Z}} = M_{\mathcal{Z}} \vec{l}_{\mathcal{Z}} \tag{4}$$

where the yawing moment, M_z, is equal to $-kpr \sin\alpha$. It can be seen from Equation (4) that the Magnus moment is an odd function in center-of-pressure location, spin rate and angle of attack. For example, the Magnus center of pressure is usually behind the center of gravity, giving a positive Magnus moment (nose to the right as viewed from the rear).

The yaw-force and yaw-moment coefficients are defined as:

$$C_Y = F_Y / QS \qquad\qquad C_n = M_{\mathcal{Z}} / QSd \tag{5}$$

The above coefficients depend upon the body pressure distribution, which, in turn, depends upon the compressibility, viscosity and unsteadiness of the flow field. To indicate the degree of simulation of these effects, it is necessary to present coefficients as functions of the appropriate flow similarity parameters.

Since the free-stream velocity is in the vicinity of the speed of sound, it is necessary to regard the medium as compressible. Simulation of compressibility effects is assured by testing at identical free-flight Mach numbers. Also, since the Magnus effect on the forebody originates entirely in the boundary layer, it is necessary to test at the anticipated Reynolds numbers to simulate viscous effects. Finally, since each surface element on a steadily spinning body experiences a cyclically changing flow field, the test must be made at a parameter which matches flow unsteadiness. In Magnus tests this flow unsteadiness parameter is designated as the reduced frequency, $\tilde{p}$. Testing at identical reduced frequencies assures a matching of the flow angularity at similarly located surface elements on geometrically similar bodies. Thus, it will be postulated in a Magnus test that the coefficients must be expressed as functions of Mach number, Reynolds number and reduced frequency, as well as body angular attitude.

If the Magnus force is assumed to be an analytic function of angle of attack and reduced frequency, the yaw-force coefficient can be expanded in a truncated Taylor series in α and $\tilde{p}$, as:

$$C_Y(\alpha, \tilde{p}) = C_Y(0,0) + \frac{\partial C_Y}{\partial \alpha}\alpha + \frac{\partial C_Y}{\partial \tilde{p}}\tilde{p} + \frac{1}{2}\left(\frac{\partial^2 C_Y}{\partial \alpha^2} + \frac{\partial^2 C_Y}{\partial \tilde{p}^2} + 2\frac{\partial^2 C_Y}{\partial \alpha \partial \tilde{p}}\right) \tag{6}$$

8

where all derivatives are evaluated at α and $\tilde{p}$ equal to zero. Since,

$$C_y(0,0) = C_y(0,\alpha) = C_y(\tilde{p},0) = 0 \qquad (7)$$

it follows that all but the cross derivatives vanish. Thus, Equation (6) becomes, as a first approximation,

$$C_y(\alpha,\tilde{p}) \simeq \frac{\partial^2 C_y}{\partial\alpha\,\partial\tilde{p}}\,\alpha\tilde{p} \equiv C_{y_{p\alpha}}\tilde{p}\alpha \qquad (8)$$

A similar relationship for the moment coefficient, C_n, would be

$$C_n(\alpha,\tilde{p}) \cong \frac{\partial^2 C_y}{\partial\alpha\,\partial\tilde{p}}\,\alpha\tilde{p} \equiv C_{n_{p\alpha}}\tilde{p}\alpha \qquad (9)$$

The terms on the right in Equations (8) and (9) are the familiar Magnus force and moment derivatives, respectively, for linear aerodynamics. It should be noted that Equations (8) and (9) are compatible with Equations (3) and (4) for small angles of attack.

Before coming to grips with an analytic description of the problem's nonlinearities, it is important to recall the methods of data acquisition. Side-force and yawing-moment measurements were made while the model was undergoing spin decay at a fixed angle of attack and immersed in a flow of constant Mach number. After tachometer and strain-gage signals are recorded, the angle of attack is changed. The model is spun again to some predetermined upper limit, the drive air is terminated and the procedure repeated. After the entire angle-of-attack range has been spanned, the Mach number is changed and the procedure repeated. Since it is noted that for configurations without fins, the Magnus force and moment coefficients are linear with spin rate, Equation (6) may be rewritten as

$$C_y(\alpha,\tilde{p}) = \partial C_y(\alpha)/\partial\tilde{p} = C_{y_p}\tilde{p} \qquad (10)$$

The variation of the Magnus effect with angle of attack is represented by the derivative, $\partial C_y(\alpha)/\partial\tilde{p}$. If the Magnus effect varies linearly with angle of attack, then Equation (10) may be replaced by Equation (8). Experiments show that, generally, the Magnus effect varies in a nonlinear fashion for angles of attack greater than two or three degrees. Thus, the wind-tunnel procedure is to obtain $\partial C_y/\partial\tilde{p}$ for several angles of attack at a fixed Mach number. Since the ballistics range data-reduction methods are based upon linear aerodynamics, the Magnus effect can only be represented by the Magnus

derivatives of Equations (8) and (9). Such a limitation is usually acceptable as ballistics range tests are usually limited to a few degrees angle of attack. Wind-tunnel measurements can be compared with ballistics range measurements by obtaining the slope through the origin of the $\partial C_y/\partial \tilde{p}$ versus angle-of-attack graphs.

This slope, $\partial/\partial\alpha(\partial C_y/\partial\tilde{p})$ or $C_{y_{p\alpha}}$ is the Magnus force derivative.

AERODYNAMIC MEASUREMENTS

As mentioned several times earlier, the aerodynamic data contained in this report were obtained in the NOL Pressurized Ballistics Range and Supersonic Tunnel No. 1. The flow environment experienced by the range and wind-tunnel models might be summarized in a plot of Reynolds number versus Mach number. Such a plot is presented in Figure 8 with the Reynolds number being based upon body diameter.

In the ballistics range, two pressurization levels were used-- one atmosphere and one-tenth of an atmosphere. These levels are also indicated in Figure 8. The wind tunnel, being a blowdown facility, has a total pressure head of one atmosphere. At the lower Mach numbers (below Mach 1.5) it will be noted that a higher Reynolds number is achieved in the wind tunnel. This higher Reynolds number occurs because the wind-tunnel model is nearly three times the linear size of the full-scale ballistics range models (2.0 inches as compared to 0.786 inch for the ballistics range model).

Figures 9 through 17 present the wind-tunnel measurements of the normal-force and pitching-moment coefficients for the Basic configuration; Figures 18 through 24 present the same information for the Smooth configuration. It will be noted that the pitching-moment coefficient is linear through the origin and remains linear up to about 10 degrees angle of attack for subsonic measurements (see, for example, Fig. 11). Supersonically, the pitching moment begins to give evidence of nonlinearities at about eight degrees (see Fig. 15). This same sort of observation can be made for the Smooth body, indicating that nose geometry rather than surface irregularities is the main contributor.

It was mentioned earlier that a variety of configurations were briefly examined in the ballistics range at the inception of this program. In addition to the Smooth configuration, these configurations consisted of a 0.3-caliber cylindrical e   :ion, a 0.6-caliber cylindrical extension and a seven-degre   .5-caliber-long boattail. The normal-force and pitchir,   _it derivatives for these configurations are compared with t . . of the Basic body in Figures 25 and 26. It will be noted, for example, that the 0.3-caliber extension gives a pitching moment about equal to that of the Basic configuration; the 0.6-caliber extension seems to make an appreciable increase in the pitching moment. The boattail configuration has a significantly lower pitching moment. It should be emphasized

that the Smooth body data, given in Figures 25 and 26, are
questionable and should not be used for comparative purposes. Due
to a defective plug design there was gas blow-by which seemed to
distort the model base. This design was corrected in later tests.

Since the most important configuration is these tests is the
Basic body, it was desired to have a fairly detailed data coverage.
Figures 27 and 28 present comparisons of ballistics range and wind-
tunnel measurements of the normal-force and pitching-moment derivatives
of the Basic body. Figure 29 gives the center-of-pressure location
from the body vertex, calculated from the data of Figures 27 and 28.

The correlation between ballistics range and wind-tunnel data is
quite satisfactory. It should be recalled from Figure 8, that
the Reynolds numbers in both facilities are fairly close up to a
Mach number of 1.5. Figure 29 shows that the center of pressure
moves rearward with increasing Mach number. Figures 30 and 31
present the normal-force and pitching-moment derivatives, respectively,
for the Smooth configuration. The data for the Smooth configuration
are much more sparse than the Basic configuration, with only one
data point available from the ballistics range. Figure 32 presents
the center-of-pressure location in calibers aft of the vertex. In
comparing Figure 29 to 32 it appears that even within the scatter
of the data, the center of pressure for the Smooth configuration
is slightly ahead of that for the Basic configuration.

One of the most important single measurement made in the
ballistics range is drag. Drag measurements for the Basic and
Smooth configurations are presented in Figure 33 in the form of
the zero-lift drag coefficient. It is quite obvious from this
figure that the Smooth configuration enjoys a significant drag
advantage over the Basic configuration.

In Figures 34 and 35 the damping-in-roll derivative, C_{ℓ_p},
and the damping-in-pitch derivative, $C_{m_q} + C_{m_{\dot{\alpha}}}$, are presented

respectively, as functions of Mach number. The damping-in-roll
derivative is reduced according to the methods of Reference (4).
The roll angle is determined by pins located in the base of the model.
The damping-in-pitch derivative, unfortunately, has a great deal
of scatter in the measurements. Since this derivative is essential
in specifying the dynamic stability criterion, S_d, there will be

some uncertainty concerning regions of dynamic stability.

Also vital in the determination of the dynamic stability of
a configuration is the Magnus effect. The Magnus effect had been
discussed earlier in the Data-Reduction Section. Magnus measure-
ments were carried out in both the wind tunnel and ballistics range.
In the wind tunnel, both the side force and yawing moment are
measured as functions of spin rate and angle of attack. As pointed

11

out in Equation (10), the force and moment are considered linear with spin rate and are expressible as force and moment derivatives with spin rate. These derivatives, $\partial C_y/\partial \tilde{p}$ and $\partial C_n/\partial \tilde{p}$, have been designated as the Magnus force and moment coefficients, C_{y_p} and C_{n_p}, respectively. Figures 36 through 41 present the Magnus force and moment coefficients for the Basic configuration and Figures 42 through 47 for the Smooth configuration. It will be noted that while the slope of the Magnus force coefficient, the Magnus force derivative, remains negative over the entire Mach number range, the Magnus moment derivative changes sign in going from subsonic to supersonic Mach numbers (compare Figure 37 to 38). The above observation indicates that the Magnus center of pressure is slightly ahead of the center of gravity subsonically and slightly aft of the center of gravity supersonically. It will be pointed out later that a Magnus center of pressure ahead of the center of gravity always results in dynamic instability. Thus, it would be expected that the Basic configuration is dynamically unstable subsonically.

Interestingly enough, the Smooth configuration appears to be dynamically stable over the whole flight regime as the slope of the Magnus moment coefficient, Magnus moment derivative, is negative for subsonic and supersonic Mach numbers (compare Figure 43 to 44). The dynamic instability of the Basic configuration is not serious as it would be expected that this projectile would only be effective in the moderately high Mach number range (Mach 2 to 3.5).

In examining the Magnus data of Figures 36 through 47 it will be noted that the variation of C_{y_p} and C_{n_p} with angle of attack is nonlinear for angles much beyond two degrees. This is particularly true for the Basic configuration. For small angles of attack there appears some justification in linearizing the Magnus effect by representing the Magnus force and moment by the Magnus derivative (see Eq. (10)). This linearization has been done for the Basic configuration and the resulting Magnus force and moment derivatives plotted as functions of Mach number in Figure 48. These data appear quite ragged because the Magnus derivative is formed by twice differentiating experimental data, once with respect to spin rate and again with respect to angle of attack.

In the ballistics range an entirely different procedure is used. Since the observed motion (as obtained from the photographic plates) is assumed to be the "solution" of a set of linear differential equations, the Magnus effect can only be expressed in terms of the Magnus derivative. Also, as measurements were made at only one center-of-gravity location, only the Magnus moment derivative is available.

Figure 49 presents the Magnus moment derivative as a function of Mach number comparing the wind-tunnel and ballistics range measurements. It will be observed that the Magnus moment changes

12

sign somewhere around a Mach number of 1.1. Thus, one would expect
that the projectile would become dynamically unstable below this
Mach number.

ANALYTIC DETERMINATION OF THE STATIC COEFFICIENTS

There are a variety of methods for predicting the normal-force
and pitching-moment derivatives as a function of Mach number.
Probably the simplest is that due to Hitchcock (Ref. (5)).
Hitchcock's method is entirely empirical and has the disadvantage
of ignoring compressibility effects. The normal-force derivative,
C_{N_α}, and the center of pressure, h, are given as follows:

$$C_{N_\alpha} = \frac{8}{\pi}\left[.653 + .0223A - .6139B - .0024C + .2635D + .6473(1/E)\right] \quad (11)$$

$$h = .0747 + .0443A + 1.019B + .8032C + .2459D + .8083(1/E) \quad (12)$$

where

A is the angle of the boattail in degrees
B is the length of the boattail in calibers
C is the length of the cylindrical part in calibers
D is the length of the ogival head in calibers
E is the radius of the ogival arc in calibers

If reference is made to Figure 27 it is possible to compare the
prediction of C_{N_α}, using Hitchcock's formula of Equation (11), with

wind-tunnel and ballistics range measurements.

With

A = 0
B = 0
C = 2.41
D = 2.49
E = 7.40

Equation (11) gives

C_{N_α} = 3.54

13

This value, which is invarient with Mach number, is higher than any measurement made in either the wind tunnel or ballistics range at any Mach number. According to Equation (12) the center of pressure is 2.17 calibers aft of the vertex. The Hitchcock relationship predicts a center of pressure which is too far aft. The pitching-moment derivative, C_{m_α}, determined from Equations (11) and (12), is 1.85. Comparison with Figure 28 shows that this value is lower then any of the measurements, regardless of Mach number. Supposedly, the empirical constants of Equations (11) and (12) could be adjusted to bring the predictions in better agreement with the measurements. However, the primary shortcoming of this method is, as pointed out earlier, its failure to account for compressibility effects.

A second method due to Wood (Ref. (6)) is available which does take into account compressibility effects. Wood defines the normal-force derivative and the pitching-moment derivative about the base, respectively, as:

$$C_{N_\alpha} = [(2S'_b/S) + .5] f_1 \qquad (13)$$

$$C_{m_\alpha}^b = \left[\frac{2 \times VOLUME}{Sd}\right] f_2 \qquad (14)$$

where $S'_b = (S + S_b)/2$ and where S and S_b are the reference area and base area, respectively. The center-of-pressure location, in calibers, forward from the base is given as,

$$H = C_{m_\alpha}^b / C_{N_\alpha} \qquad (15)$$

The pitching-moment derivative about the center of gravity is easily written from Equations (14) and (15) as,

$$C_{m_\alpha} = (H - G) C_{N_\alpha} \qquad (16)$$

where G is the location of the center of gravity, in calibers, forward of the base. The functions, f_1 and f_2, are empirical

functions of the fineness ratio and the Mach number. These functions are equal to unity for Mach numbers between 0 and unity and are available, in graphical form, for Mach numbers in excess

14

of unity. Graphs of f_1 and f_2 are available in both References (6) and (7).

Table 1 presents a listing of a BASIC program to calculate the normal-force and pitching-moment derivatives and center-of-pressure location aft of the vertex. In order to use the f_1 and f_2 functions in the program, a seventh-order polynomial was fitted to these graphs. These polynomials, together with Equations (13) through (16), were formulated in the BASIC language to provide a fairly good semiemphirical estimate of the normal-force and pitching-moment derivatives and the center of pressure. Estimates of C_{N_α}, C_{m_α} and center-of-pressure location from Wood's method are compared with wind-tunnel and ballistics range measurements in Figures 27, 28 and 29. The agreement may be considered fair and probably limited to preliminary design estimates.

BASIC COMPUTER PROGRAM FOR THE RAPID DETERMINATION OF PROJECTILE STABILITY

In this section, a computer program developed for the rapid evaluation of the stability of an unguided weapon is described. This program assumes that the forces and moments acting on the body arise from linear aerodynamic loads and a constant gravitational field. More elaborate simulation of projectile characteristics is certainly possible in six-degree-of-freedom programs, such as Reference (8). While the increased precision of such programs is obvious, the lengthy table preparation and long computation time often discourages the use of such programs. For example, it is not uncommon to have a computation time 2000 times longer than real time. In this program only two second-order differential equations are solved. Other relationships, which might be written in the form of differential equations, are approximately integrated and it is these analytic approximations that are programmed. The assumption of linear aerodynamics avoids lengthy tables. This latter assumption may not be severely restricting, as a designer's first performance studies are usually limited to estimates of the stability derivatives. Even in considering operational vehicles, satisfactory performance usually restricts the projectile to small angular excursions.

This program was written, primarily, for spin-stabilized projectiles although it is entirely adequate, within the restrictions of the force and moment representations, to spinning fin-stabilized weapons as well. Regardless of the stabilization characteristics of the weapon, the program operates in the following manner: A particle trajectory is calculated to provide the dynamic pressure, velocity and Mach number. These quantities are then used to calculate the reduced frequency, the yaw of repose, the damping stability parameter and the gyroscopic stability parameter.

15

Various print statements provide these quantities as a tabular function of altitude and time.

In carrying out the computation there are three distinct sets of equations. First, two second-order differential equations, nonlinearily coupled through aerodynamic drag, are used to provide a particle trajectory program. This particle trajectory "locates" the weapon as it moves through a uniform gravitational field subject to aerodynamic drag. Since a solution in closed-form is out of the question, it was necessary to solve these equations using numerical integration.

The second set of equations provides reduced frequency as a function of arc length. If the Mach number is assumed to be constant, this equation may be integrated to give reduced frequency as a function of arc length. If changes in Mach number affect the value of the drag and roll-damping coefficients, it is necessary to carry out the integration piecewise over intervals of constant Mach number. Such a procedure avoids a lengthy numerical integration procedure and keeps the program formulation within a reasonable length.

Finally, a third set of equations is needed to describe the angular motion of the body. Two coupled second-order differential equations are integrated to express the yaw and pitch motion of the vehicle about its velocity vector. The integrals of these equations are used to formulate the gyroscopic and damping stability parameters. As in the case of the spin-rate equation, this integral of the angular motion is valid only over intervals of constant Mach number. The result is that the above-mentioned stability criteria will vary with Mach number.

The sketch given below illustrates the variables used in the trajectory equations. It will be assumed that all motion takes place in a vertical plane, with the "y" axis vertical (defined positive upwards) and the "x" axis horizontal (position forward in the directions of flight).

16
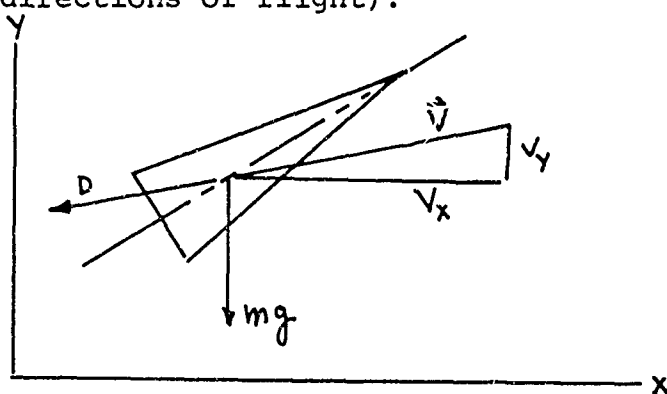
If the gravitational and drag forces are resolved into the vertical and horizontal components (according to the above sketch) the equation of vertical and horizontal motion may be written as,

$$\frac{dV_x}{dt} = -\frac{D\cos\theta}{m} = -\frac{DV_x}{mV} \qquad (17a)$$

$$V_x = dx/dt \qquad (17b)$$

$$\frac{dV_y}{dt} = -\frac{D\sin\theta}{m} - g = -\frac{D}{m}\frac{V_y}{V} - g \qquad (17c)$$

$$V_y = dy/dt \qquad (17d)$$

Where Equations (17) have been rewritten in alternate form by replacing $\cos\theta$ by V_x/V and $\sin\theta$ by V_y/V. If the following substitutions are made:

D = Al	x = X	y = Y
m = W	$\frac{dx}{dt}$ = X1	$\frac{dy}{dt}$ = Y1
g = 32.174	V_x = Q	V_y = P
V = V	$\frac{dV_x}{dt}$ = Q1	$\frac{dV_x}{dt}$ = P1

Equations (17) may now be expressed in terms of computer variables as,

$$Q1 = -\left(\frac{Al}{W*V}\right)*Q \qquad (18a)$$

$$X1 = Q \qquad (18b)$$

$$P1 = \left(\frac{Al*P}{W*V}\right) - 32.174 \qquad (18c)$$

$$Y1 = P \qquad (18d)$$

17

All computer variables are defined in terms of problem variables in Table 2.

The second equation needed in the stability analysis is that relating spin rate to some independent variable, such as time or range. The most straightforward approach is to first state the following easily established identity.

$$\frac{d}{dt}\left(\frac{p}{V}\right) = \frac{1}{V}\frac{dp}{dt} - \frac{p}{V^2}\frac{dV}{dt} \tag{19}$$

where p is the spin rate, t is the time and V is the free-stream airspeed. From the roll-damping equation, or the equation relating deceleration to the roll-damping moment, we have,

$$\frac{dp}{dt} = \frac{C_{\ell_p}QSd}{I_{xx}}\left(\frac{pd}{2V}\right) = \left(\frac{C_{\ell_p}\rho VS K_x^{-2}}{4m}\right)p \tag{20}$$

where I_{xx} is the moment of inertia about the longitudinal axis, C_{ℓ_p} the damping-in-roll derivative, m the mass and K_x the nondimensional radius of gyration defined as I_{xx}/m. Next, the drag equation can be written as

$$\frac{dV}{dt} = -\frac{C_D Q S}{m} = -\frac{C_D \rho V^2 S}{2m} \tag{21}$$

Inserting Equations (20) and (21) into identity, (19) gives

$$\frac{d}{dt}\left(\frac{p}{V}\right) = \left(\frac{\rho S V}{2m}\right)\left(\frac{p}{V}\right)\left[\frac{1}{2}K_x^{-2}C_{\ell_p} + C_D\right] \tag{22}$$

The above equation may be rewritten changing the independent variable from time, t, to downrange distance, x, through the following operator

$$\frac{d}{dt}(\quad) = V_x\frac{d}{dx}(\quad)$$

18

Equation (22) then becomes,

$$\frac{d}{dx}\left(\frac{p}{V}\right) = \left(\frac{V}{V_x}\right)\left(\frac{\rho S}{2m}\right)\left[\frac{1}{2}K_x^{-2}C_{\ell_p} + C_D\right]\left(\frac{p}{V}\right) \tag{23}$$

Equation (23) can be rearranged to give,

$$\frac{d(p/V)}{p/V} = \left(\frac{1}{Cos\theta}\right)\left(\frac{\rho S}{2m}\right)\left[\frac{1}{2}K_x^{-2}C_{\ell_p} + C_D\right]dx \tag{24}$$

where $\cos\theta = V_x/V$. An exact integral of Equation (24) in closed-

form is impossible because $\cos\theta$ is a function of x, which can only
be known by integrating the particle trajectory. However, if
the integration is carried out over a short enough time interval
that $\cos\theta$ may be replaced by a constant value, say its value at
the beginning of an interval "i," the integral of Equation (24) may
be written as,

$$\left(\frac{p}{V}\right)_{i+1} = \left(\frac{p}{V}\right)_i \exp\left\{\left(\frac{1}{Cos\theta_i}\right)\left(\frac{\rho S}{2m}\right)\left[\frac{1}{2}K_x^{-2}C_{\ell_p} + C_D\right](x-x_o)\right\} \tag{25}$$

If the number 5 is attached to a symbol to mean the value at the
beginning of an interval, it is possible to rewrite Equation (25)
in computer variables.

$$E5 = EXP((V5/Q5)*(((R*S)/(2*W))*(K6*II)*.5*E+A)*(X-X5) \tag{26}$$

$$P7 = (P5*V)/V5$$

Now P5, the value at the beginning of the next interval, is
P5 = P7*E5. Again, reference is made to Table 2 for the definition
of the computer variables in terms of the problem variables.

Equations (17) describe the position of the projectile as
a function of time as it moves through a uniform gravity field.
It is obvious that no interaction is assumed between the angular
motion of the body and its trajectory. This is obviously a
simplifying assumption, but is justified on the grounds that the
angular motion of a stable projectile should be small and, therefore
interaction terms, such as lift force, Magnus force and angular
dependent drag, can be neglected. The question arises as to how
one can be sure that the angular motion will remain small under

response to an initial disturbance. In order to answer this question, two stability criteria will be developed to provide the necessary and sufficient conditions that the projectile's angular motion will not grow in response to a disturbance. These criteria will be formulated in terms of the body's mass distribution, spin rate and Magnus, damping and static aerodynamic characteristics.

Murphy, in Reference (2) Equations 4.24 and 4.25, introduces the complex variable

$$\bar{\xi} = \frac{V + iW}{V} \tag{27a}$$

which, for small angles of attack and sideslip, becomes,

$$\bar{\xi} = \beta + i\alpha \tag{27b}$$

The above formalism allows the differential equations of lateral motion to be expressed in terms of a single second-order differential equation, rather than in two second-order equations in the real variables v/V and w/V or β and α. As indicated by Murphy in Equation 6.12 of Reference (2), this equation of motion becomes

$$\bar{\xi}'' + (H + iP)\bar{\xi}' - (M + iPT)\bar{\xi} = G \tag{28}$$

where

$$H = \left(\frac{\rho Sd}{2m}\right)\left[C_{N\alpha} - 2C_D - \frac{1}{2}K_y^{-2}(C_{m_q} + C_{m_{\dot\alpha}})\right] \tag{29a}$$

$$M = \left(\frac{\rho Sd^3}{2I_y}\right)\left[C_{m\alpha}\right] \tag{29b}$$

$$T = \left(\frac{\rho Sd}{2m}\right)\left[C_{N\alpha} - C_D + \frac{1}{2}K_y^{-2}C_{m_{p\alpha}}\right] \tag{29c}$$

$$G \simeq \frac{Pgd}{V^2} \tag{29c}$$

Equations (29a) and (29c) differ from those given in Reference (2) (see Eq. 6.12), in that the coefficients $C_{m_q} + C_{m_{\dot\alpha}}$ and $C_{m_{p\alpha}}$ are

multiplied by 1/2. This factor of 1/2 is necessary as NOL dynamic moments are nondimensionalized with respect to pd/2V whereas in Reference (2), pd/V is used. This factor of 1/2 occurred earlier in Equation (23).

20

Since Equation (28) is linear, its solution is given as,

$$\vec{\xi} = (K_{10} e^{i\phi_0}) e^{(\lambda_1 + i\phi_1' s)} + (K_{20} e^{i\phi_{20}}) e^{(\lambda_2 + i\phi_2' s)} + \vec{\xi}_g \qquad (30)$$

Since the requirement for stability is that

$$\lim_{s \to \infty} \vec{\xi} \to 0$$

it is necessary and sufficient that λ_1 and λ_2 are both negative.

The exponentials of Equation (30) may be written as,

$$\lambda_{1,2} + i\phi_{1,2}' = \frac{1}{2}\left[iP - H \pm \sqrt{4M + H^2 - P^2 + 2iP(2T - H)} \right] \qquad (31)$$

If the Magnus-lift coupling term, T, and the damping term, H, are neglected, one has

$$\lambda_{1,2} + i\phi_{1,2}' = \frac{1}{2}\left[iP \pm \sqrt{4M - P^2} \right]$$
$$= \frac{P}{2}\left[i \pm i\sqrt{1 - 1/s_g} \right] \qquad (32)$$

where $1/S_g = 4M/P^2$ and is designated as the reciprocal of the gyroscopic stability parameter. Thus, in a spin-stabilized vehicle it is necessary that $1/S_g$ be less than unity for the vehicle to be stable. A fin-stabilized vehicle will always be gyroscopically stable as M is negative. If $1/S_g$ is greater than unity, λ would equal $1/\sqrt{1/S_g - 1}$ and, being positive, would result in divergence of the projectile from its initial conditions.

If $1/S_g$ is less than unity and λ_1 and λ_2 are both zero,

$$\phi_{1,2}' = \frac{P}{2}\left[1 \pm \sqrt{1 - 1/s_g} \right] \qquad (33)$$

21

Equation (33) followed from Equation (31) after T and H were set equal to zero. The exact values of the frequencies ϕ_1' and ϕ_2' will vary with the relative magnitudes of T, H, M and P; however, Equation (33) is usually an excellent approximation for the modal frequencies ϕ_1' and ϕ_2'. The criteria for such a approximation is that:

$$\phi_1' \, \phi_2' \gg \lambda_1, \lambda_2$$

Murphy (Ref. (2)) then goes on to show that, regardless of the values of ϕ_1', ϕ_2', λ_1 and λ_2, one may write,

$$\lambda_{1,2} = -\frac{H}{2}\left[1 \mp \frac{P}{[\phi_1' - \phi_2']}(S_d - 1)\right] \tag{34}$$

where $S_d = 2T/H$ or the ratio of the Magnus-lift coupling to the

damping. It follows, from Equation (33), that $P/[\phi_1 - \phi_2]$

must be less than unity for a statically stable missile and greater than unity for a statically unstable missile. In either case, Equation (34) may be rewritten using Equation (33) to give:

$$\lambda_{1,2} = -\frac{H}{2}\left[1 \mp \frac{(S_d - 1)}{\sqrt{1 - 1/S_g}}\right] \tag{35}$$

Conditions for stability $(\lambda_1, \lambda_2 < 0)$ are that

$$1 > \left|\frac{S_d - 1}{\sqrt{1 - 1/S_g}}\right|$$

or equivalently

$$1 > \frac{(S_d - 1)^2}{1 - 1/S_g}$$

The boundary between stability and instability follows as

$$\frac{1}{S_g} = S_d(2 - S_d) \tag{36}$$

which is Equation 7.7 of Reference (2).

22

A dynamically stable model must have an inverse gyroscopic stability parameter less than that given by Equation (36).

If a trajectory is determined for a given projectile and if $1/Sg$ and S_d are calculated at a fixed interval, then the locus

of the curve in the $1/Sg - S_d$ plane readily indicates the stability over its flight path.

It is possible now to write $1/Sg$ and S_d in terms of the

aerodynamic coefficients and projectile mass, mass distribution and geometry. In terms of problem variables, Sg is:

$$\frac{1}{S_g} = \frac{P^2}{4M} = \frac{2 I_{xx}^2 P^2}{I_{xx}(\pi \rho d^3 V^2 C_{m\alpha})} \tag{37a}$$

or in terms of computer variables,

$$SI = \frac{(2 * (I1 \uparrow 2) * (P5 \uparrow 2)}{I2 * 3.1416 * R * (D5 \uparrow 3) * (V \uparrow 2) * B} \tag{37b}$$

similarly,

$$S_d = \frac{2T}{H} = \frac{2(C_{N\alpha} - C_D) + \frac{1}{2} K_x^{-2} C_{mp\alpha}}{(C_{N\alpha} - 2C_D - \frac{1}{2} K_y^{-2}(C_{mq} + C_{m\alpha}))} \tag{38a}$$

and in terms of computer variables,

$$S2 = \frac{2 * (D - A) + .5 * (K6 / I1) * F}{D - 2 * A - .5 * (K6 / I2) * C} \tag{38b}$$

It has been shown that the solution of Equation (30) will be stable if $1/Sg$ has a value no greater than that given by Equation (36).

The third term on the right in Equation (30) is the steady-state value of ξ, this term is designated as ξg and called the yaw of repose. This term is, according to Murphy (Ref. (2), Eq. 6.13),

23

$$\xi_g = \left[\frac{-P}{M + iPT} \right] \frac{gd}{V_o^2} \tag{39}$$

Inserting the appropriate values for M, P and T from Equations (29), the above expression becomes, after rationalizing the denominator:

$$\xi_g = \frac{I_x \rho g \cos\theta}{\frac{1}{2}\rho S d C_{m_\alpha} V_o^3} \left(-1 + i \frac{C_{m_{p\alpha}}}{C_m} \frac{\rho d}{V_o} \right) \tag{40a}$$

Since pd/V_o is the order of 0.1, the imaginary terms in Equation (40a) can be ignored. If this is done, it is possible to rewrite Equation (40a) in terms of the computer variables as,

$$S3 = \frac{(I1 * P5 * 64.348 * Q/V)}{(R * S * D5 * (V\wedge 3) * B)} \tag{40b}$$

In calculating Sg (Eqs. (37)) it is necessary to insert a value for the density. The density, of course, changes with altitude and this change is assumed in this report to be exponential with altitude, y, as:

$$\rho = \rho_o e^{-ky} \tag{41a}$$

The main assumption in deriving Equation (41a) is that the atmosphere is isothermal. In computer variables, Equation (41a) becomes

$$R = .002377 * EXP(-.31582 E-4 * Y) \tag{41b}$$

The aerodynamic coefficients which are necessary to calculate S_d, Sg and ξg are entered into the program as a table with Mach number. Mach number is, of course, the ratio of the body's speed to the speed of sound as

24

$$M = V/C \tag{42}$$

The body's speed is obtained in the particle trajectory program, Equations (17). The speed of sound varies solely with the temperature for an ideal gas and in the English units may be given as,

$$c = 49.0 \sqrt{T + 460} \tag{43}$$

where T is in degrees Fahrenheit and c is in feet per second. The speed of sound may be written as

$$c = c_0 + \frac{\partial c}{\partial y} y = c_0 + \frac{\partial c}{\partial T} \frac{\partial T}{\partial y} y \tag{44}$$

where

$$\frac{\partial c}{\partial T} = \overline{49}^2 / 2 c_0$$

from Equation (43) and $\partial T / \partial y$ (partial derivative) will be taken at -0.0039 degrees Fahrenheit per foot. Thus, Equation (44) may be written as

$$c = 1117 - .0042 y \tag{45}$$

The Mach number may be written in computer variables as

$$M = V / (1117 - .0042 * Y) \tag{46}$$

Equation (44) and, hence, Equation (46) are assumed to be valid only up to 36,000 feet. Above this altitude the temperature and, therefore, the speed of sound are assumed to be constant. In this case, Equation (46) will be replaced by

$$M = V / 971 \tag{47}$$

Table 2 gives the correspondence between the computer variables, as used in the BASIC language, and the problem variables, most of which have been defined in the list of symbols. The general rules of the BASIC language and terminal apply. One need only supply the input data starting on line 1890 (see Table 2). Data are input in the following order:

T5	initial time (seconds)
XO	initial horizontal displacement (feet)
YO	initial vertical displacement (feet)
VO	platform velocity relative to inertial space (feet per second)
V1	projectile muzzle velocity (feet per second)
ϕ	initial flight path angle (degrees)
H	program parameter to control integration step size (seconds)
N	program parameter to control the print-out frequency (integer multiple of H)
W	mass of projectile (slugs)
D5	diameter of projectile (feet)
I1	axial moment of inertia (slug-ft^2)
I2	transverse moment of inertia (slug-ft^2)
P5	initial spin rate (radians per second)
Z9	an integer designating the table length (number of Mach number entries - maximum value is ten)

Following the above data are the tables. The tables are supplied per line:

M(J)	Mach number
A(J)	C_D
B(J)	C_{m_α}
C(J)	$C_{m_q} + C_{m_{\dot\alpha}}$
D(J)	C_{N_α}
E(J)	C_{ℓ_p}
F(J)	$C_{m_{p\alpha}}$

26

The input data should appear as follows:

1890 DATA	T5, XO, YO, VO, V1, O
1900 DATA	H, N
1910 DATA	W, D5, I1, I2, P5
1920 DATA	Z9
1930 DATA	M(1), A(1), B(1), C(1), D(1), E(1), F(1)
1940 DATA	M(2), A(2), B(2), C(2), D(2), E(2), F(2)
19.. DATA	M(Z9), A(Z9), B(Z9), C(Z9), C(Z9), E(Z9)

Typical output from the program is shown in Table 4. As indicated, the first part of the output is the coefficient table. After this table is printed, the quantitites H and N are printed. These numbers indicate the step size and print-out frequency, respectively. The remainder of the print out is the trajectory parameters and stability derivatives (as defined in Table 1).

These data are presented in pairs. Each pair contains TIME (seconds), X (horizontal distance - feet), Y (vertical distance - feet), V (speed relative to inertial space - feet per second), p (spin rate - radians per second), 1/Sg (inverse gyroscopic stability parameter), S_d (damping stability parameter), Yaw

of repose (radians), pd/2V (reduced frequency), MACH (Mach number). Following the initial conditions is a print out of the above trajectory constants at the appropriate step dictation by the quantities H and N. The program automatically terminates at zero altitude. It will be noted, in Table 3, that the projectile velocity relative to inertial space, V, is calculated in line 430 from the platform velocity and muzzle velocity.

STABILITY ANALYSIS

In considering the stability of the projectile the analyst must, in some way, limit the infinite number of initial conditions in altitude and velocity that the projectile theoretically might encounter. A relatively small number of initial conditions can be chosen which will represent typical operating conditions. Since the 20mm projectile under consideration is intended for general purpose, one must consider firings from high-speed aircraft, helicopters and ground.

In order to represent firings or launchings from high-speed aircraft, the gyroscopic stability factor was calculated at the muzzle for launchings from aircraft flying at 300, 475 and 600 knots and at altitudes of 0, 5000, 10,000 and 15,000 feet. In addition, since

atmospheric conditions are influential, it was decided to carry out identical calculations for a cold day (-65°F) and a standard day (-59°F). Using the program described in the preceding section, the gyroscopic stability factor was rapidly and easily determined for these 24 various launchers.

Figure 50 presents results for the cold day and Figure 51 for the standard day. A comparison of these figures indicates that the most critical firing condition of those studied occurs on a cold day in firing from an aircraft having a 600 know airspeed at sea level. Clearly, the projectile's stability decreases with an increase in speed and decrease in altitude of the launch aircraft and with decreasing ambient temperature. Both Figures 50 and 51 indicate that the projectile is gyroscopically stable for all conditions studied.

It was stated in Equation (36) that the necessary and sufficient condition for projectile dynamic stability is that

$$1/S_g < 1 \qquad\qquad 0 < S_d < 2 \tag{48a}$$

and

$$\frac{1}{S_g} < S_d(2 - S_d) \tag{48b}$$

It can be shown that a good approximation to Equation (38a) might be written neglecting the normal-force, C_{N_α}, and the drag, C_D, contributions

$$S_d \cong \frac{I_{yy} C_{m_{p\alpha}}}{I_{xx}(C_{m_q} + C_{m_{\dot\alpha}})} \tag{49}$$

Now since $C_{m_q} + C_{m_{\dot\alpha}}$ will always be negative, it can be seen that the sign of S_d will be identical to the sign of the Magnus derivative, $C_{m_{p\alpha}}$. It will be noted, in Figure 49, that the Magnus derivative changes sign from positive to negative in going from supersonic to subsonic flight. Thus, in light of Equations (48), the projectile will be unstable for subsonic flight. Figures 35 and 49 also point out that there is considerable scatter in both the damping-in-pitch

derivative and the Magnus derivative. There might be some doubt as to the projectile satisfying the condition that $S_d < 2$. The stability conditions, as specified by $1/Sg$ and S_d, can now be examined for a number of representative operational conditions.

Since projectile stability becomes more severe the higher the platform velocity, it was decided to examine the trajectory of the projectile fired from an aircraft flying at an airspeed of 600 knots and at several altitudes. In Figures 52 through 55, the reciprocal of the gyroscopic stability factor is plotted versus the damping stability factor for launchings from an aircraft having an airspeed of 600 knots and altitudes, respectively, of 15,000, 10,000, 5,000 and 500 feet. Certain conclusions about projectile stability may now be drawn from these figures.

In Figure 52 it will be noted that the projectile remains gyroscopically stable throughout the entire flight. This conclusion was made on the basis of Figures 50 and 51. More significantly, the dynamic stability factor decreases steadily with diminishing flight speed. Thus, an error made in the location of S_d due to scatter is not too serious as the damping stability factor decreases steadily through the flight. In comparing Figures 52 through 55 it will be noted that stability becomes more critical at the lower altitudes, not only gyroscopic stability, as pointed out earlier, but damping stability as well. It is interesting to note that at 15,000 feet the unstable conditions are encountered at between six to seven seconds after firing and around 13,000 feet downrange. By contrast, at 500 feet instability is encountered at less than four seconds and at a downrange distance of about 7500 feet. In both extremes, projectile velocities are comparable at the onset of instability.

Since the projectile under consideration is general purpose, is was decided to examine its stability under conditions of horizontal firing from a stationary platform and a 45-degree firing from the ground. From the stationary platform the instability is encountered at less than three seconds and about 5,000 feet downrange. For ground firing at 45 degrees, the instability occurs at an altitude and range both of about 3500 feet (see Figs. (56) and (57), respectively).

CONCLUSIONS

This report has presented aerodynamic data on the U. S. Navy's general purpose 20-millimeter projectile. The data were obtained in both a pressurized aeroballistics range and in a supersonic wind tunnel. A computer analysis was carried out to determine the stability of the projectile under several operational situations. It may be concluded that the projectile is both gyroscopically and dynamically stable under all conditions

29

examined. Gyroscopic stability becomes lessened with decreasing altitude and temperature and increasing platform velocity. The dynamic stability decreases with decreasing altitude, although it is relatively insensitive to platform velocity.

In addition to the above computer stability analysis, attempts were made to calculate the normal-force and pitching-moment derivatives, C_{N_α} and C_{m_α}, respectively, using Wood's

semiempirical method. The agreement is considered only fair.

REFERENCES

(1)   "Aero- and Hydroballistics Research Facilities at the Naval Ordnance Laboratory," NOLR 1264, Jul 1967.

(2)   Murphy, C. H., "Free-Flight Motion of Symmetric Missiles," BRL Report 1216, Ballistics Research Laboratories, Aberdeen Proving Ground, Jul 1963.

(3)   Knadler, Charles, "A Wind Tunnel Free-Flight Data-Reduction Program for Either Spinning or Nonspinning Models Utilizing Data from a Single Plane," NOLTR 68-87, Jun 1968.

(4)   Nicolaides, J. D., "On the Pure Rolling Motion of Winged and/or Finned Missiles in Varying Supersonic Flight," BRL Report 799, Ballistics Research Laboratories, Aberdeen Proving Ground, 1952.

(5)   Hitchcock, H. P., "Aerodynamic Data for Spinning Projectiles," BRL Report 620, Ballistics Research Laboratories, Aberdeen Proving Ground, 1947.

(6)   Wood, R. M., "Quick Methods for Estimating the Static Aerodynamic Coefficients of Shell," BRL Report 854, Ballistics Research Laboratories, Aberdeen Proving Ground, 1954.

(7)   Engineering Design Handbook, "Design for Control of Projectile Flight Characteristics," AMCP 706-242, Army Material Command, 1966.

(8)   DeGrafft, W. D., "An IBM 7090 Six-Degree-of-Freedom Trajectory Program," NOLTR 64-225, 1965.

TABLE 1
PROGRAM FOR CALCULATION OF NORMAL FORCE AND PITCHING MOMENT DERIVATIVES FOR A SHELL

```
100 REM THIS PROGRAM CALCULATES NORMAL FORCE AND PITCHING MOMENT
110 REM DERIVATIVES AND CENTER OF PRESSURE FOR A SHELL.
120 REM THIS IS A SEMI-EMPIRICAL METHOD BASED UPON BRL854
130 REM C1 IS THE NORMAL FORCE DERIVATIVE
140 REM C2 IS THE PITCHING MOMENT DERIVATIVE ABOUT THE BASE
150 REM C3 IS THE PITCHING MOMENT ABOUT THE CENTER OF GRAVITY
160 REM S IS THE STATIC MARGIN
170 REM CO IS THE CENTER OF PRESSURE IN CALIBERS FROM THE NOSE
180 REM R IS THE FINENESS RATIO ,BODY VOLUME/(REF. AREAXDIAMETER)
190 REM G IS THE LOCATION OF THE CG FROM THE BASE
200 REM L IS THE LENGTH OF THE BODY IN CALIBERS
210 REM T IS THE CENTER OF PRESSURE AFT OF THE VERTEX (IN CAL.)
220 REM A1 IS THE RATIO OF EFFECTIVE BOATTAIL CROSSECTIONAL AREA
230 REM TO REFERENCE AREA,(AB+AR)/2*AR WHERE AB IS BOATTAIL AREA
240 REM AND AR IS THE REFFERENCE AREA
250 FOR I = 1 TO 15
260 READ M
270 LET R = 3.83148
280 LET L = 4.9
290 LET A1 =1
300 LET N0=.14331
310 LET N1=-9.32777E-2
320 LET N2=.453401
330 LET N3=.581451
340 LET N4=-4.97192
350 LET N5=6.97863
360 LET N6=-3.80723
370 LET N7=.736042
380 LET M0=.192947
390 LET M1=-.112361
400 LET M2=.872645
410 LET M3=-2.37587
420 LET M4=1.33114
430 LET M5=.924154
440 LET M6=-1.07323
450 LET M7=.26358
460 LET G=2.21
470 IF M>1 THEN 510
480 LET F1 = 1
490 LET F2 = 1
500 GOTO 580
510 LET N = SQR((M↑2)-1)/R
520 LET F1=N0+N1*N+N2*(N↑2)+N3*(N↑3)+N4*(N↑4)+N5*(N↑5)
530 LET F1=F1+N6*(N↑6)+N7*(N↑7)
540 LET F2=M0+M1*N+M2*(N↑2)+M3*(N↑3)+M4*(N↑4)+M5*(N↑5)
550 LET F2=F2+M6*(N↑6)+M7*(N↑7)
560 LET F1 = F1*SQR((M↑2)-1)+1
570 LET  F2 = (F2)*SQR((M↑2)-1)+1
580 LET C1 = (2*A1+.5)*F1
590 LET C2=2*R*F2
600 LET C=C2/C1
610 LET T = L -C
620 LET S=C-G
630 LET C3=C1*S
640 IF I>1 THEN 670
650 PRINT "PITCH.MOM.","NOR.FORCE","STAT.MAR.","C.P.","MACH NO."
660 PRINT
670 PRINT C3,C1,S,T,M
680 NEXT I
690 DATA .4,1.,1.2,1.5,1.75,2,2.5,3,3.5
700 END
```

Table 2

CORRESPONDENCE BETWEEN COMPUTER AND PROBLEM VARIABLES

Computer Variable	Problem Variable	Definition
A	C_D	drag coefficient, current value
A1	D	drag, $C_D \rho S V^2/2$
A(Z)	--	drag coefficient array
B	C_{m_α}	pitching-moment derivative, current value
B(Z)	--	pitching-moment array
C	$C_{m_q} + C_{m_{\dot\alpha}}$	damping-in-pitch derivative, current value
C(Z)	--	damping-in-pitch derivative array
D	C_{N_α}	normal-force derivative
D1	--	variable used in Runge Kutta
D2	--	variable used in Runge Kutta
D5	d	diameter of projectile, reference length (feet)
D(Z)	--	normal-force derivative array
E	C_{ℓ_p}	damping-in-roll derivative
E1	--	variable used in Runge Kutta
E2	--	variable used in Runge Kutta
E5	--	exponential part of Pd/2V formula
E(Z)	--	damping-in-roll derivative array
F	$C_{n_{p\alpha}}$	Magnus moment derivative
F(Z)	--	Magnus moment derivative array
G	--	counter
G5	--	switching variable
H	--	step size
I	--	counter
I1	I_{xx}	axial moment of inertia (slug-ft^2)
I2	I_{yy}	transverse moment of inertia (slug-ft^2)

Table 2 (Cont'd)

Computer Variable	Problem Variable	Definition
J	--	index variable
K1	--	variable used in Runge Kutta
K2	--	variable used in Runge Kutta
K3	--	variable used in Runge Kutta
K4	--	variable used in Runge Kutta
K6	md^2	mass times reference length squared $(slug\text{-}ft^2)$
L1	--	variable used in Runge Kutta
L2	--	variable used in Runge Kutta
L3	--	variable used in Runge Kutta
L4	--	variable used in Runge Kutta
M	--	Mach number
M1	--	variable used in Runge Kutta
M2	--	variable used in Runge Kutta
M3	--	variable used in Runge Kutta
M4	--	variable used in Runge Kutta
M(Z)	--	Mach number array
N	--	print-out frequency
N1	--	variable used in Runge Kutta
N2	--	variable used in Runge Kutta
N3	--	variable used in Runge Kutta
N4	--	variable used in Runge Kutta
$\emptyset$	$\emptyset_o$	initial flight path angle in degrees
P	V_y	dy/dt velocity in vertical direction in ft/sec
PO	--	variable used in Runge Kutta
P1	--	dP/dt, $\dot{P}$, dV_y/dt
P5	p	current value of spin rate in rad/sec
P7	--	nonexponential part of pd/2V formula
P8	pd/2V	current value of pd/2V
Q	V_x	dx/dt, velocity in horizontal direction in ft/sec

33

Table 2 (Cont'd)

Computer Variable	Problem Variable	Definition
QO	--	variable used in Runge Kutta
Q1	--	dQ/dt, $\dot{Q}$, dVx/dt
Q5	Vxo	previous value of Vx in ft/sec
R	ρ	density slugs/ft^3
S	S	reference area $\pi d^2/4$ in ft^2
S1	Sg	gyroscopic stability factor
S2	S_d	dynamic stability factor
S3	$\delta\gamma$	yaw angle of repose in rad
T	t	time in seconds
TO	--	variable used in Runge Kutta
T5	to	initial time in seconds
V	v	velocity of projectile relative to inertial space
VO	--	velocity of platform relative to inertial space
V1	--	muzzle velocity
V2	v^2	total velocity squared in ft^2/sec^2
V5	vo	previous value of V in ft/sec
W	m	mass of projectile in slugs
X	x	horizontal distance in feet
XO	--	variable used in Runge Kutta
X1	dx/dt	horizontal velocity
X5	Xo	previous value of X in feet
Y	y	vertical distance in feet
YO	--	variable used in Runge Kutta
Y1	dy/dt	vertical velocity
Z	--	index variable
Z9	--	table length

TABLE 3
BASIC PROGRAM FOR THE CALCULATION OF PROJECTILE STABILITY

```
100 REM THE PURPOSE OF THIS PROGRAM IS TO OBTAIN THE STABILITY
110 REM OF A PROJECTILE IN TERMS OF THE RECIPROCAL OF THE
120 REM GYROSCOPIC STABILITY FACTOR AND THE DAMPING STABILITY
130 REM FACTOR.  THE FOLLOWING IS A LISTING OF THE REQUIRED
140 REM INPUTS TO THIS PROGRAM.
150 REM T5 IS THE INITIAL TIME(SECONDS)
160 REM XO IS THE INITIAL HORIZONTAL DISPLACEMENT(FEET)
170 REM YO IS THE INITIAL VERTICAL DISPLACEMENT(FEET)
180 REM V IS THE VEL. OF PROJ. REL. TO INERTIAL SPACE(FT/SEC.)
190 REM VO IS THE PLATFORM VELOCITY REL. TO INERT. SPACE (FT/SEC)
200 REM V1 IS THE PROJECTILE MUZZLE VELOCITY )FT/SEC)
210 REM 0 IS THE INITIAL FLIGHT PATH ANGLE(DEGREES)
220 REM H IS PROGRAM PARAMETER TO CONTROL INT. STEP SIZE(SEC.)
230 REM N IS PROGRAM PARAMETER TO CONTROL PRINT-OUT FREQUENCY
240 REM      (INTEGER MULTIPLE OF H)
250 REM W IS THE MASS OF THE PROJECTILE (SLUGS)
260 REM D5 IS THE DIAMETER OF THE PROJECTILE(FEET)
270 REM I1 IS THE AXIAL MOMENT OF INERTIA(SLUG-FT SQ.)
280 REM I2 IS THE TRANSVERSE MOMENT OF INERTIA (SLUG-FT SQ.)
290 REM Z9 IS AN INTEGER INDICATING THE LENGTH OF THE TABLES
300 REM (NUMBER OF MACH NUMBER ENTRIES-MAXIMUM NO. IS 10)
310 REM THE TABLES ARE SUPPLIED PER LINE AS FOLLOWS:
320 REM M(J) IS THE MACH NUMBER
330 REM A(J) IS THE DRAG COEFFICIENT,CD
340 REM B(J) IS THE PITCH. MOMENT DERIVATIVE, CMA
350 REM C(J) IS THE DAMPING-IN-PITCH DERIVATIVE,CMO+CMA
360 REM D(J) IS THE NORMAL FORCE DERIVATIVE,CNA
370 REM E(J) IS THE DAMPING-IN-ROLL DERIVATIVE,CLP
380 REM F(J) IS THE MAGNUS DERIVATIVE,CMPA
390 PRINT "                   PROJECTILE STABILITY PROGRAM"
400 PRINT
410 READ T5,XO,YO,VO,V1,0,H,N
420 LET V = VO + V1
430 READ W,D5,I1,I2,P5
440 DIM M(10), A(10), B(10), C(10), D(10),E(10), F(10)
450 READ Z9
460 PRINT "COEFFICIENT TABLE"
470 PRINT " M        A        B        C        D        E        F"
480 FOR J=1 TO Z9
490 READ M(J), A(J), B(J), C(J), D(J), E(J), F(J)
500 PRINT M(J);A(J);B(J);C(J);D(J);E(J);F(J)
510 NEXT J
520 LET Z=1
530 LET S=(3.14159*D5†2)/4
540 LET PO=V*SIN(0/57.296)
550 LET 00=V*COS(0/57.296)
560 LET K6=(W*(D5†2))
570 LET TO=T5
580 PRINT
590 PRINT "FOR H ="H;"N ="N
600 PRINT
610 PRINT
620 PRINT "TIME","X","Y","V","P"
630 PRINT
640 PRINT "1/SG","SD","YAW OF REPOSE","PD/2V","MACH"
650 PRINT
660 PRINT
670 PRINT "INTITIAL CONDITONS:"
680 PRINT
690 LET T=TO
700 LET TO=T5
710 LET X=XO
720 LET Y=YO
730 LET 0=00
```

```
740 LET P=P0
750 LET X5=X
760 LET U5=U
770 LET V5=V
780 GOSUB 1620
790 LET G5=0
800 LET G=0
810 LET I = N
820 LET G=G+1
830 IF G5=0 THEN 1400
840 LET G5=1
850 GOSUB 1560
860 LET K1=Y1*H
870 LET N1=X1*H
880 GOSUB 1590
890 LET L1=P1*H
900 LET M1=Q1*H
910 LET T=T0+H/2
920 LET Y=Y0+K1/2
930 LET X=X0+N1/2
940 LET P=P0+L1/2
950 LET Q=Q0+M1/2
960 GOSUB 1560
970 LET K2=Y1*H
980 LET N2=X1*H
990 GOSUB 1590
1000 LET L2=P1*H
1010 LET M2=Q1*H
1020 LET Y=Y0+K2/2
1030 LET X=X0+N2/2
1040 LET P=P0+L2/2
1050 LET Q=Q0+M2/2
1060 GOSUB 1560
1070 LET K3=Y1*H
1080 LET N3=X1*H
1090 GOSUB 1590
1100 LET L3=P1*H
1110 LET M3=Q1*H
1120 LET T=T0+H
1130 LET Y=Y0+K3
1140 LET X=X0+N3
1150 LET P=P0+L3
1160 LET Q=Q0+M3
1170 GOSUB 1560
1180 LET K4=Y1*H
1190 LET N4=X1*H
1200 GOSUB 1590
1210 LET L4=P1*H
1220 LET M4=Q1*H
1230 LET D1=(K1+K4)/6+(K2+K3)/3
1240 LET E1=(N1+N4)/6+(N2+N3)/3
1250 LET D2=(L1+L4)/6+(L2+L3)/3
1260 LET E2=(M1+M4)/6+(M2+M3)/3
1270 LET Y0=Y0+D1
1280 LET X0=X0+E1
1290 LET P0=P0+D2
1300 LET Q0=Q0+E2
1310 LET T0=T5+H*G
1320 LET T=T0
1330 LET Y=Y0
1340 LET X=X0
1350 LET P=P0
1360 LET Q=Q0
1370 GOSUB 1620
```

36

(CONT'D)

```
1380 IF Y<=0 THEN 1400
1390 IF G<I THEN 820
1400 LET B=B(Z)+((B(Z+1)-B(Z))*(M-M(Z)))/(M(Z+1)-M(Z))
1410 LET C=C(Z)+((C(Z+1)-C(Z))*(M-M(Z)))/(M(Z+1)-M(Z))
1420 LET D=D(Z)+((D(Z+1)-D(Z))*(M-M(Z)))/(M(Z+1)-M(Z))
1430 LET F=F(Z)+((F(Z+1)-F(Z))*(M-M(Z)))/(M(Z+1)-M(Z))
1440 LET S1=(2*(I1†2)*(P5†2))/(I2*3.1416*R*(D5†3)*(V†2)*B)
1450 LET S1=1/S1
1460 LET S2=(2*(D-A+.5*(K6/I1)*F))/(D-(2*A)-.5*(K6/I2)*C)
1470 LET S3=(I1*P5*64.348*(O/V))/(R*S*D5*(V†3)*B)
1480 PRINT T,X,Y,V,P5
1490 PRINT S1,S2,S3,P8,M
1500 PRINT
1510 PRINT
1520 IF Y<=0 THEN 2030
1530 IF G5=0 THEN 840
1540 LET I = I + N
1550 GOTO 820
1560 LET X1=0
1570 LET Y1=P
1580 RETURN
1590 LET P1=-((A1)/(W*V))*P-32.174
1600 LET U1=-((A1)/(W*V))*O
1610 RETURN
1620 LET V2=P*P+U*O
1630 LET V=SOR(V2)
1640 IF Y<36500 THEN 1670
1650 LET M=V/971
1660 GO TO 1680
1670 LET M=V/(1117-.0042*Y)
1680 IF M<=M(Z+1) THEN 1720
1690 LET Z=Z+1
1700 IF Z> Z9 THEN 1880
1710 GO TO 1680
1720 IF M>=M(Z)    THEN 1760
1730 LET Z=Z-1
1740 IF Z<1 THEN 1880
1750 GO TO 1720
1760 LET A=A(Z)+((A(Z+1)-A(Z))*(M-M(Z)))/(M(Z+1)-M(Z))
1770 LET R=.002377*EXP(-.31582E-4*Y)
1780 LET A1=(A*S*R*V2)/2
1790 LET E=E(Z)+((E(Z+1)-E(Z))*(M-M(Z)))/(M(Z+1)-M(Z))
1800 LET P7=(P5*V)/V5
1810 LET E5=EXP((V5/Q5)*(((R*S)/(2*W))*((K6/I1)*.5*E+A)*(X-X5)))
1820 LET P5=P7*E5
1830 LET P8=(P5*D5)/(2*V)
1840 LET X5=X
1850 LET O5=O
1860 LET V5=V
1870 RETURN
1880 PRINT "ERROR MACH NO. = "M" NOT IN DATA "
1890 DATA 0,0,1000,1010,2700,0
1900 DATA .1,10
1910 DATA .0100578,.06562,.5283E-5,.601331E-4,10285
1920 DATA 10
1930 DATA 0,.25,2.5,-22.5,1,-.044,-1
1940 DATA .8,.275,2.84,-22.5,2.19,-.039,-.76
1950 DATA 1,.435,2.98,-22.5,2.42,-.0375,-.45
1960 DATA 1.1,.515,3.06,-22.5,2.52,-.037,-.2
1970 DATA 1.2,.523,3.09,-22.5,2.63,-.0365,.15
1980 DATA 1.5,.5,3.13,-22.5,2.9,-.0345,.75
1990 DATA 2,.412,2.92,-22.5,3.22,-.0315,1.15
2000 DATA 2.5,.33,2.48,-22.5,3.5,-.0285,1.2
2010 DATA 3,.285,1.88,-22.5,3.4,-.025,1.3
2020 DATA 5,.275,1.88,-22.5,3.4,-.025,1.35
2030 END
```

TABLE 4 SAMPLE OUTPUT FROM BASIC STABILITY PROGRAM
PROJECTILE STABILITY PROGRAM

COEFFICIENT TABLE

M	A	B	C	D	E	F
0	.95	2.5	-22.5	1	-.044	-1
.5	.275	2.54	-22.5	2.19	-.039	-.76
1	.435	2.98	-22.5	2.42	-.0375	-.45
1.1	.515	3.06	-22.5	2.52	-.037	-.2
1.2	.523	3.09	-22.5	2.63	-.0365	.15
1.5	.5	3.13	-22.5	2.9	-.0345	.75
2	.412	2.92	-22.5	3.22	-.0315	1.15
2.5	.33	2.48	-22.5	3.5	-.0285	1.2
3	.285	1.88	-22.5	3.4	-.025	1.3
5	.275	1.58	-22.5	3.4	-.025	1.35

FOR H = .1 N = 10

TIME	X	Y	V	P
1/SG	SD	YAW OF REPOSE	PD/2V	MACH

INITIAL CONDITIONS:

0	0	1000	3710	10285
.538756	1.55077	7.12572E-5	9.09571E-2	3.33393
1.	3086.47	985.713	2560.05	9033.62
.469929	1.4607	1.34782E-4	.115776	2.30043
2.	5240.29	948.669	1800.31	8129.82
.333251	1.17706	3.00232E-4	.148163	1.6175
3.	6781.79	894.587	1326.18	7445.86
.216424	.534758	6.84708E-4	.184213	1.19127
4.	7958.41	824.715	1063.04	6898.39
.155043	-.033804	1.28484E-3	.212915	.95465
5.	8944.59	736.226	929.799	6481.
.130926	-.198919	1.8462E-3	.228696	.834718
6.	9823.76	626.746	846.664	6150.03
.119228	-.270147	2.33565E-3	.233327	.759771
7.	10625.8	496.081	780.785	5875.84
.11054	-.305803	2.84106E-3	.246913	.700308
8.	11363.2	345.051	726.424	5644.65
.1034	-.335741	3.36913E-3	.254949	.65118
9.	12045.2	174.379	681.208	5451.
9.74168E-2	-.361018	3.90519E-3	.262545	.610255
10.	12679.2	-15.2999	643.423	5290.76
9.23185E-2	-.382419	4.43269E-3	.269791	.575995
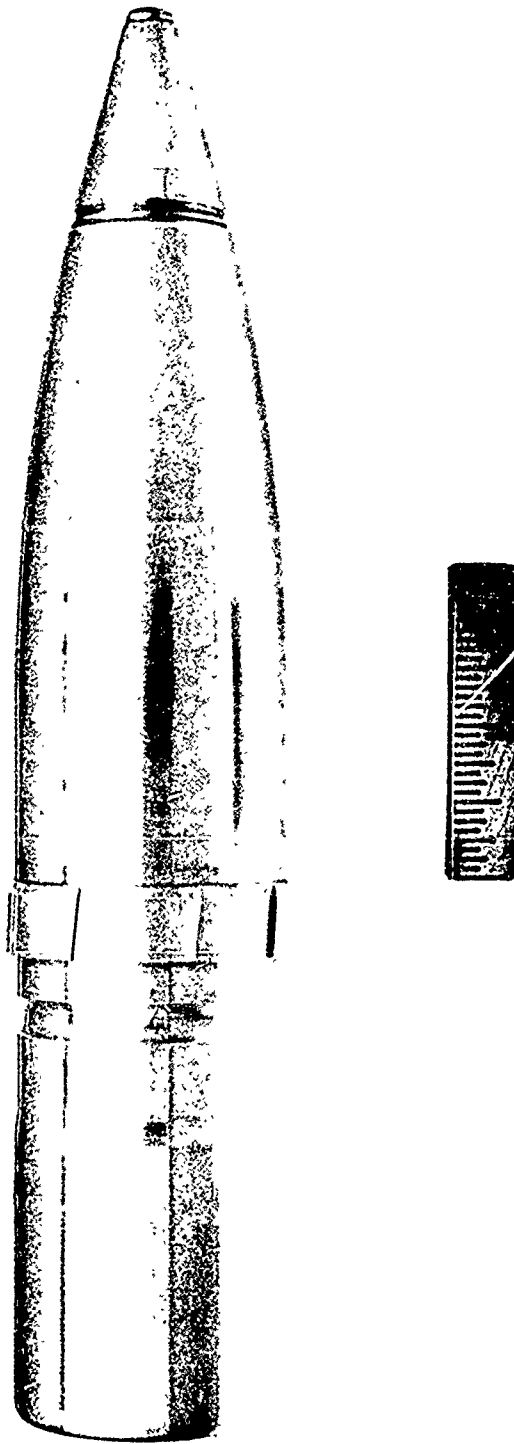
FIG. 1 BASIC CONFIGURATION OF THE 20 MM GENERAL PURPOSE PROJECTILE

39
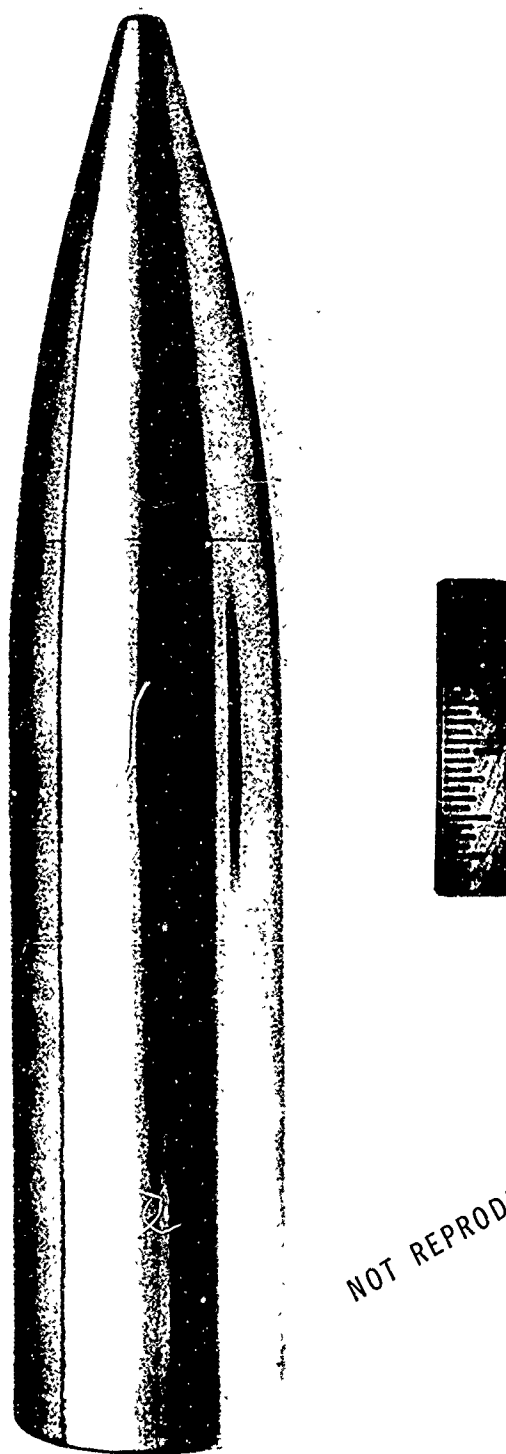
NOT REPRODUCIBLE

FIG. 2 SMOOTH CONFIGURATION OF THE 20 MM GENERAL PURPOSE PROJECTILE

ALL DIMENSIONS IN INCHES
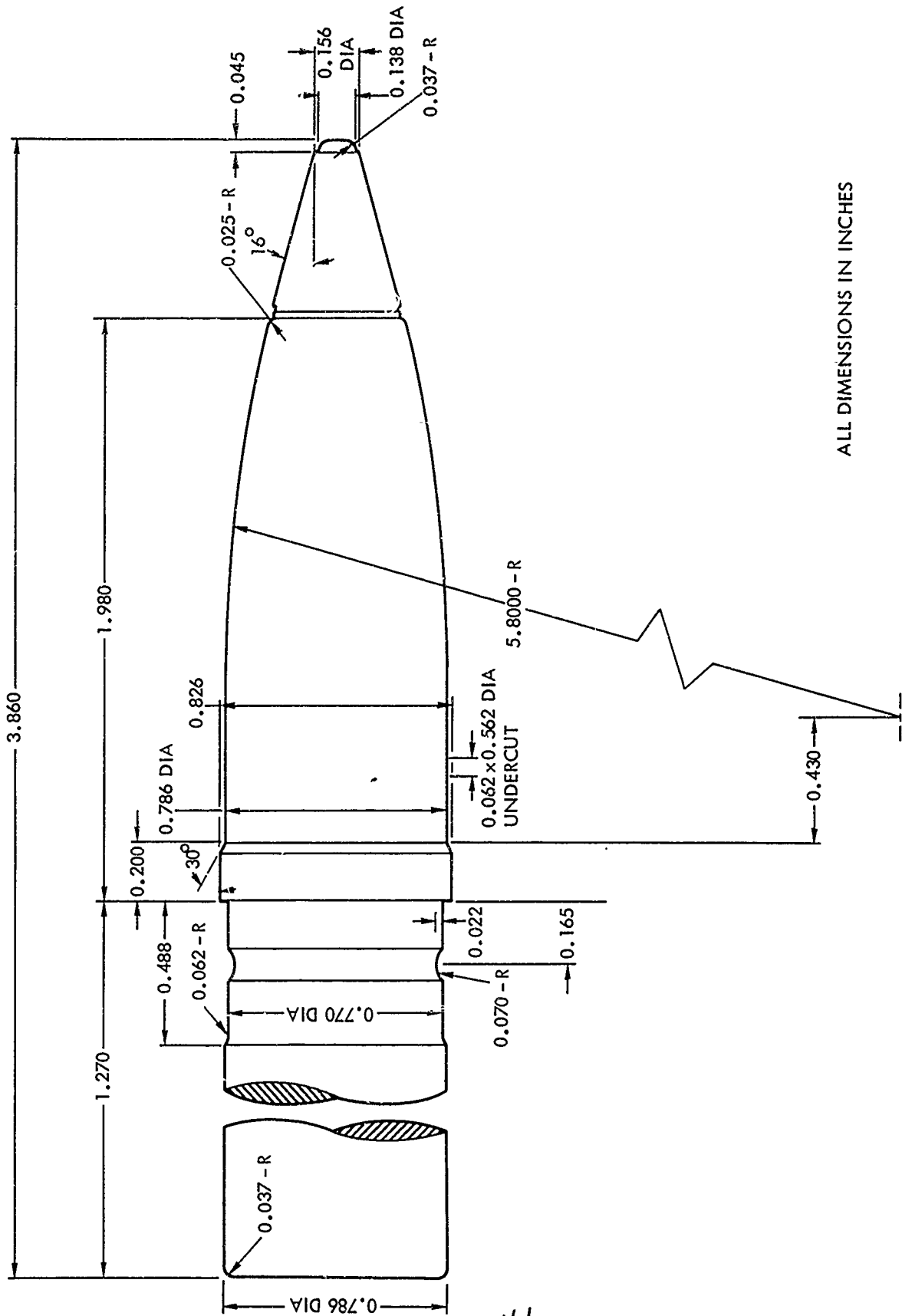
FIG. 3 GEOMETRIC DETAILS OF BASIC CONFIGURATION OF 20 MM GENERAL PURPOSE PROJECTILE

41

MAGNETIC
TACHOMETER

BALL BEARING

AIR
EXHAUST

AIR
INLET

MAGNUS FLEXURE

MULTI - STAGE
AIR TURBINE
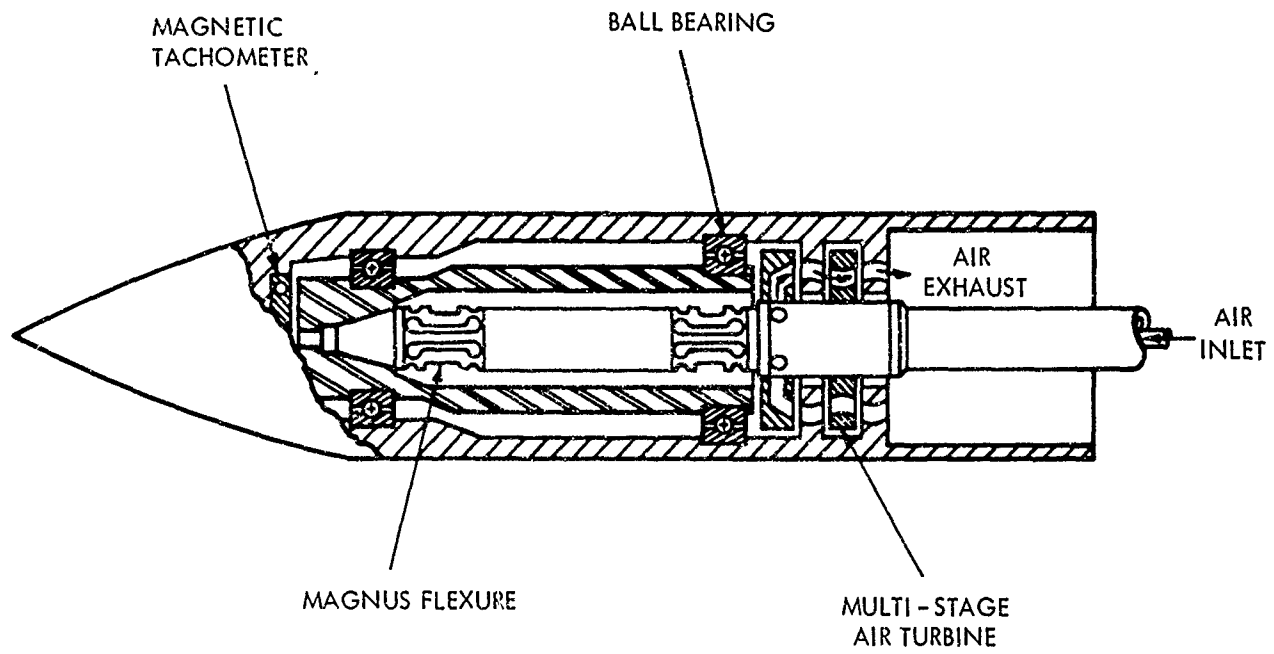
FIG. 4 MAGNUS BALANCE DETAILS

MAGNUS BRIDGE
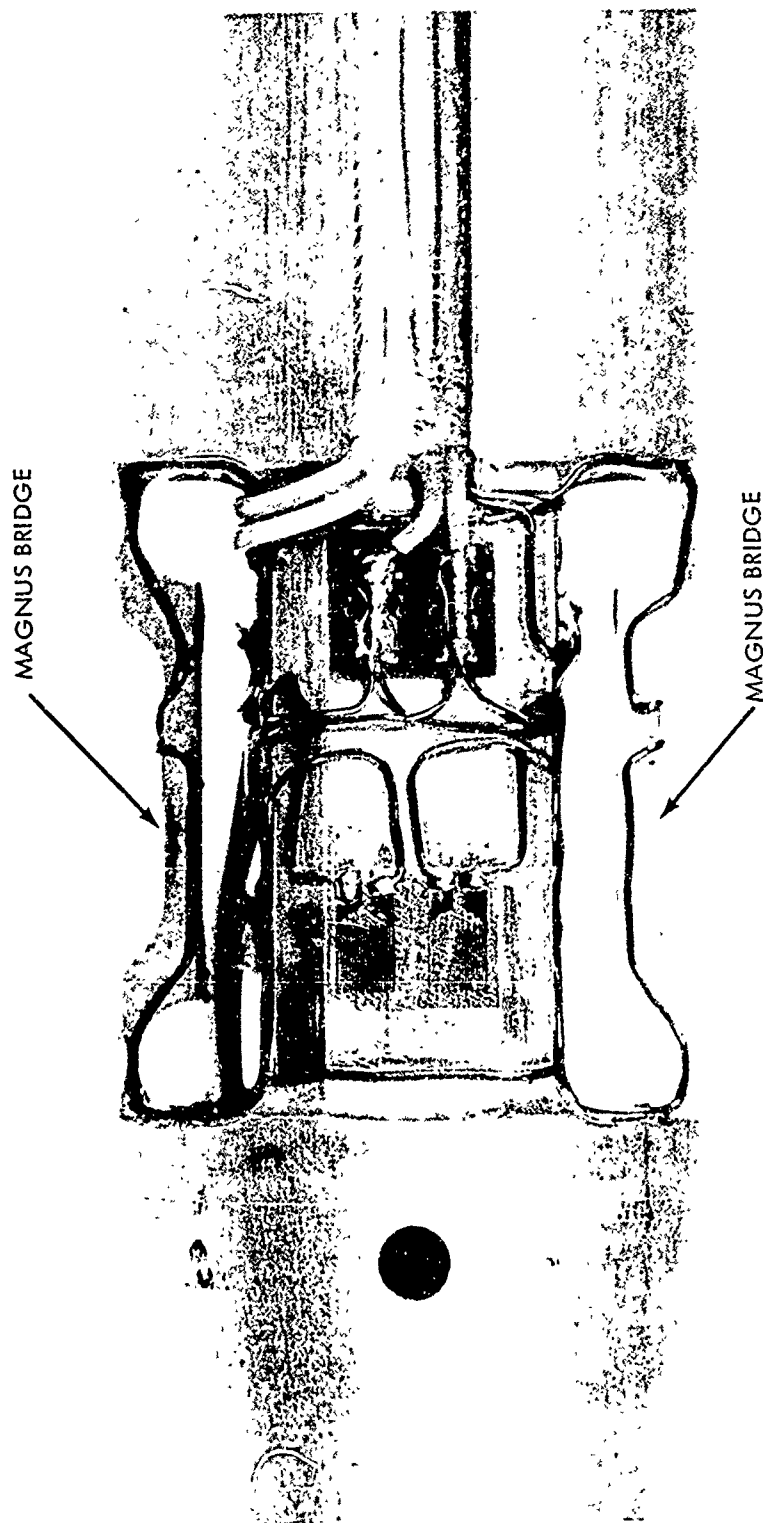
MAGNUS BRIDGE

FIG. 5 MAGNUS BRIDGE DETAILS

43
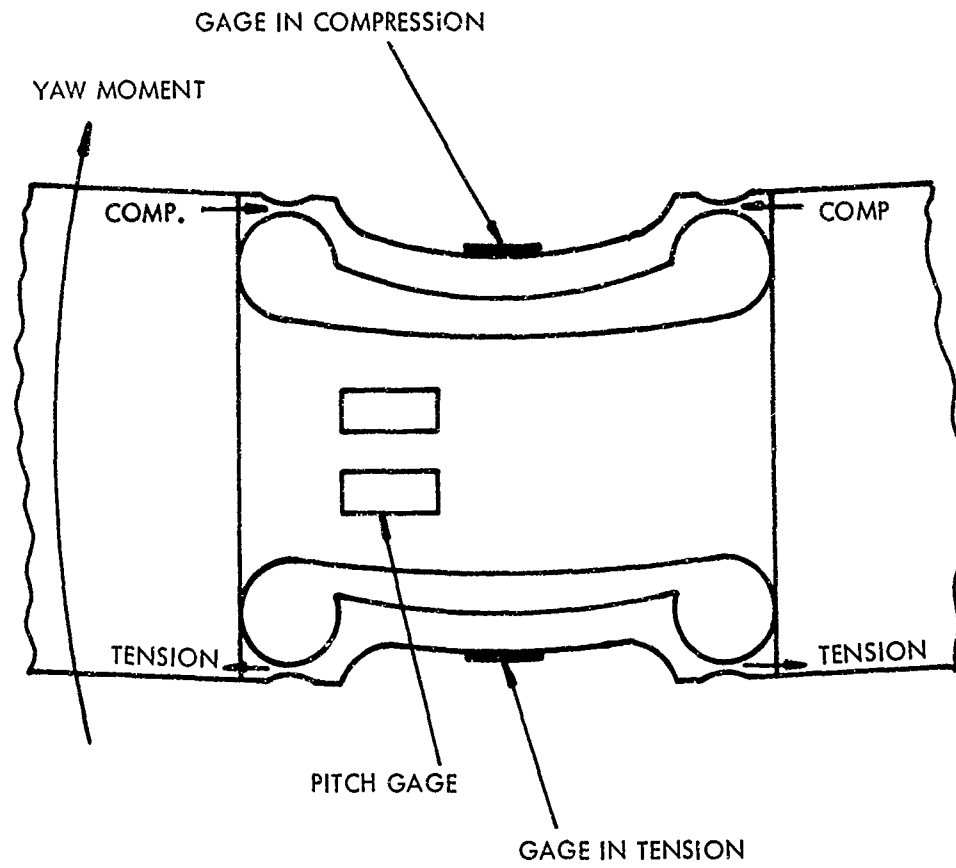
FIG. 6 MAGNUS BRIDGE UNDER YAW MOMENT
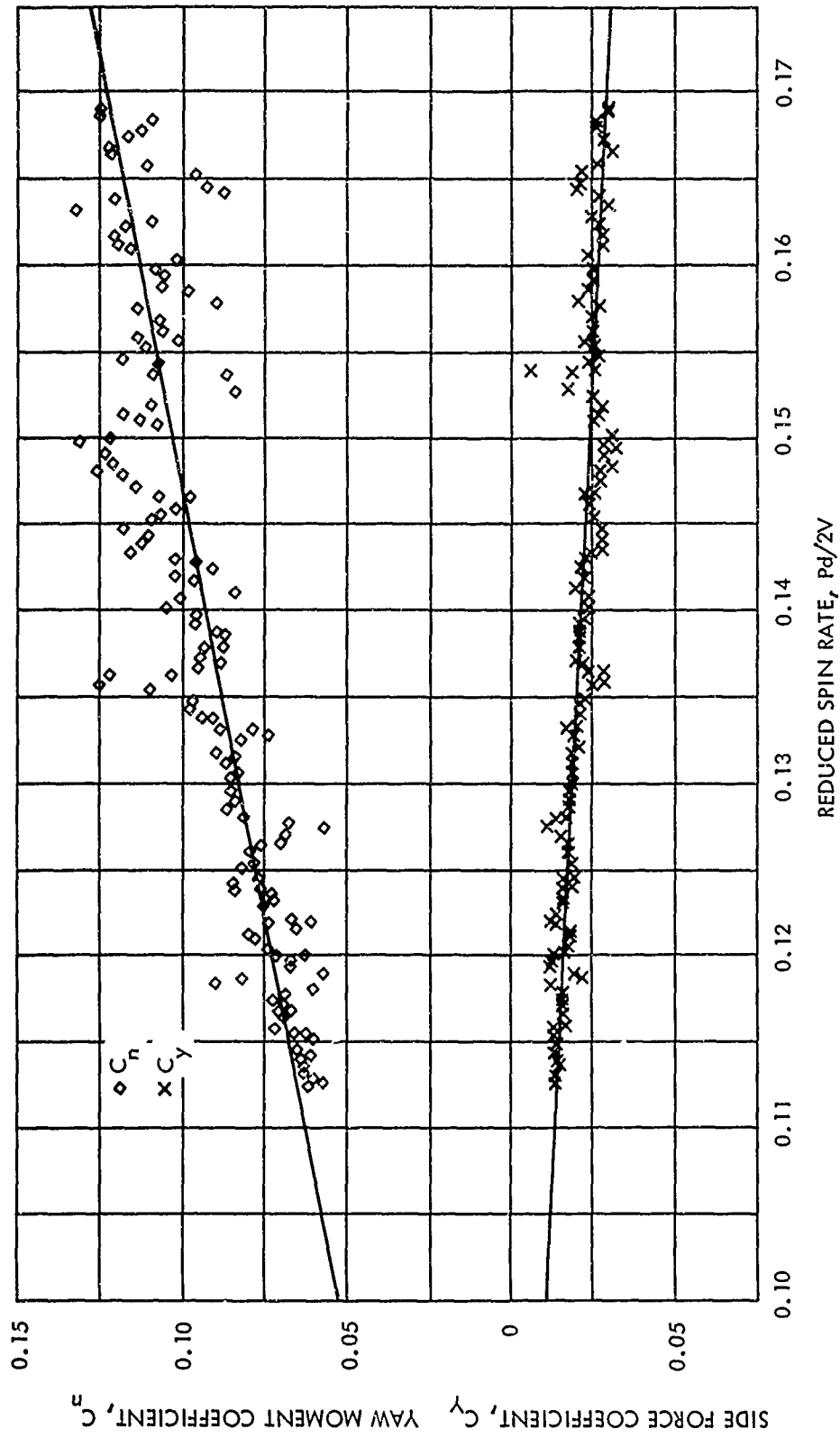
FIG. 7 SIDE FORCE AND YAW MOMENT COEFFICIENT VS REDUCED FREQUENCY FOR THE BASIC CONFIGURATION
AT A MACH NUMBER OF 3.02 AND AN ANGLE OF ATTACK OF 15 DEGREES
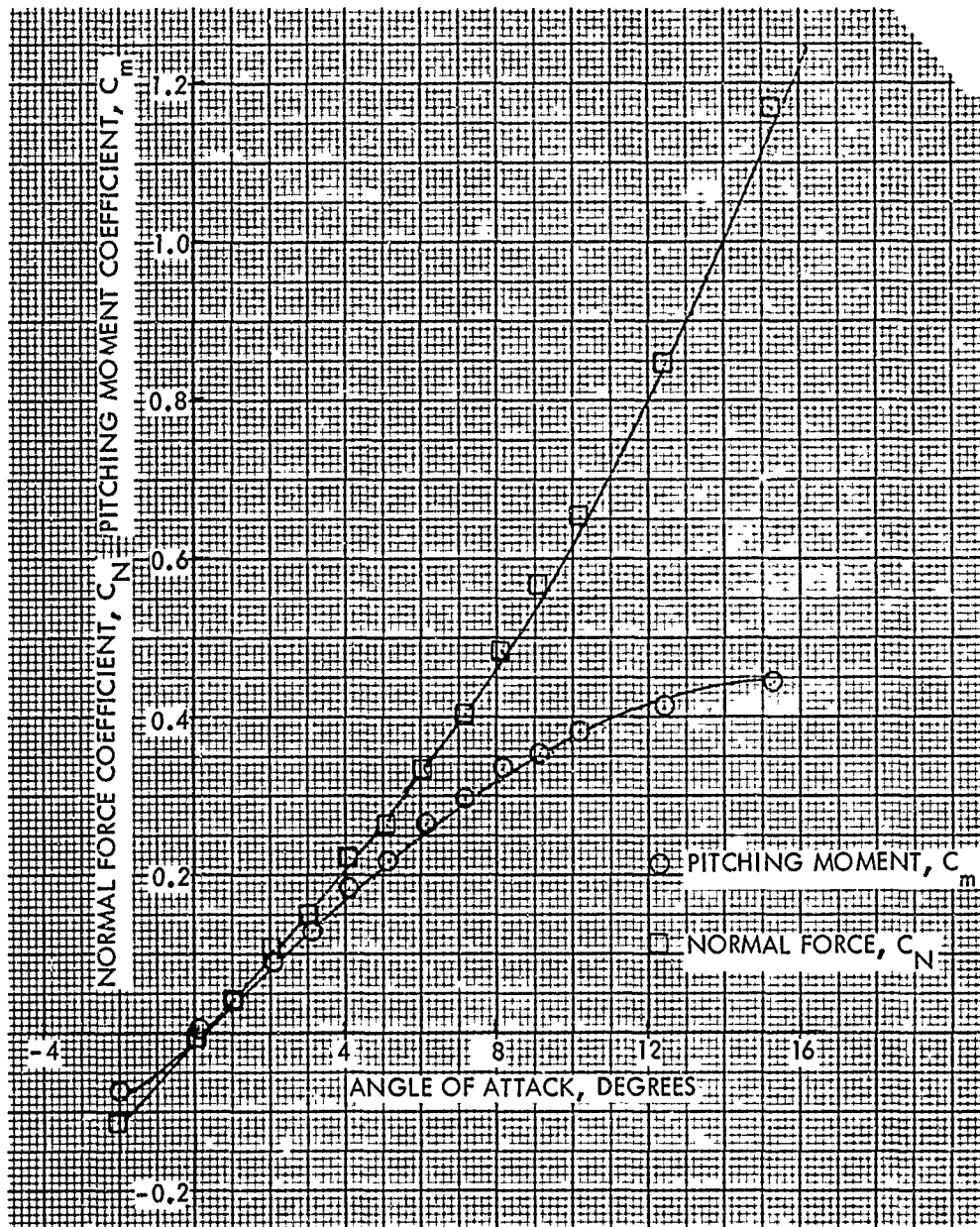
45
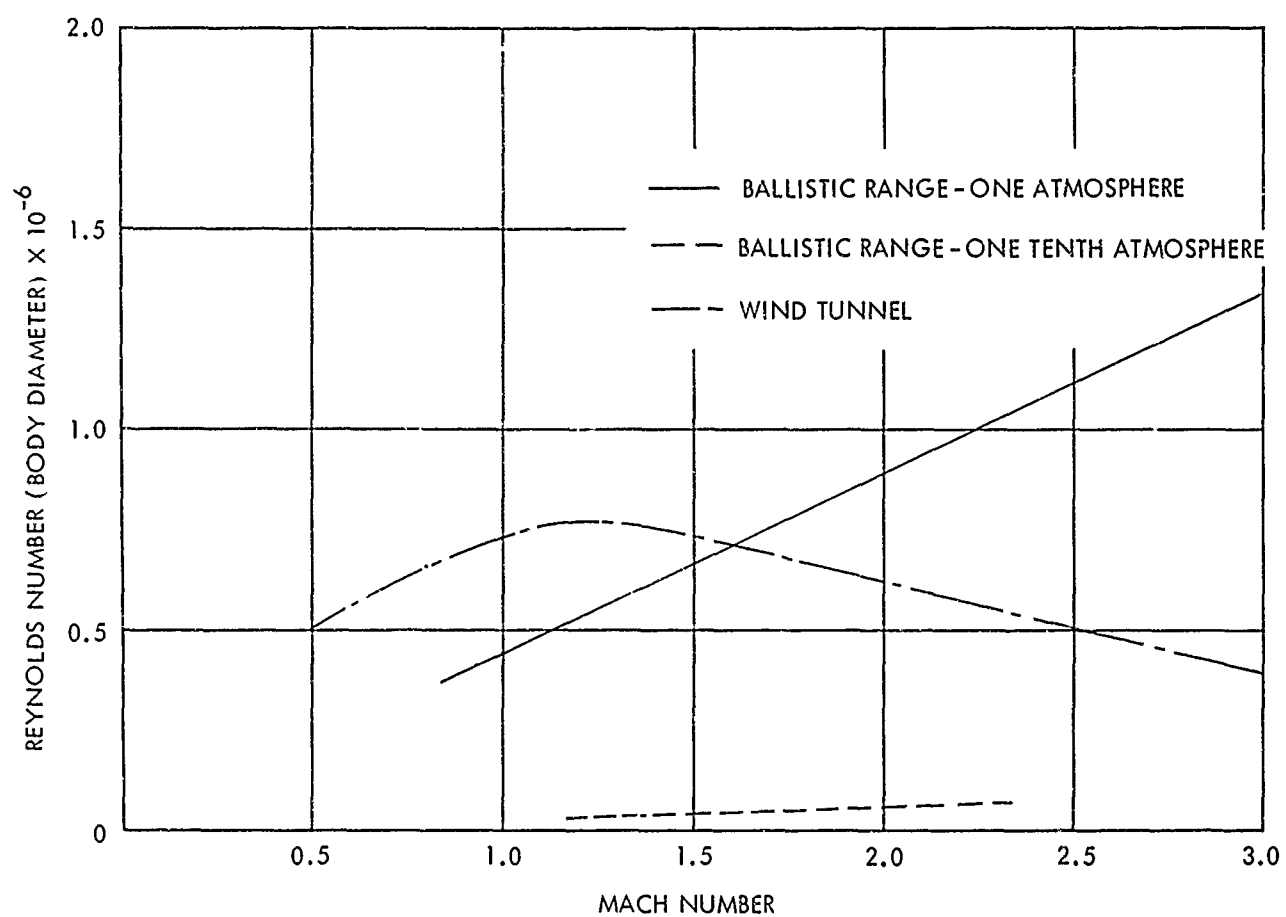
FIG. 8 REYNOLDS NUMBER VERSUS MACH NUMBER
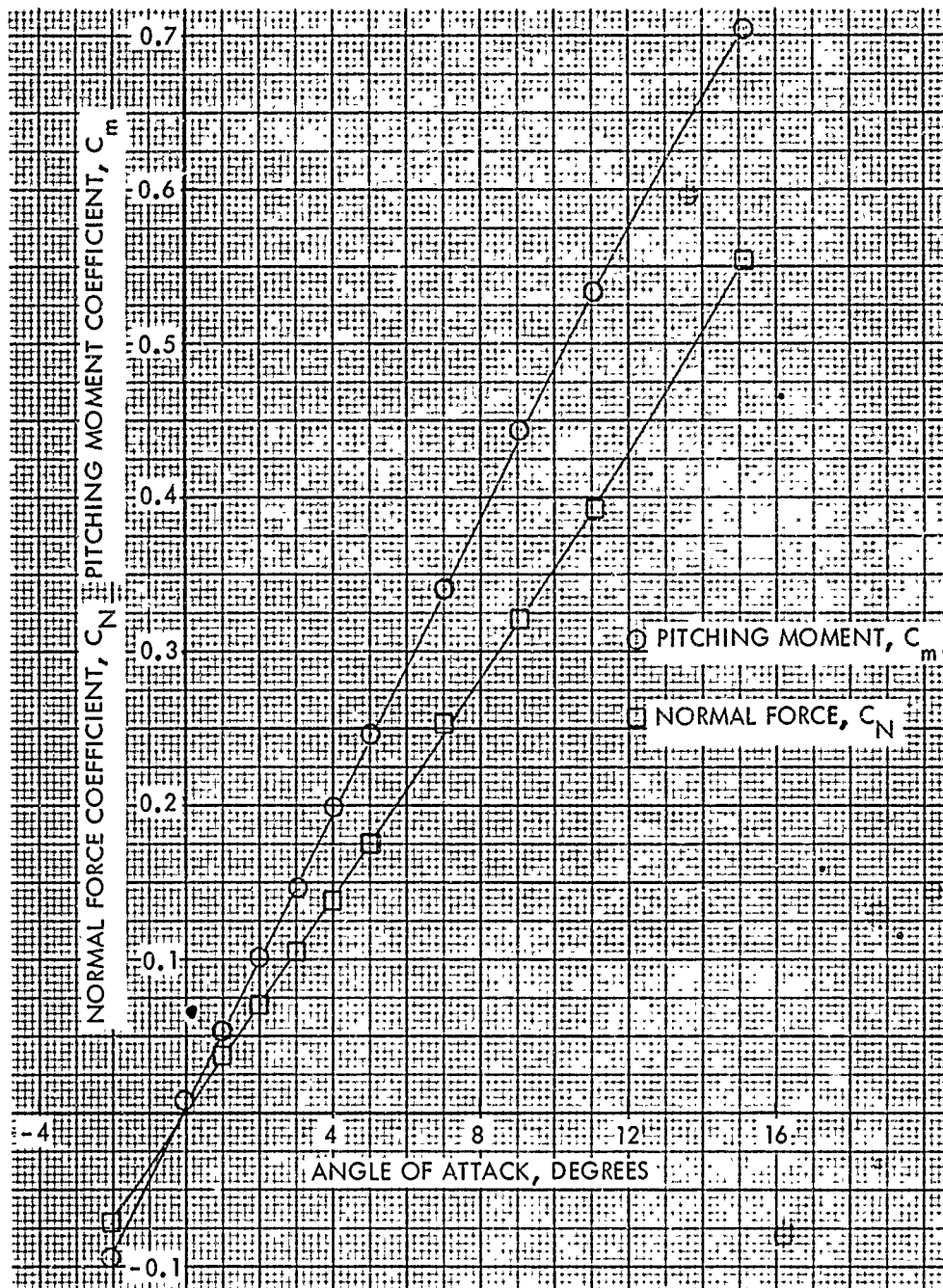
FIG. 9 NORMAL FORCE AND PITCHING MOMENT COEFFICIENTS VERSUS ANGLE OF ATTACK ᴀᴛ
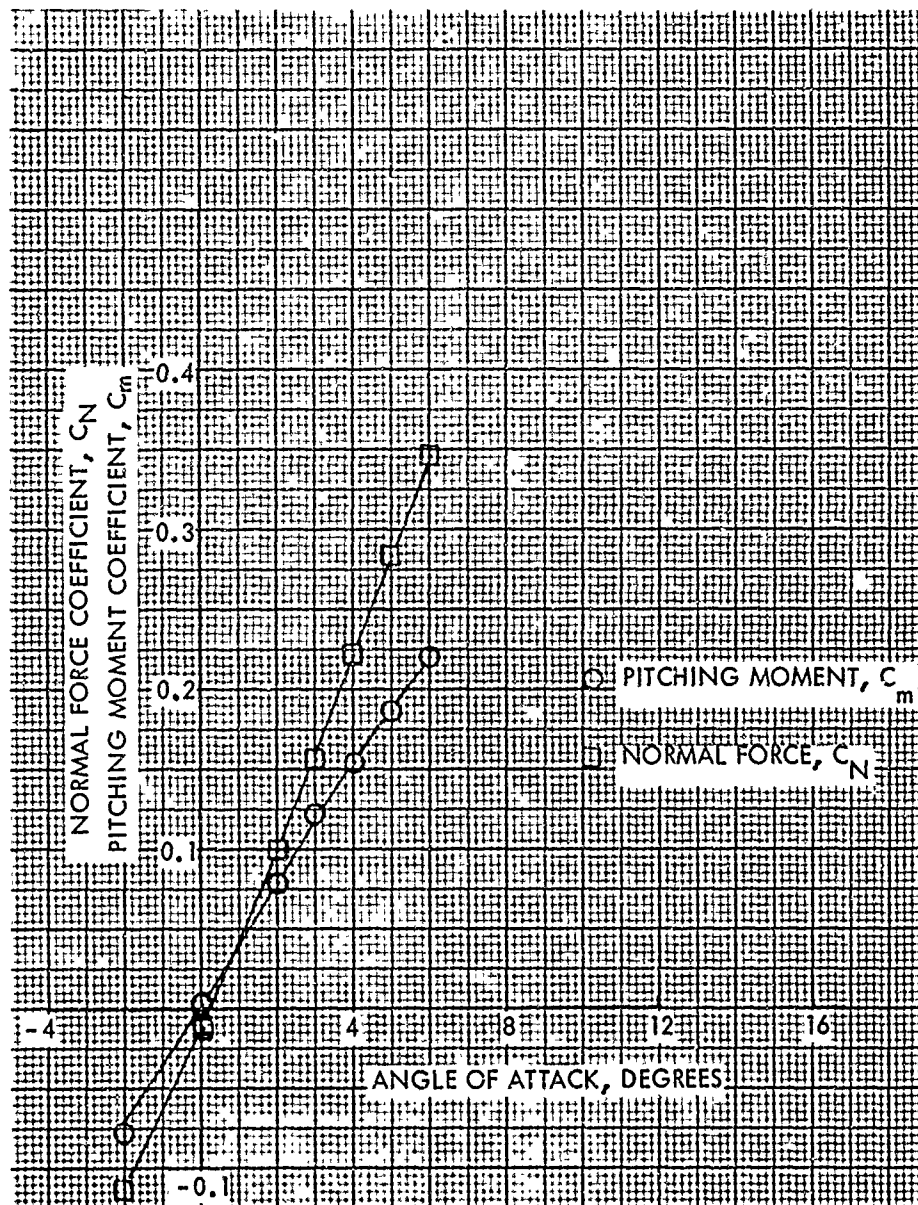A MACH NUMBER OF 0.59 FOR THE BASIC CONFIGURATION

41
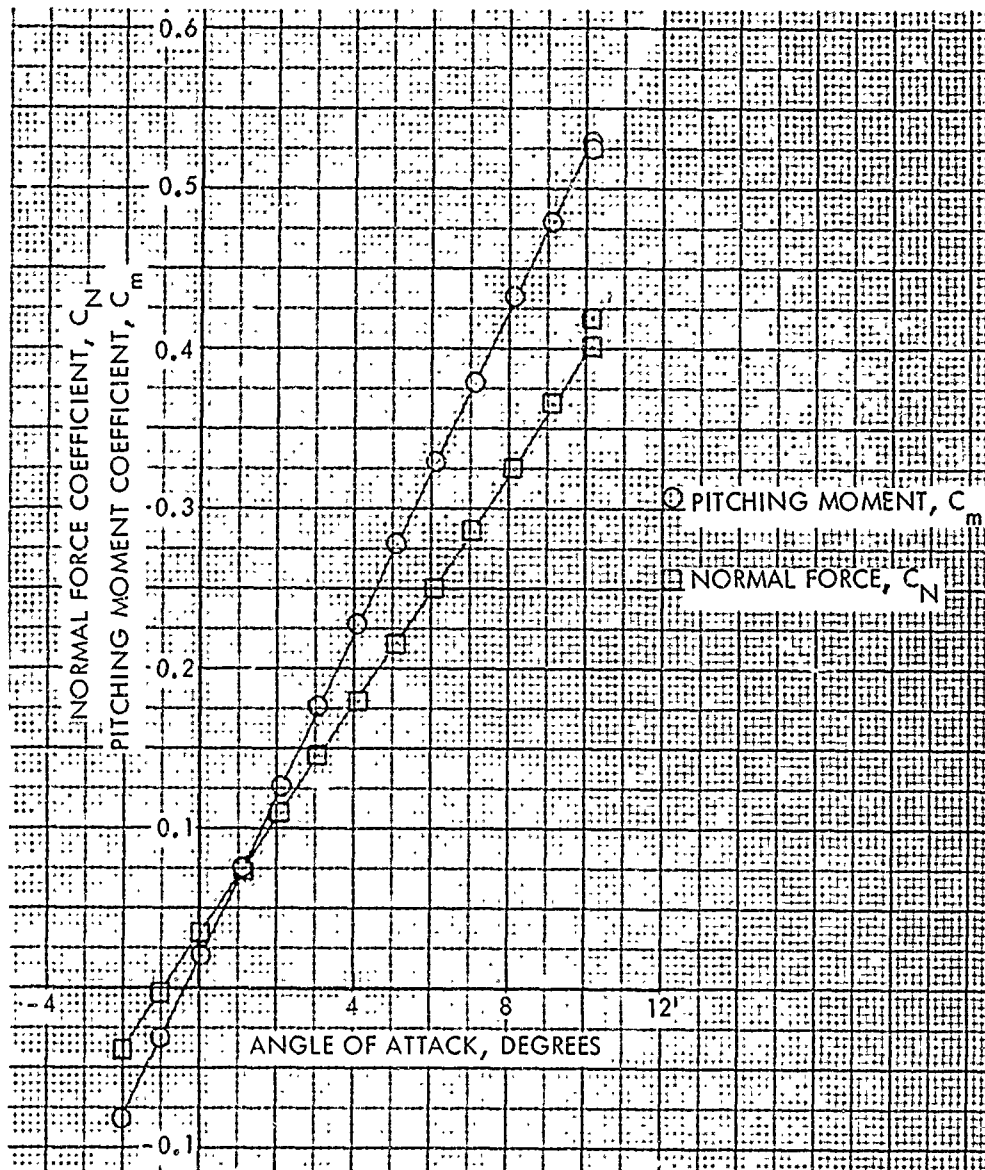
FIG. 10 NORMAL FORCE AND PITCHING MOMENT COEFFICIENTS VERSUS ANGLE OF ATTACK AT
A MACH NUMBER OF 0.79 FOR THE BASIC CONFIGURATION
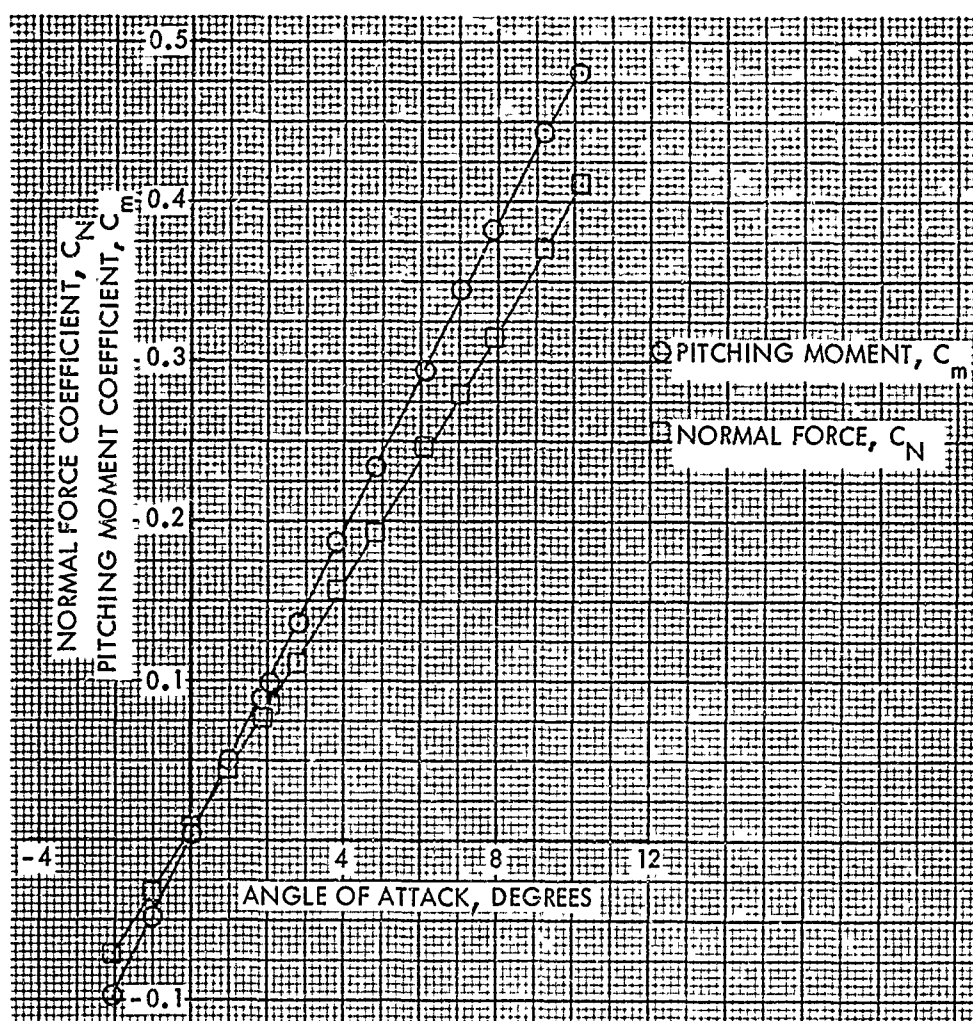
FIG. 11 NORMAL FORCE AND PITCHING MOMENT COEFFICIENTS VERSUS ANGLE OF ATTACK AT
A MACH NUMBER OF 0.90 FOR THE BASIC CONFIGURATION

49
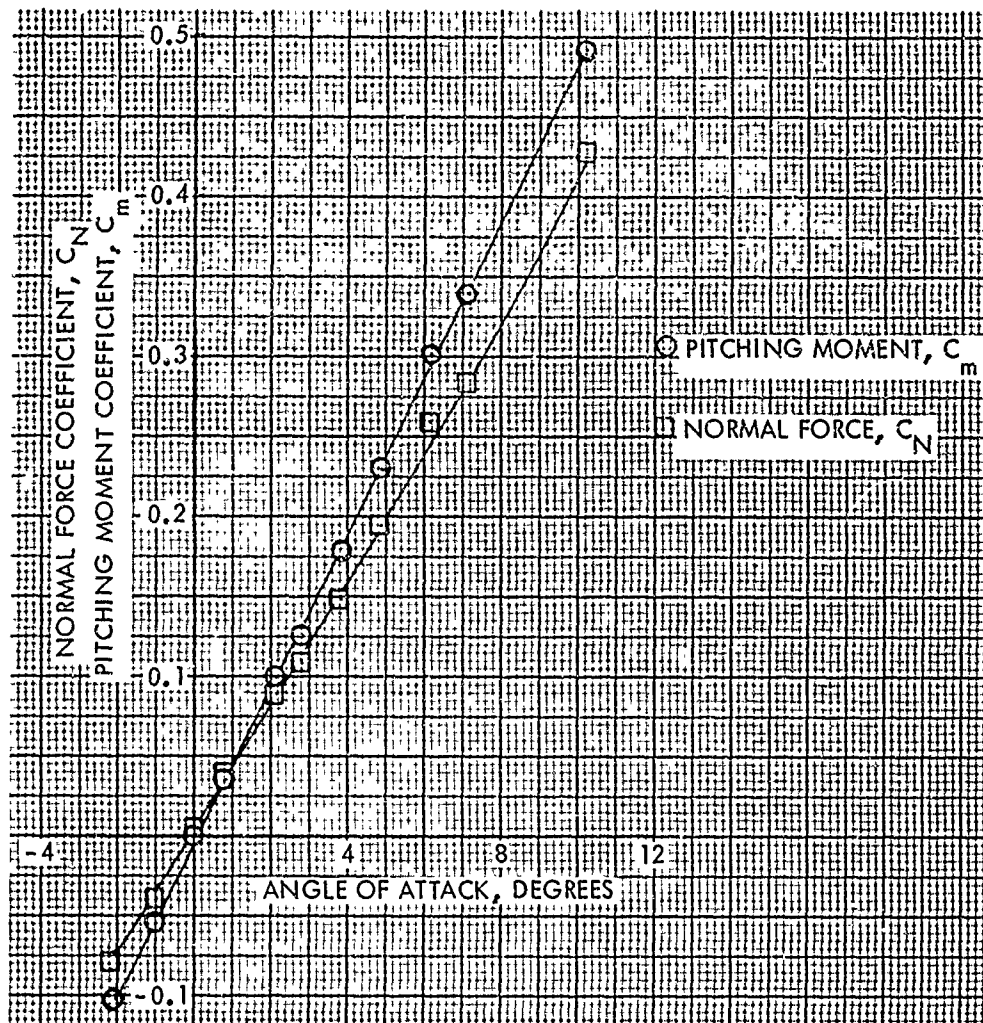
FIG. 12 NORMAL FORCE AND PITCHING MOMENT COEFFICIENTS VERSUS ANGLE OF ATTACK AT
A MACH NUMBER OF 0.93 FOR THE BASIC CONFIGURATION
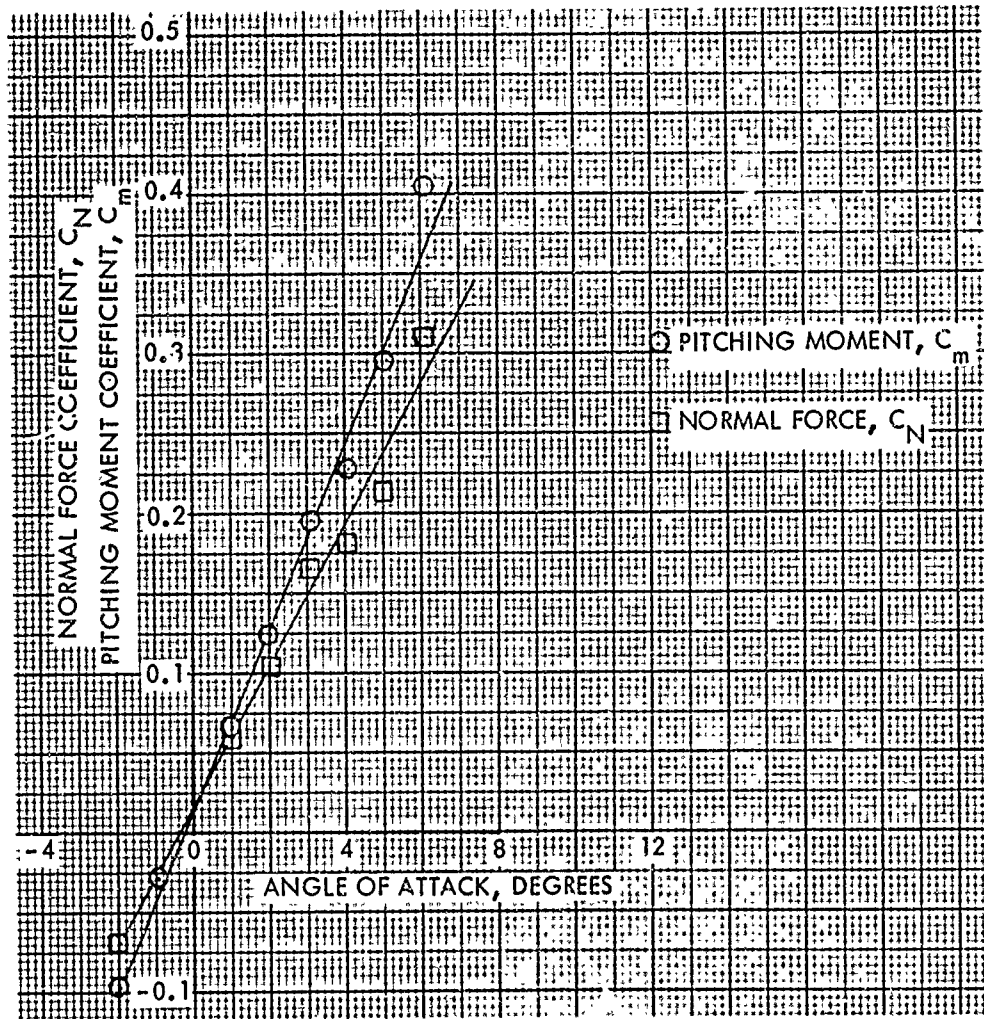
FIG. 13 NORMAL FORCE AND PITCHING MOMENT COEFFICIENTS VERSUS ANGLE OF ATTACK AT A MACH NUMBER OF 1.05 FOR THE BASIC CONFIGURATION

51
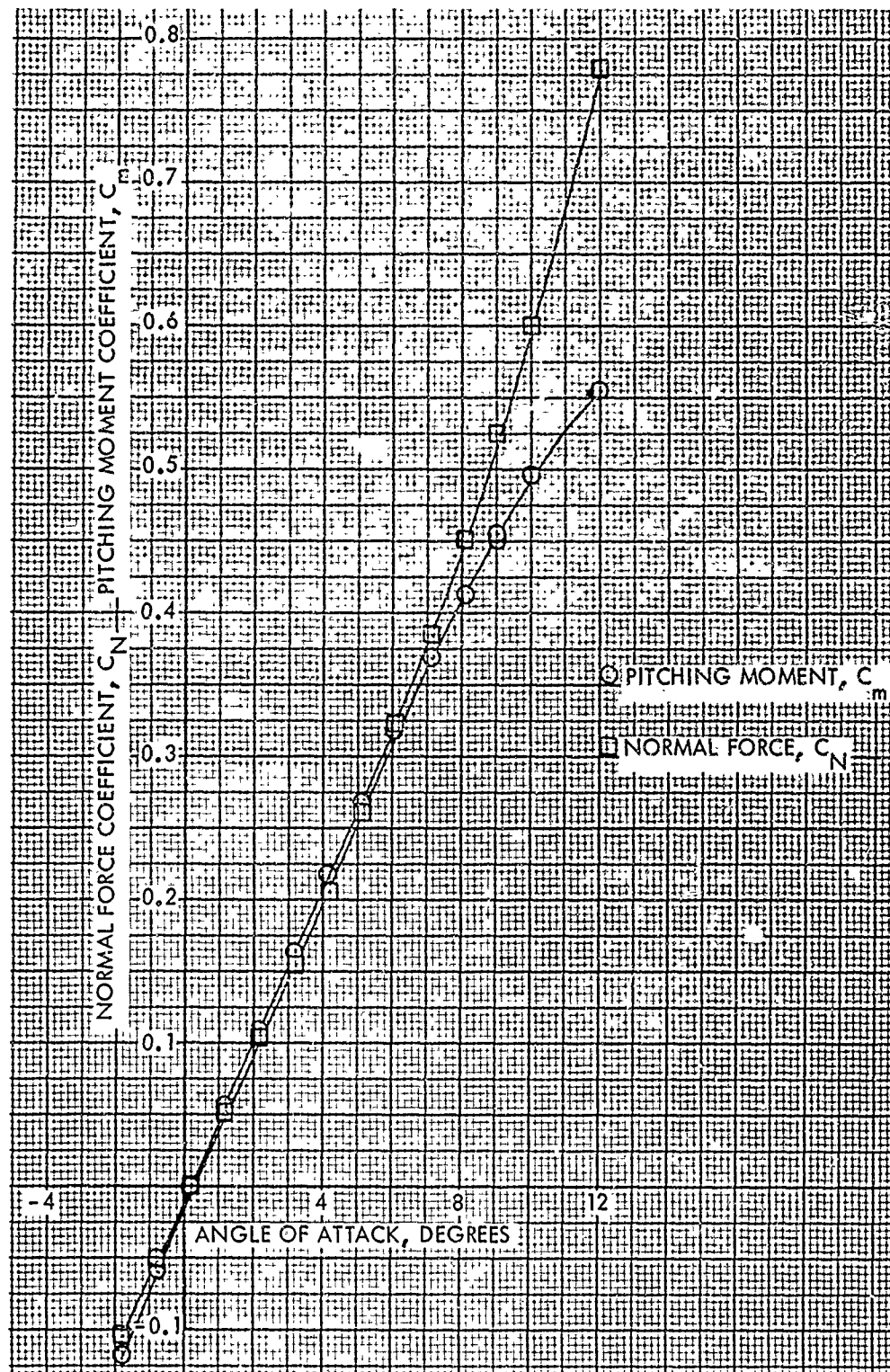
FIG. 14 NORMAL FORCE AND PITCHING MOMENT COEFFICIENTS VERSUS ANGLE OF ATTACK
A MACH NUMBER OF 1.76 FOR THE BASIC CONFIGURATION
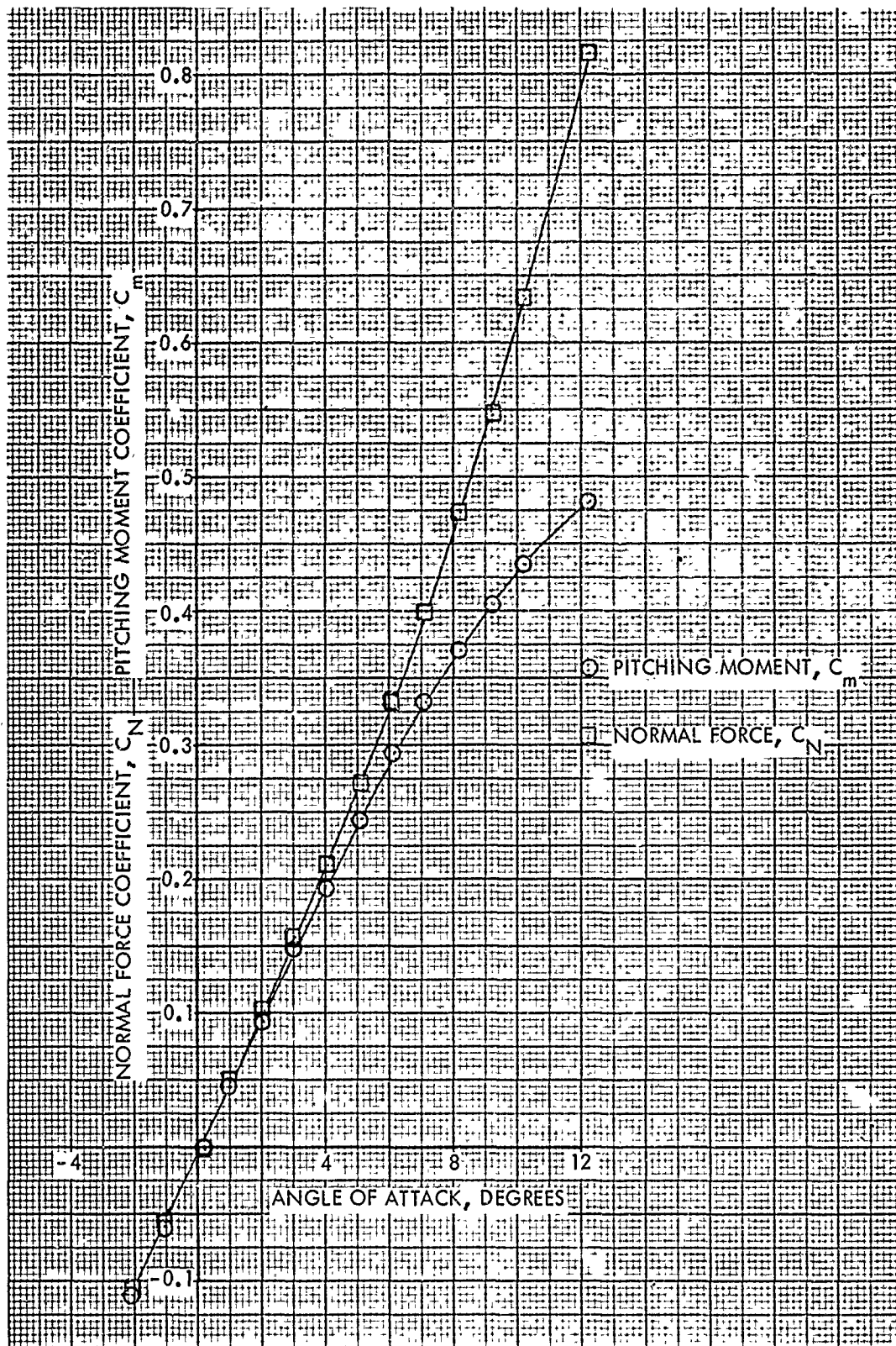
FIG. 15 NORMAL FORCE AND PITCHING MOMENT COEFFICIENTS VERSUS ANGLE OF ATTACK A MACH NUMBER OF 2.0 FOR THE BASIC CONFIGURATION

53
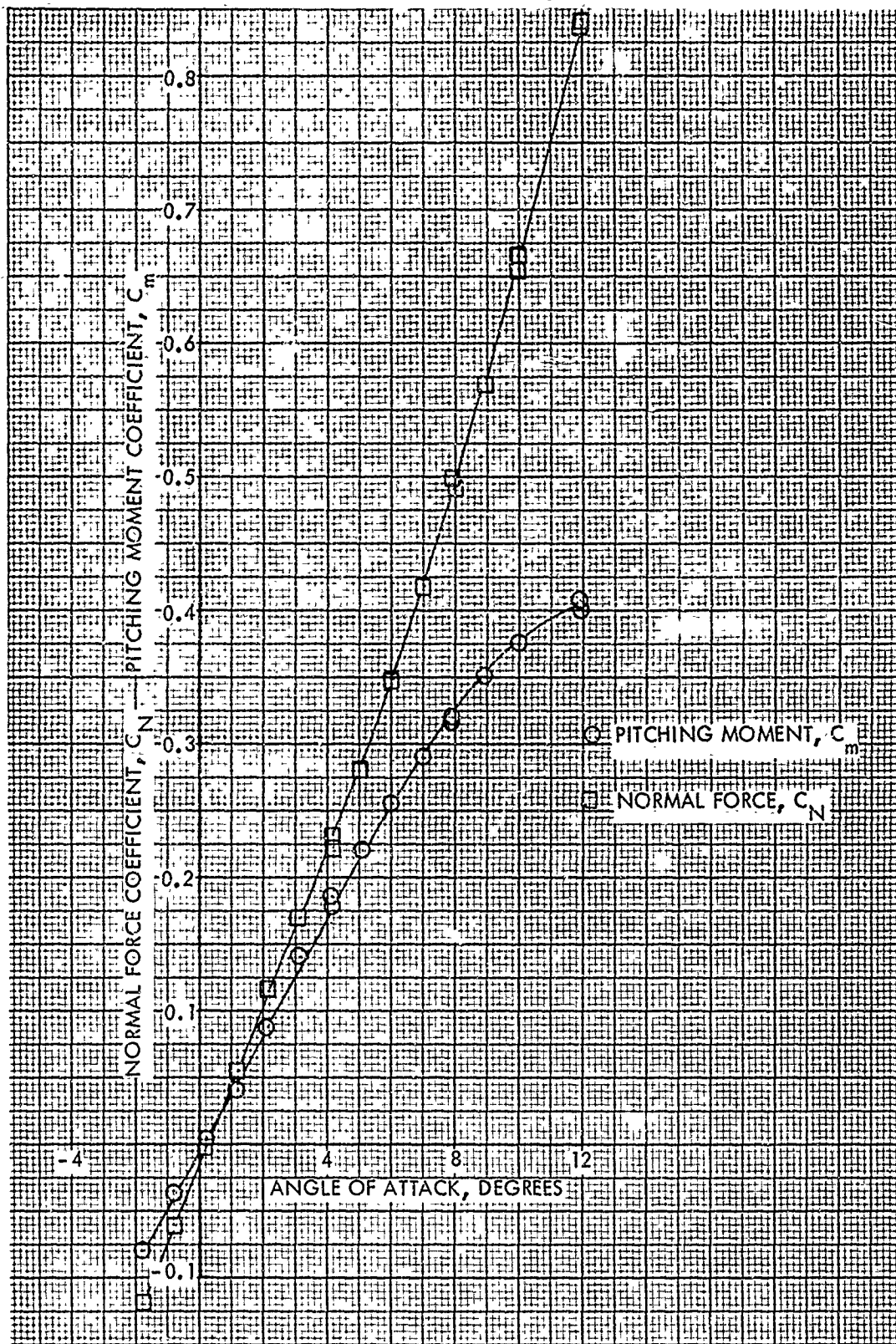
FIG. 16 NORMAL FORCE AND PITCHING MOMENT COEFFICIENTS VERSUS ANGLE OF ATTACK AT A MACH NUMBER OF 2.5 FOR THE BASIC CONFIGURATION
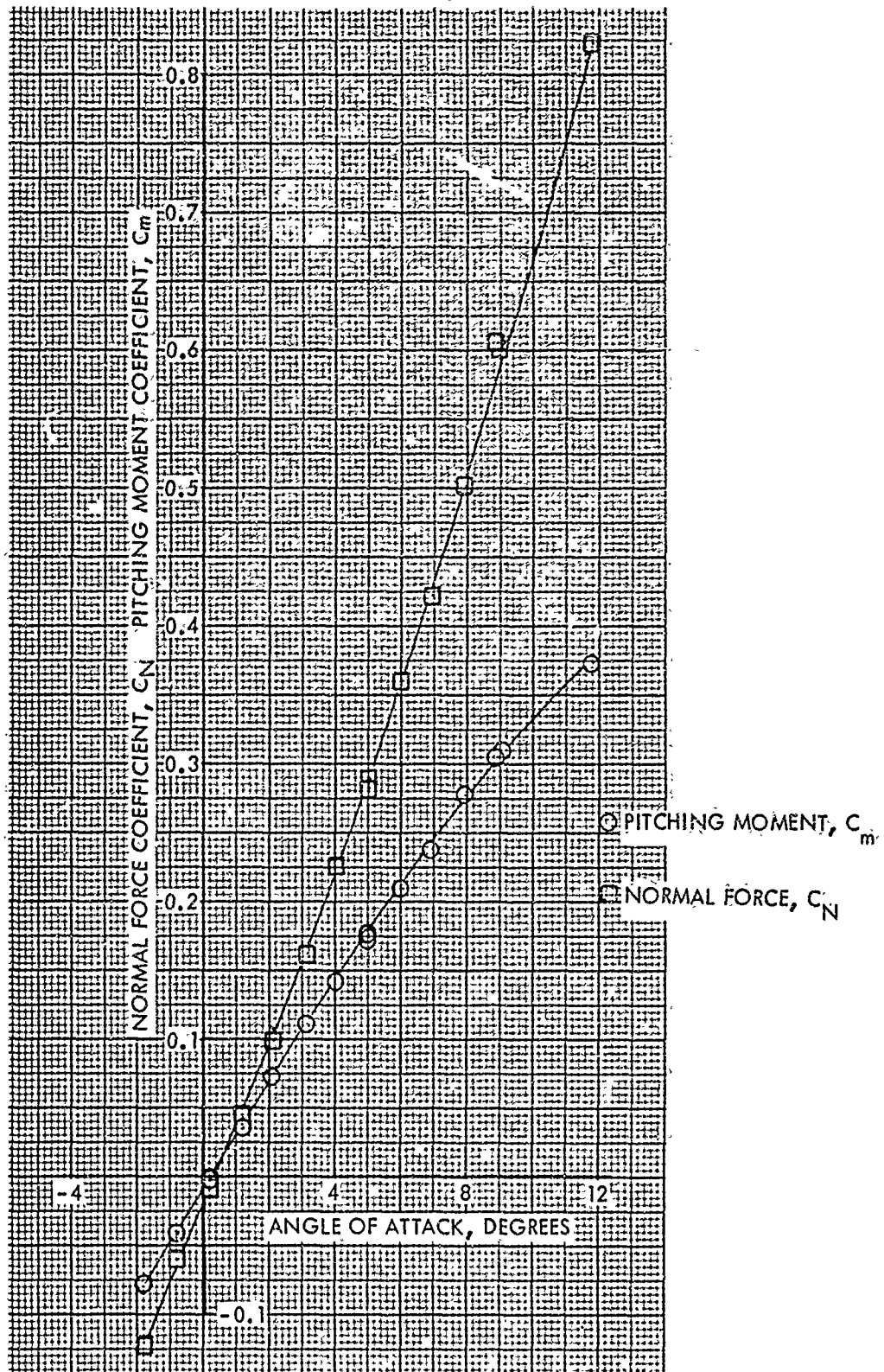
FIG. 17 NORMAL FORCE AND PITCHING MOMENT COEFFICIENTS VERSUS ANGLE OF ATTACK AT
A MACH NUMBER OF 3.0 FOR THE BASIC CONFIGURATION
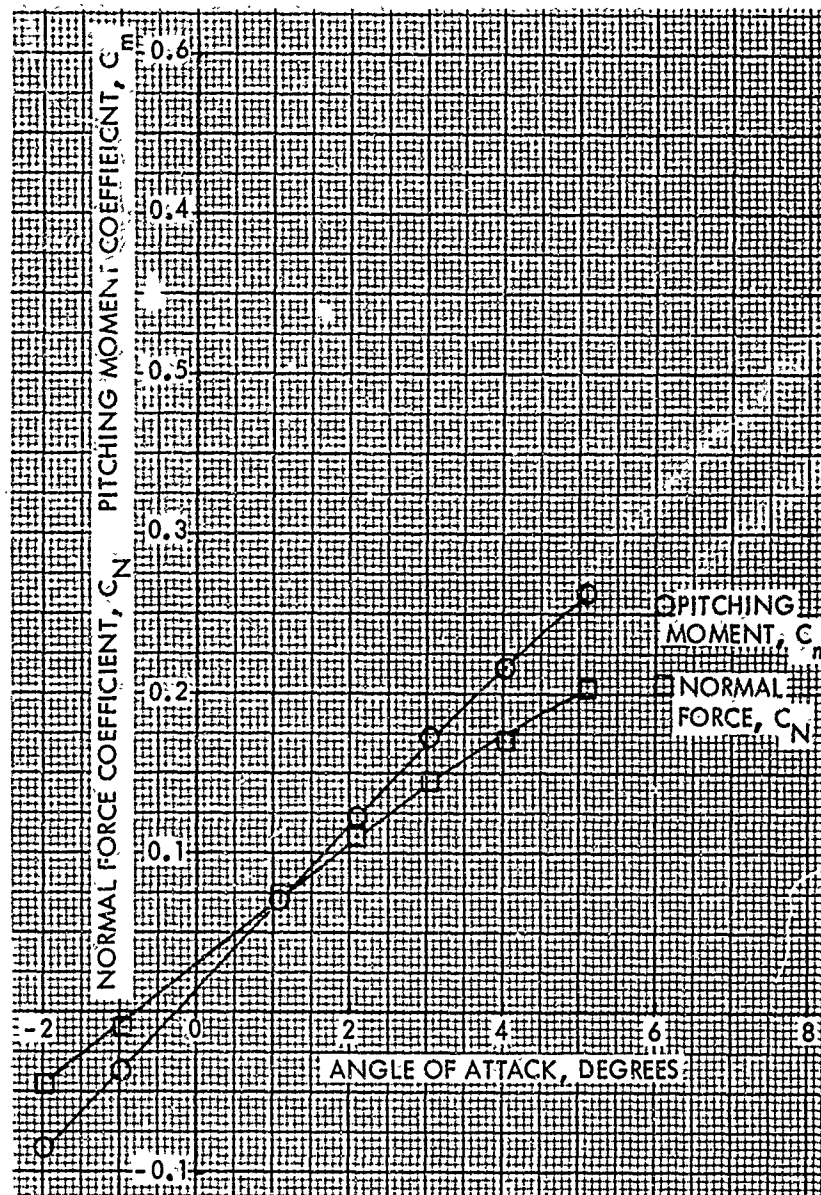
FIG. 18 NORMAL FORCE AND PITCHING MOMENT COEFFICIENT VERSUS ANGLE OF ATTACK AT
A MACH NUMBER OF 0.80 FOR THE SMOOTH CONFIGURATION
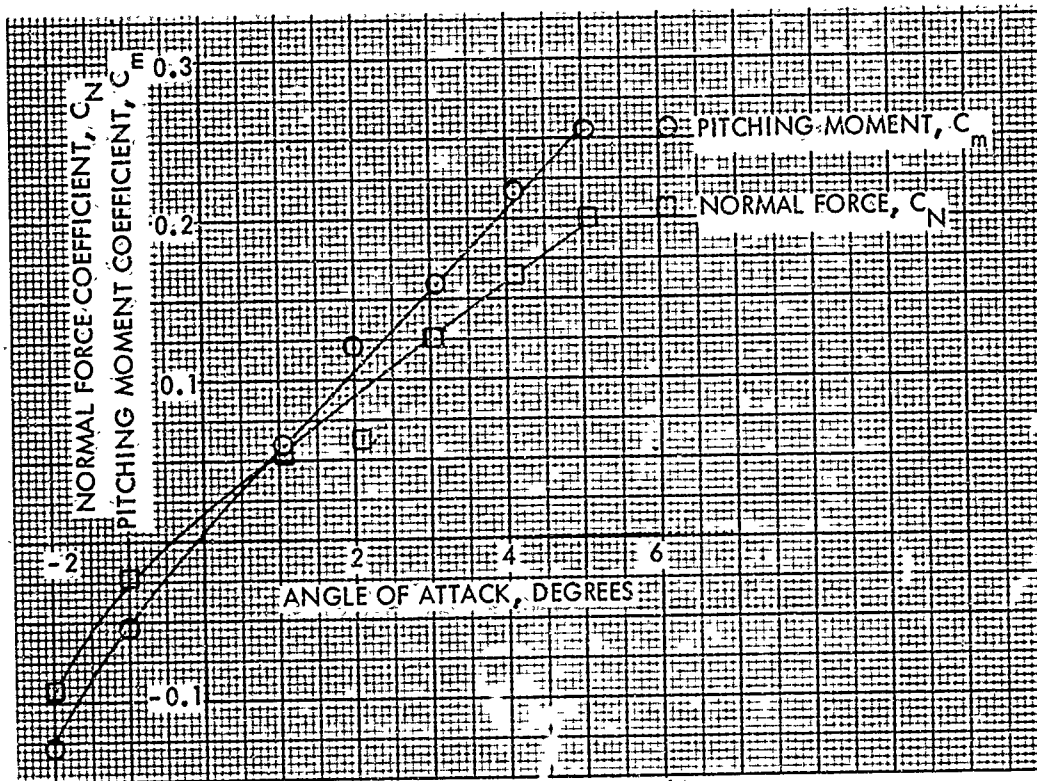
FIG. 19 NORMAL FORCE AND PITCHING MOMENT COEFFICIENTS VERSUS ANGLE OF ATTACK AT A MACH NUMBER OF 0.95 FOR THE SMOOTH CONFIGURATION

59
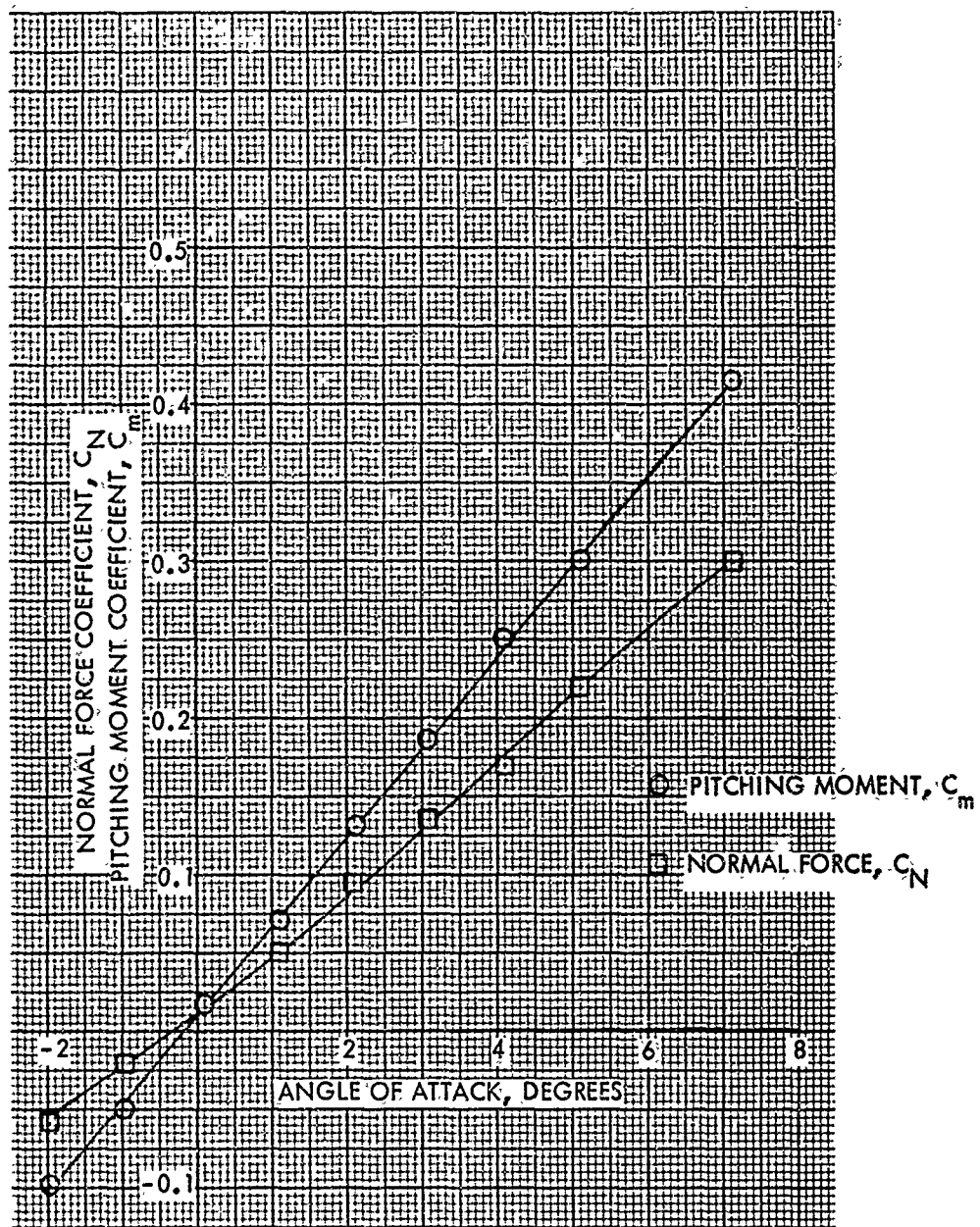
FIG. 20 NORMAL FORCE AND PITCHING MOMENT COEFFICIENTS VERSUS ANGLE OF ATTACK AT
A MACH NUMBER OF 1.05 FOR THE SMOOTH CONFIGURATION
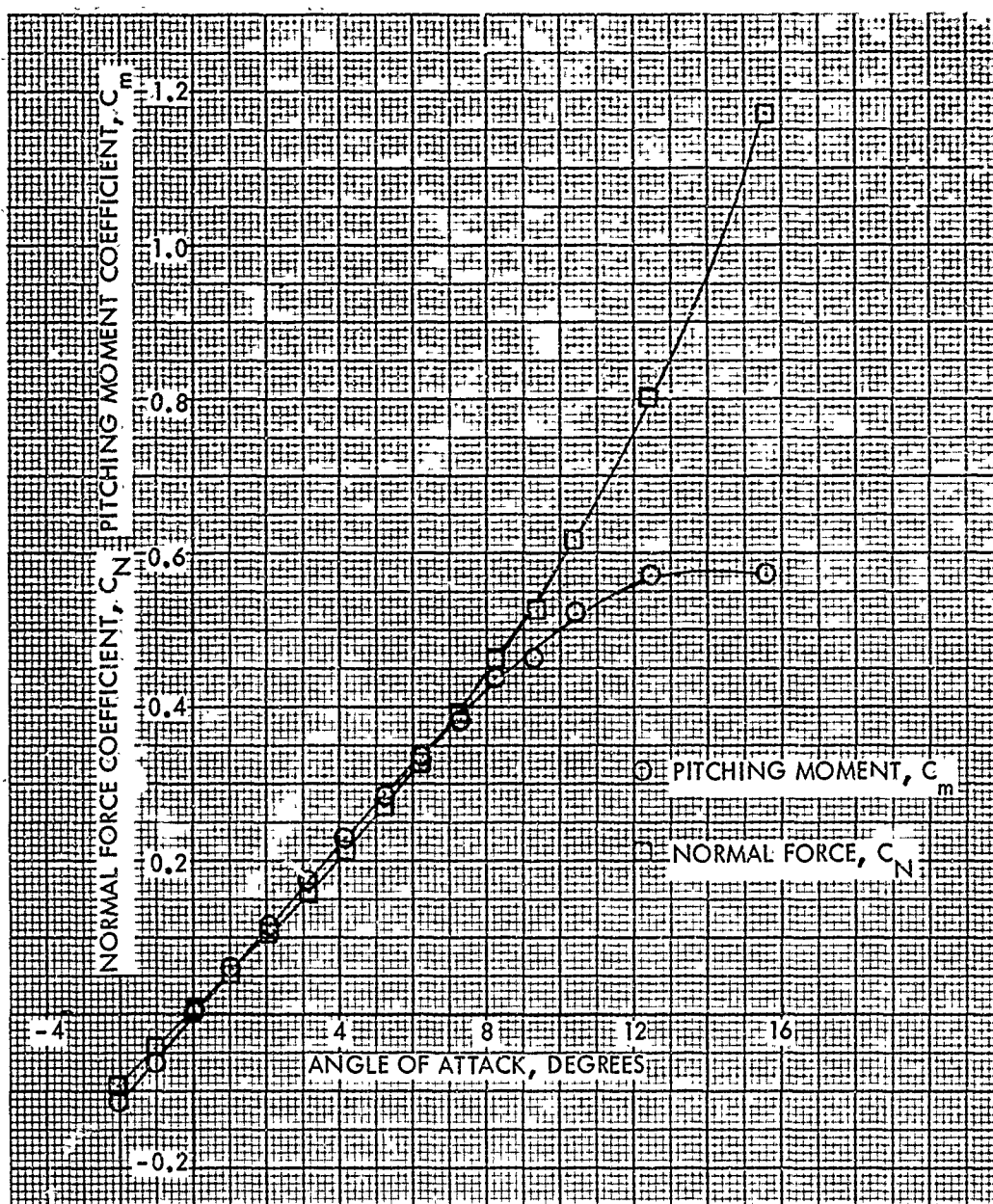
FIG. 21 NORMAL FORCE AND PITCHING MOMENT COEFFICIENTS VERSUS ANGLE OF ATTACK AT A MACH NUMBER OF 1.76 FOR THE SMOOTH CONFIGURATION

61
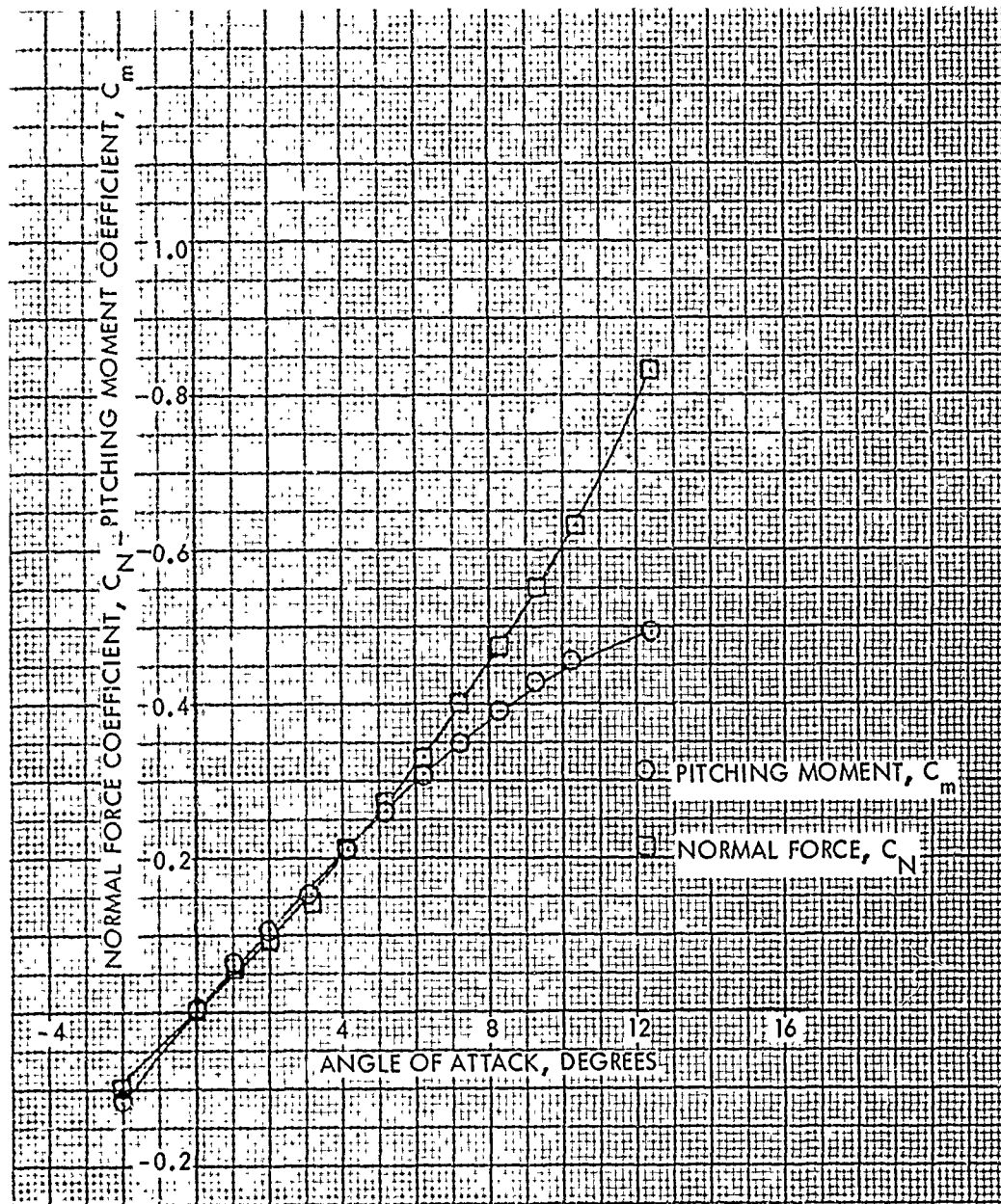
FIG. 22 NORMAL FORCE AND PITCHING MOMENT COEFFICIENTS VERSUS ANGLE OF ATTACK AT
A MACH NUMBER OF 2.0 FOR THE SMOOTH CONFIGURATION

FIG. 23 NORMAL FORCE AND PITCHING MOMENT COEFFICIENTS VERSUS ANGLE OF ATTACK AT
A MACH NUMBER OF 2.5 FOR THE SMOOTH CONFIGURATION

63

FIG. 24 NORMAL FORCE AND PITCHING MOMENT COEFFICIENTS VERSUS ANGLE OF ATTACK AT A MACH NUMBER OF 3.00 FOR THE SMOOTH CONFIGURATION
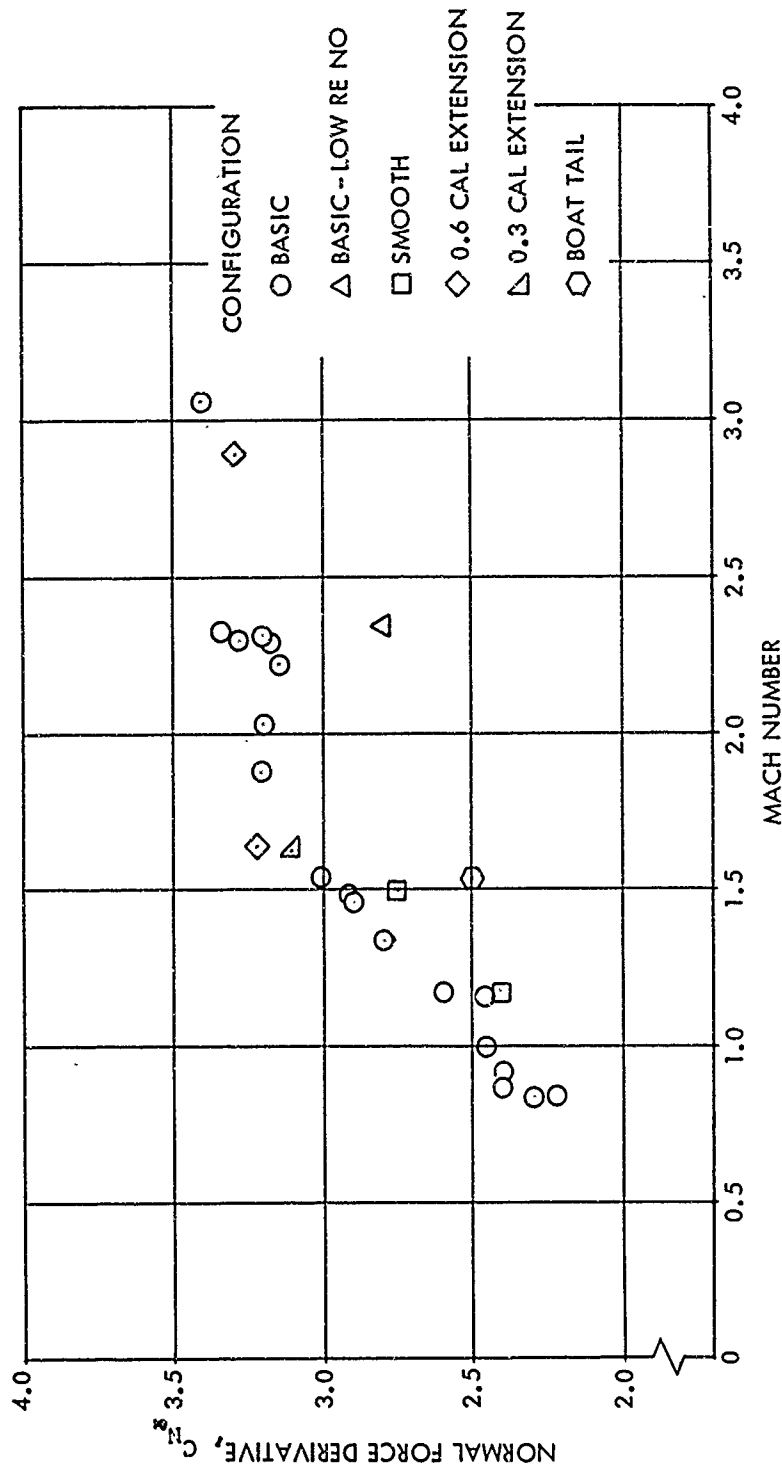
FIG. 25 NORMAL FORCE DERIVATIVE VERSUS MACH NUMBER FROM BALLISTIC RANGE MEASUREMENTS
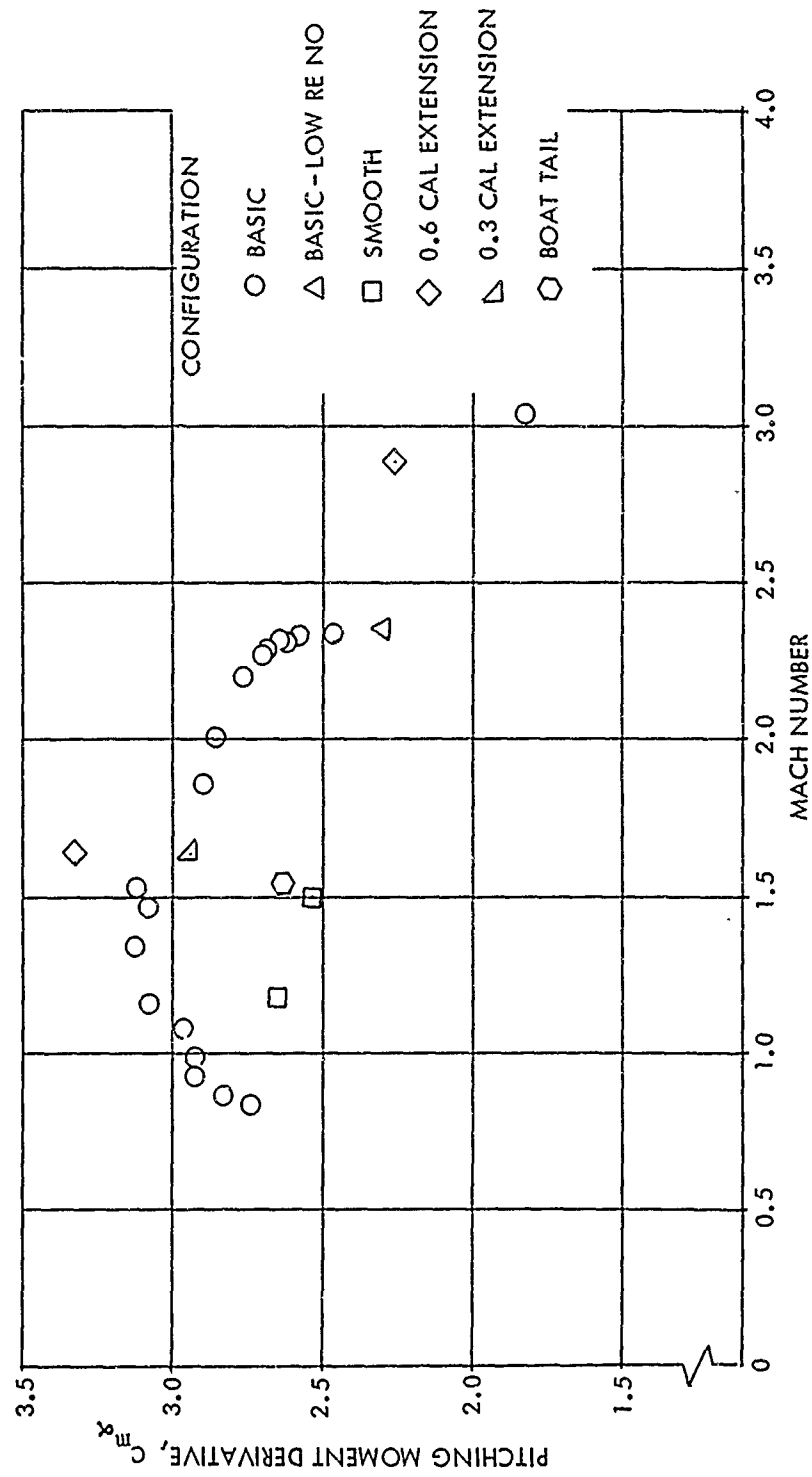
FIG. 26 PITCHING MOMENT DERIVATIVE VERSUS MACH NUMBER FROM BALLISTIC RANGE MEASUREMENTS
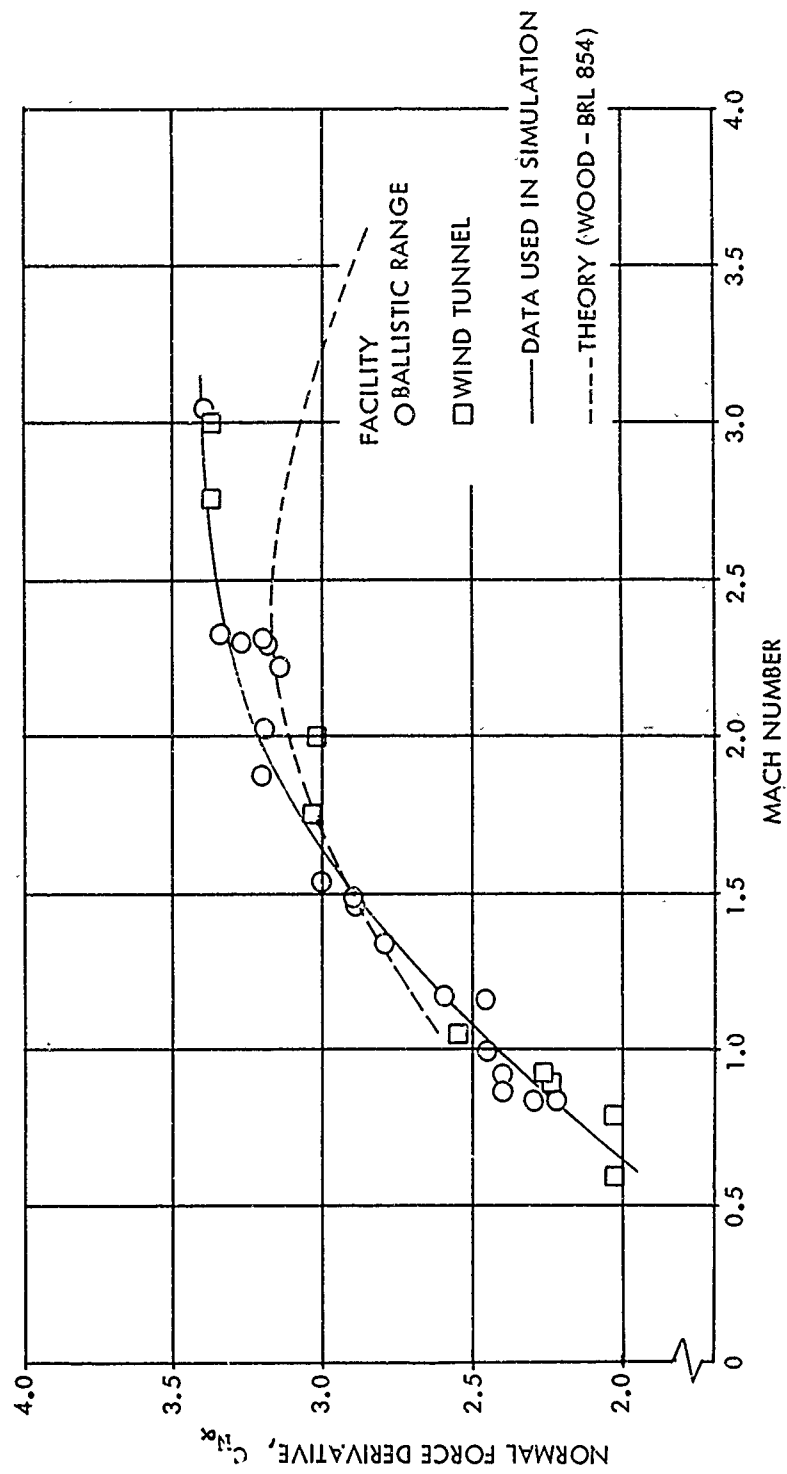
FIG. 27 NORMAL FORCE DERIVATIVE VERSUS MACH NUMBER FROM BALLISTIC RANGE AND WIND TUNNEL MEASUREMENTS FOR THE BASIC CONFIGURATION
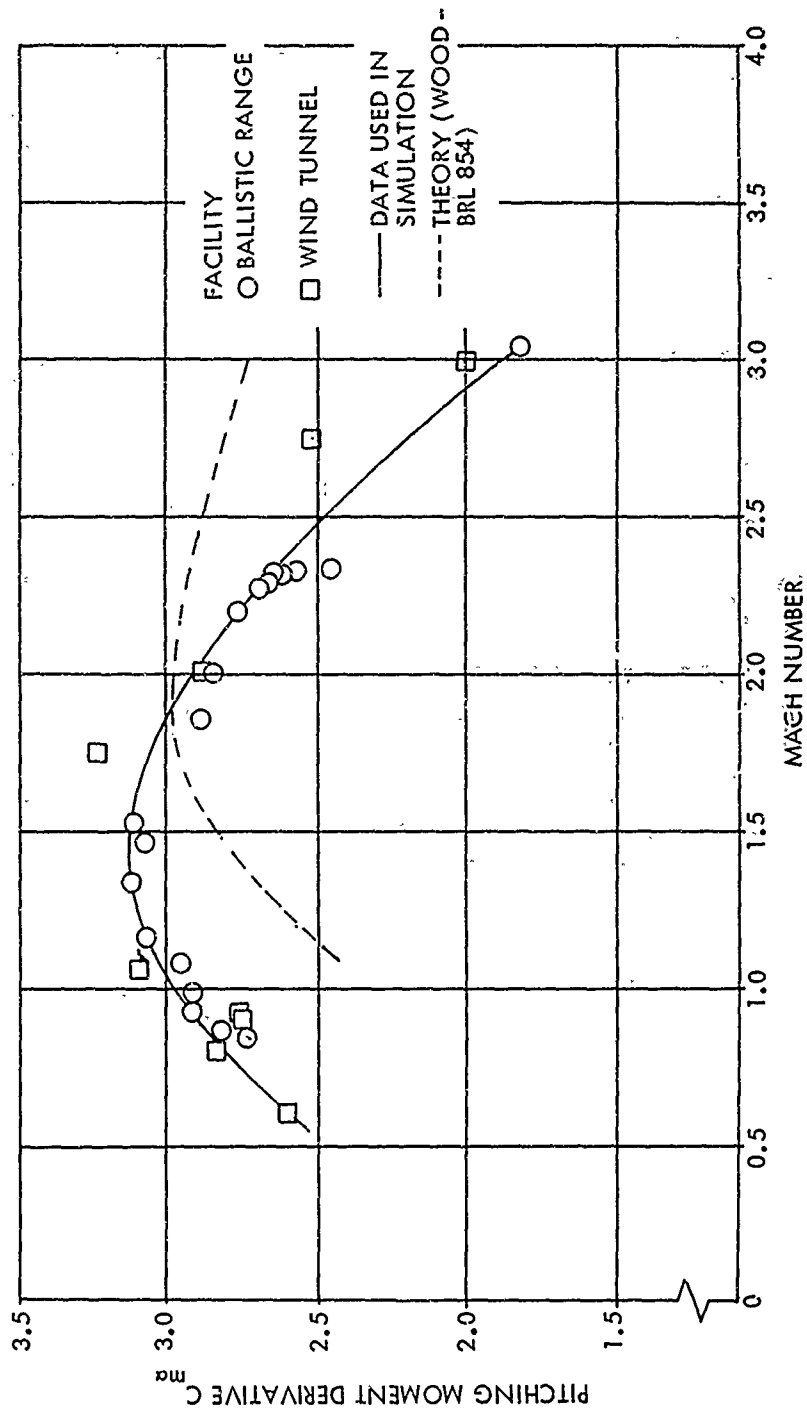
FIG. 28 PITCHING MOMENT DERIVATIVE VERSUS MACH NUMBER FROM BALLISTIC RANGE AND WIND TUNNEL MEASUREMENTS FOR THE BASIC CONFIGURATION
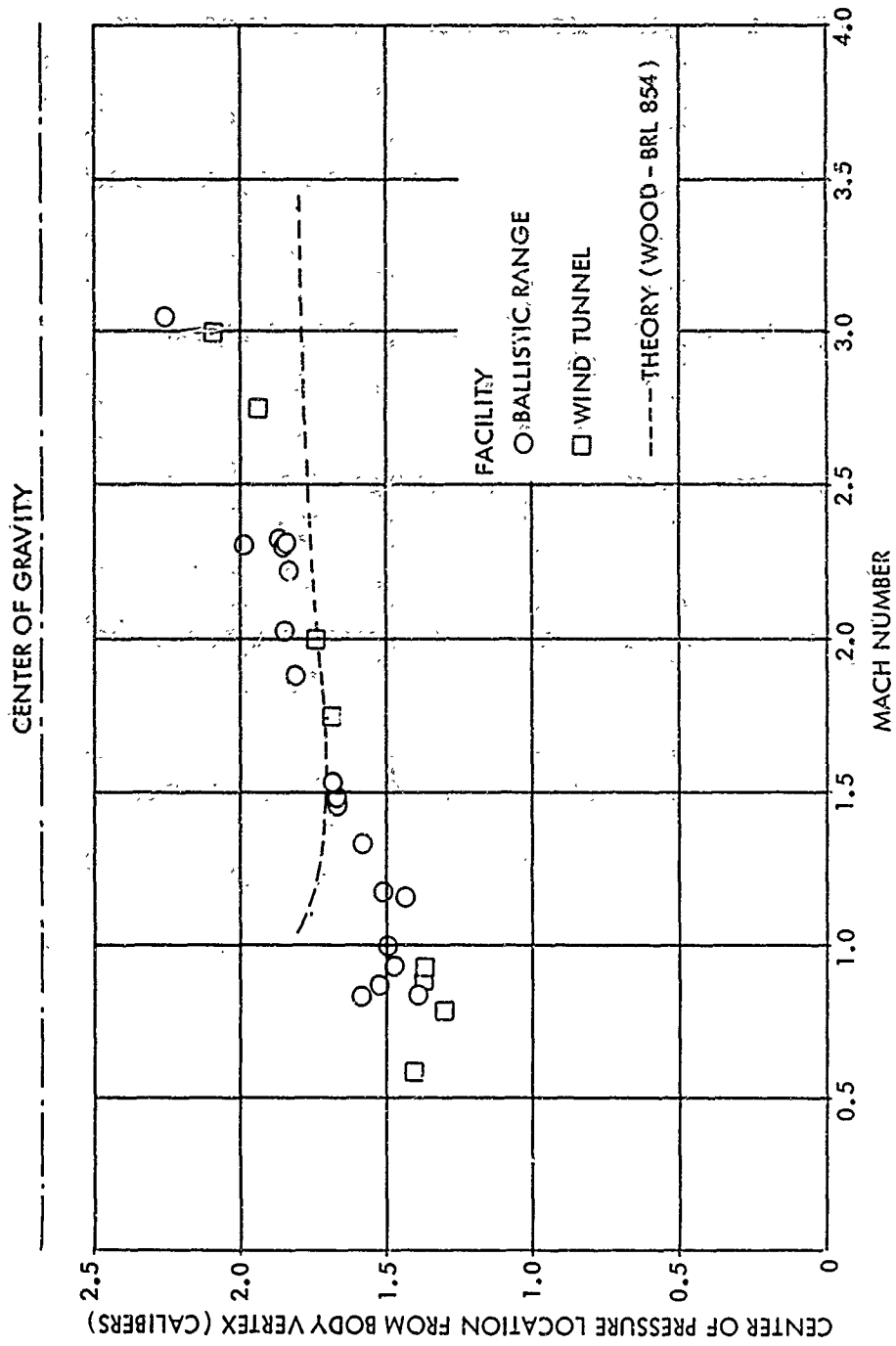
FIG. 29 CENTER OF PRESSURE FROM BODY VERTEX VERSUS MACH NUMBER FROM BALLISTIC RANGE AND WIND TUNNEL MEASUREMENTS FOR THE BASIC CONFIGURATION
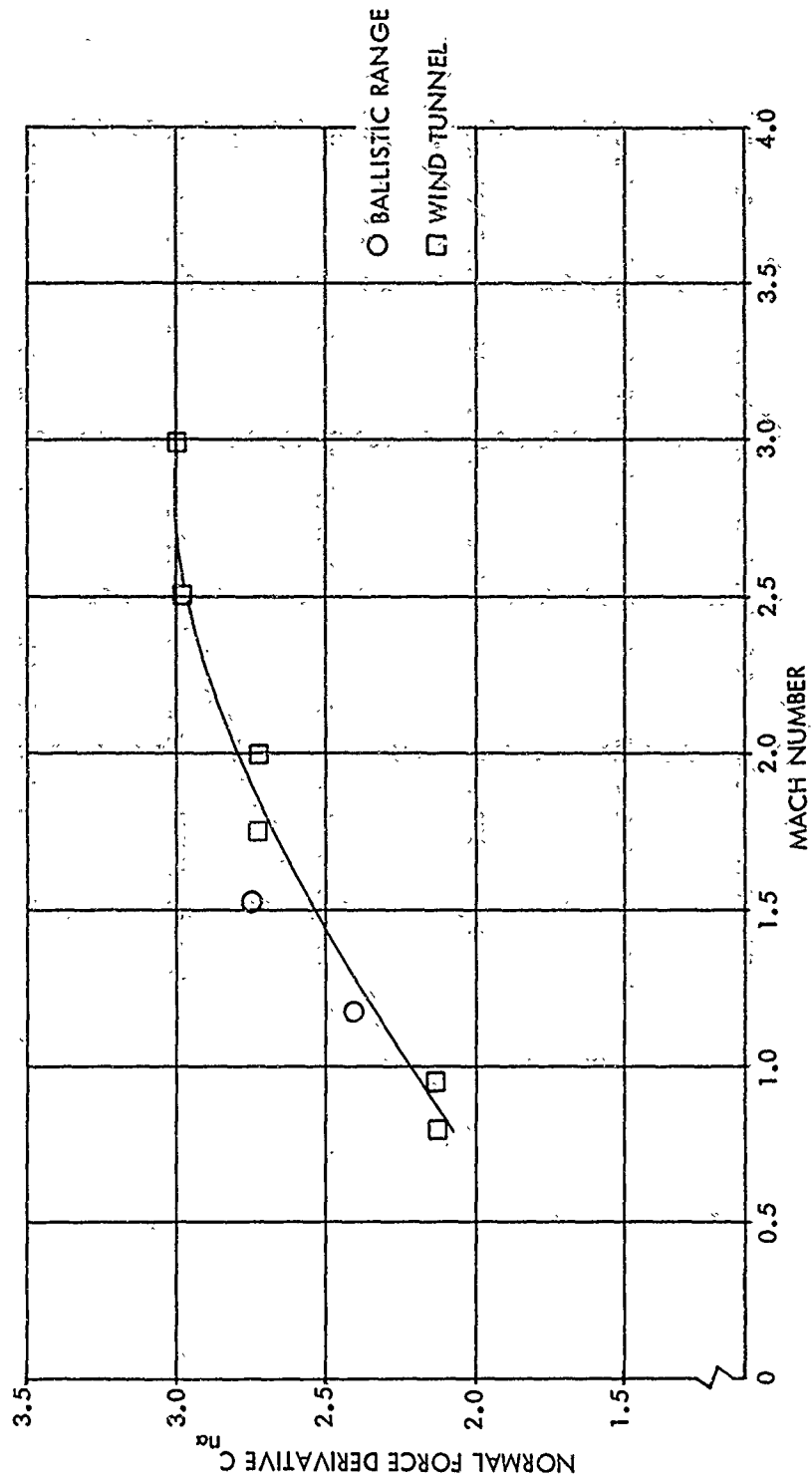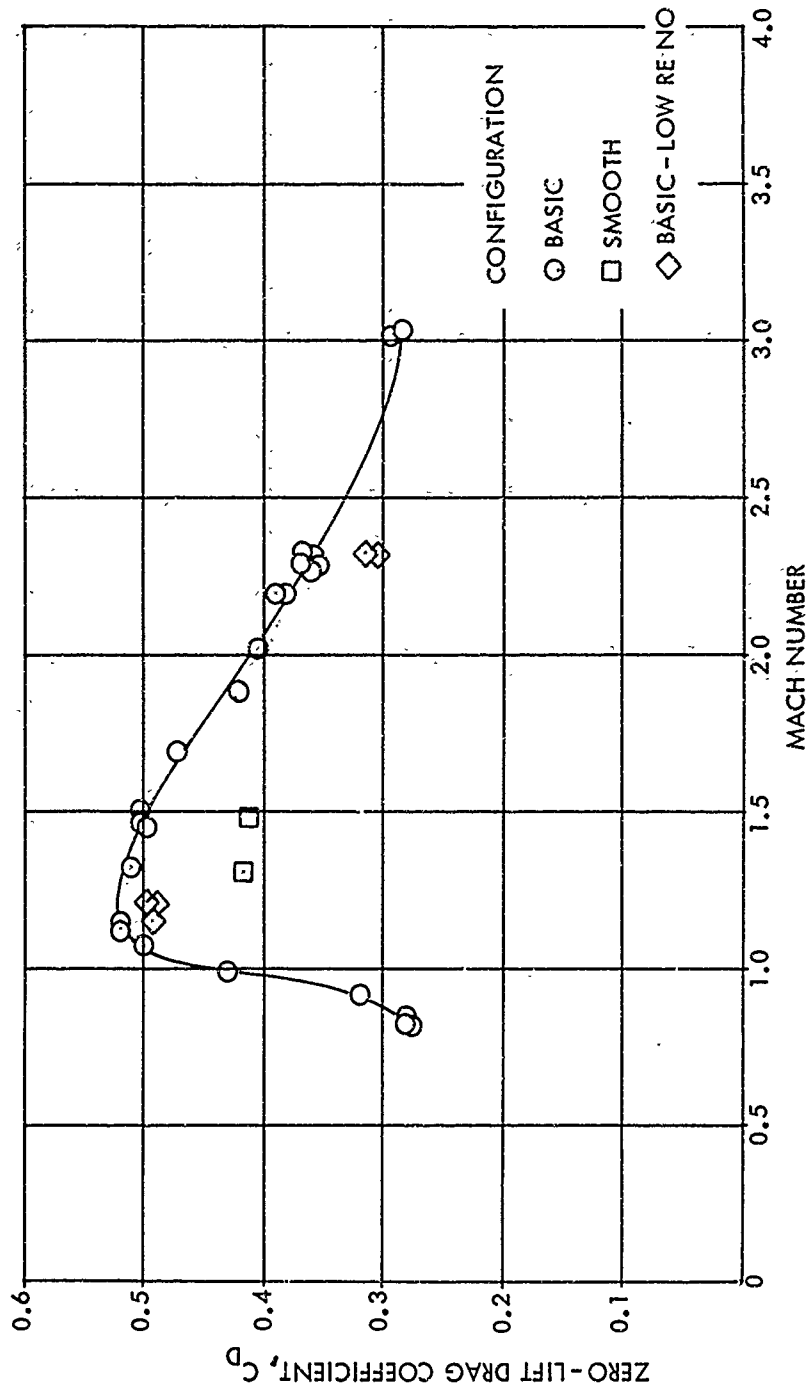
FIG. 30 NORMAL FORCE DERIVATIVE VERSUS MACH NUMBER FROM BALLISTIC RANGE AND WIND TUNNEL MEASUREMENTS FOR THE SMOOTH CONFIGURATION
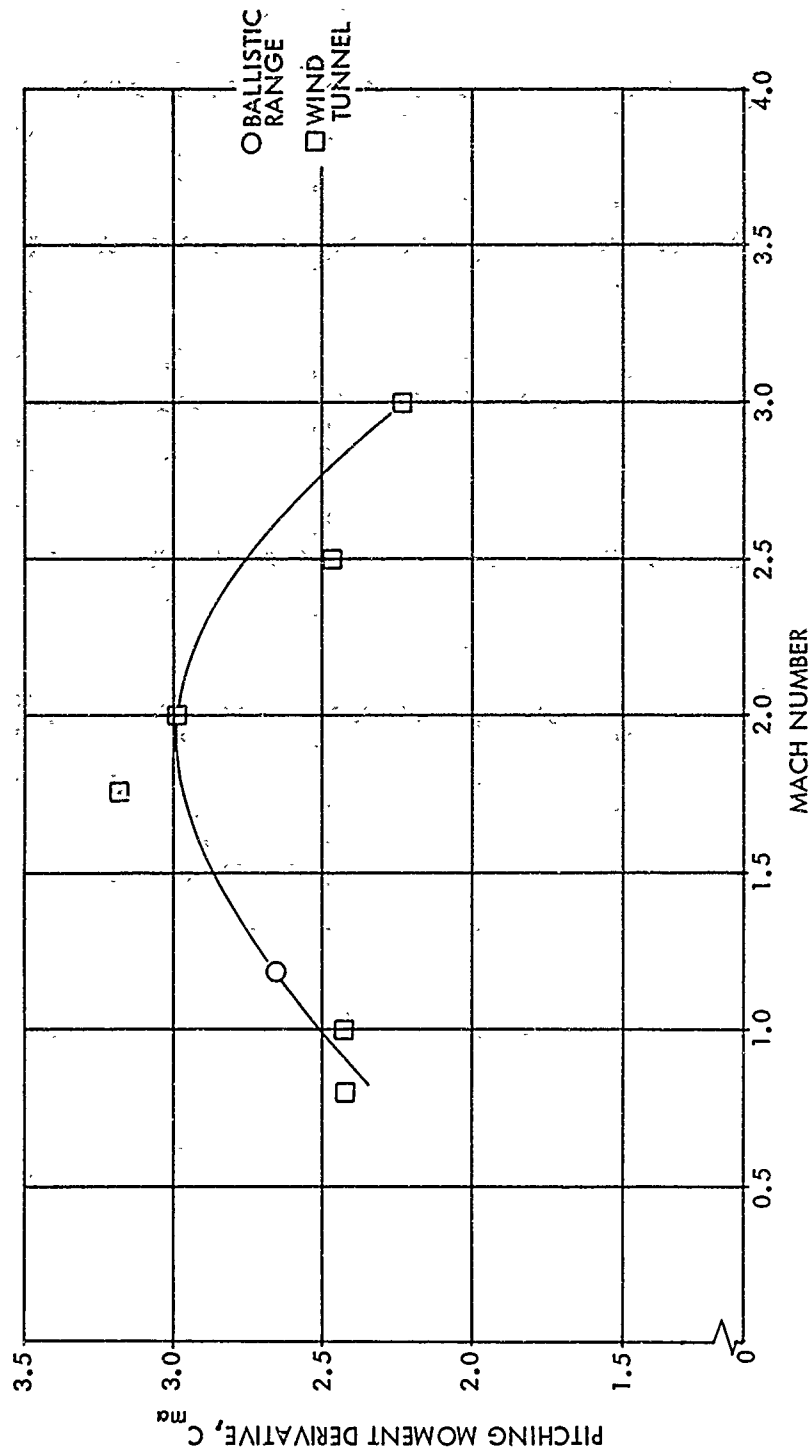
FIG. 31 PITCHING MOMENT DERIVATIVE VERSUS MACH NUMBER FROM BALLISTIC RANGE AND WIND TUNNEL MEASUREMENTS FOR THE SMOOTH CONFIGURATION

71
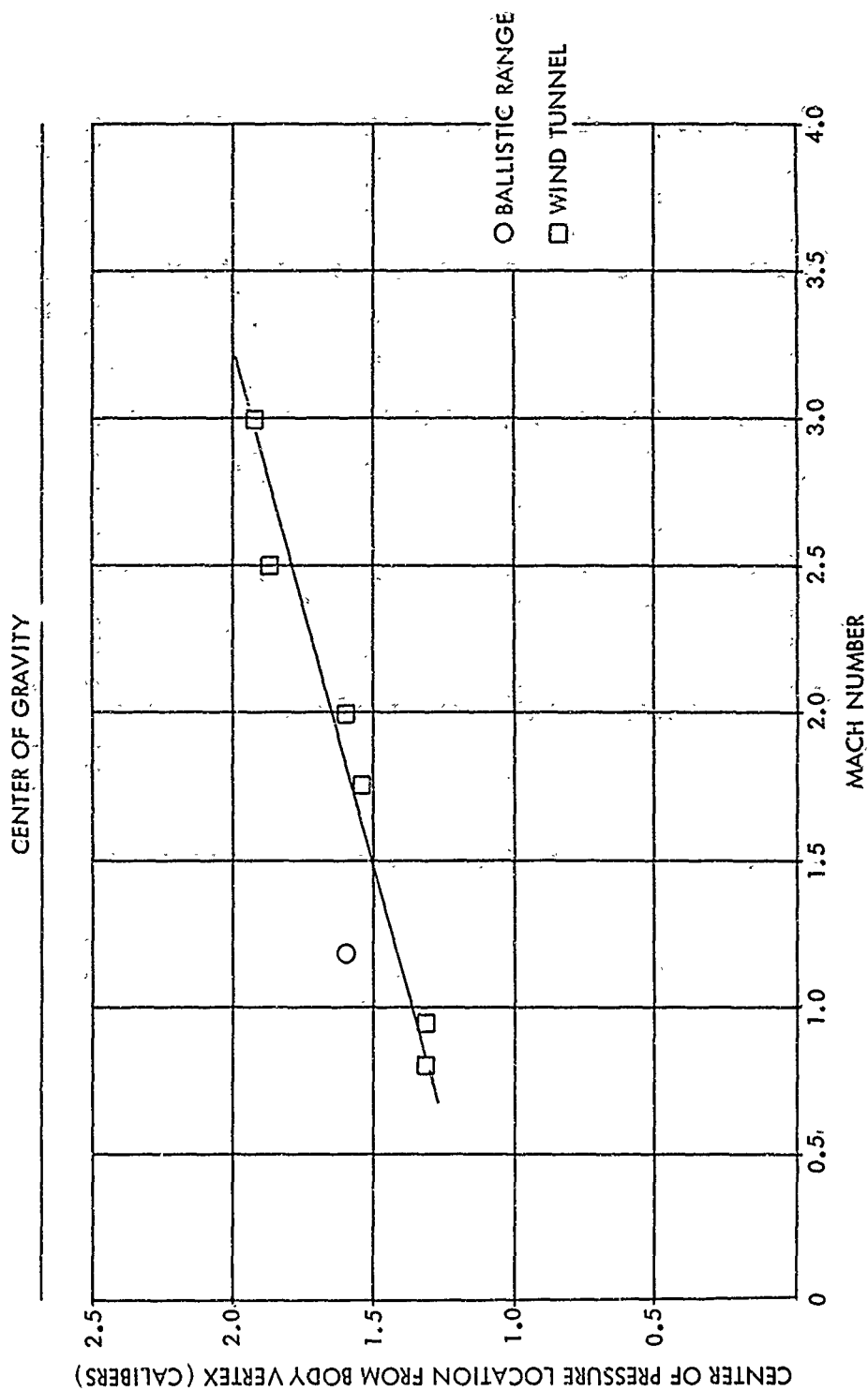
FIG. 32 CENTER OF PRESSURE LOCATION FROM BODY VERTEX VERSUS MACH NUMBER FROM BALLISTIC RANGE AND WIND TUNNEL MEASUREMENTS FOR THE SMOOTH CONFIGURATION

FIG. 33 DRAG COEFFICIENT VERSUS MACH NUMBER FROM BALLISTIC RANGE MEASUREMENTS

73
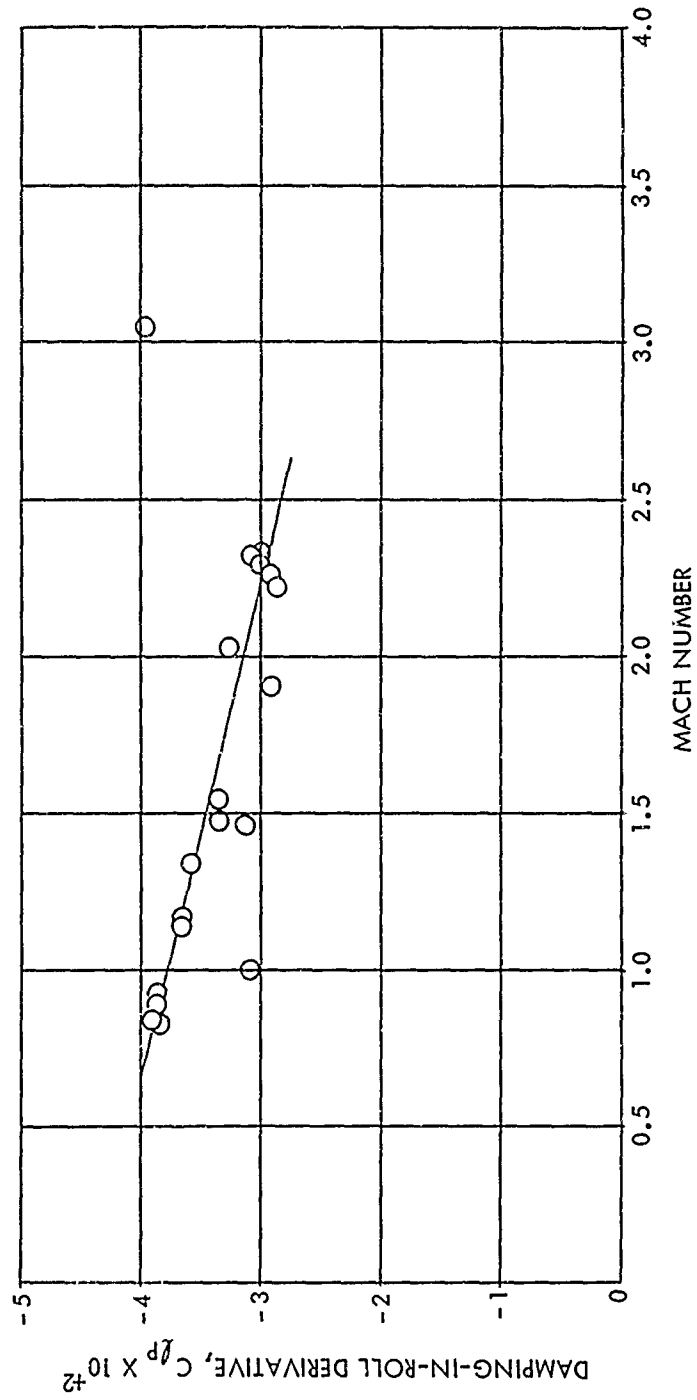
FIG. 34 DAMPING–IN ROLL DERIVATIVE VERSUS MACH NUMBER FROM BALLISTIC RANGE
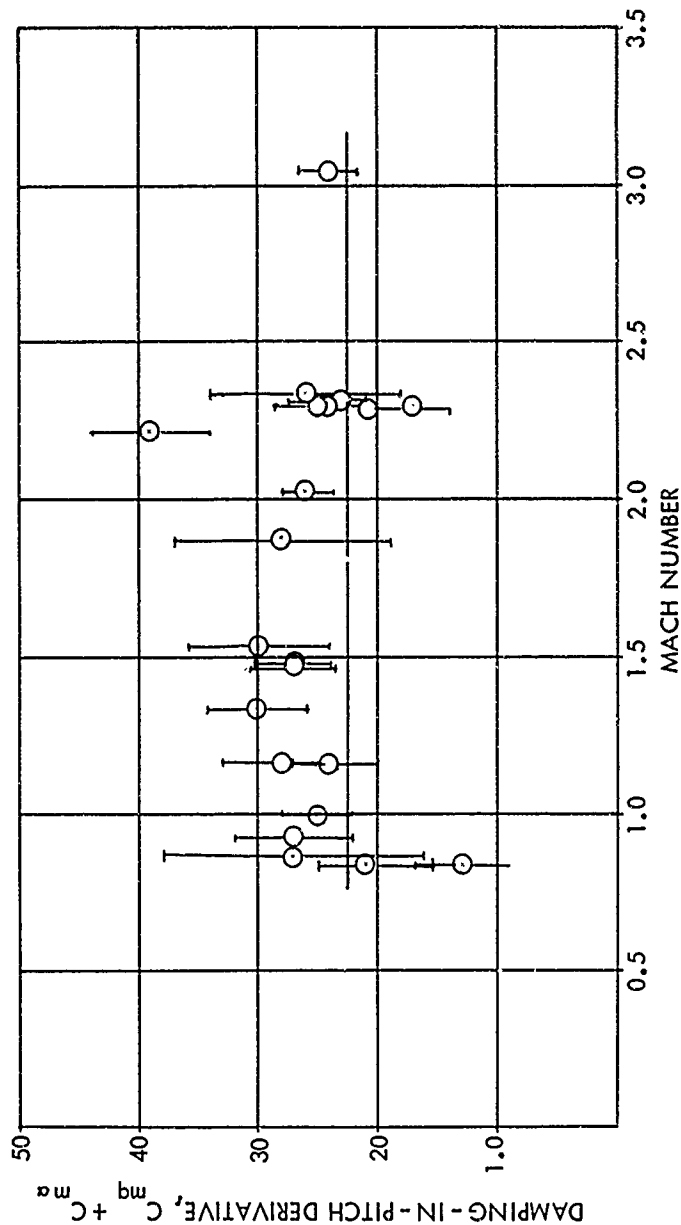MEASUREMENTS FOR THE BASIC CONFIGURATION

FIG. 35 DAMPING – IN – PITCH DERIVATIVE VERSUS MACH NUMBER FROM BALLISTIC RANGE
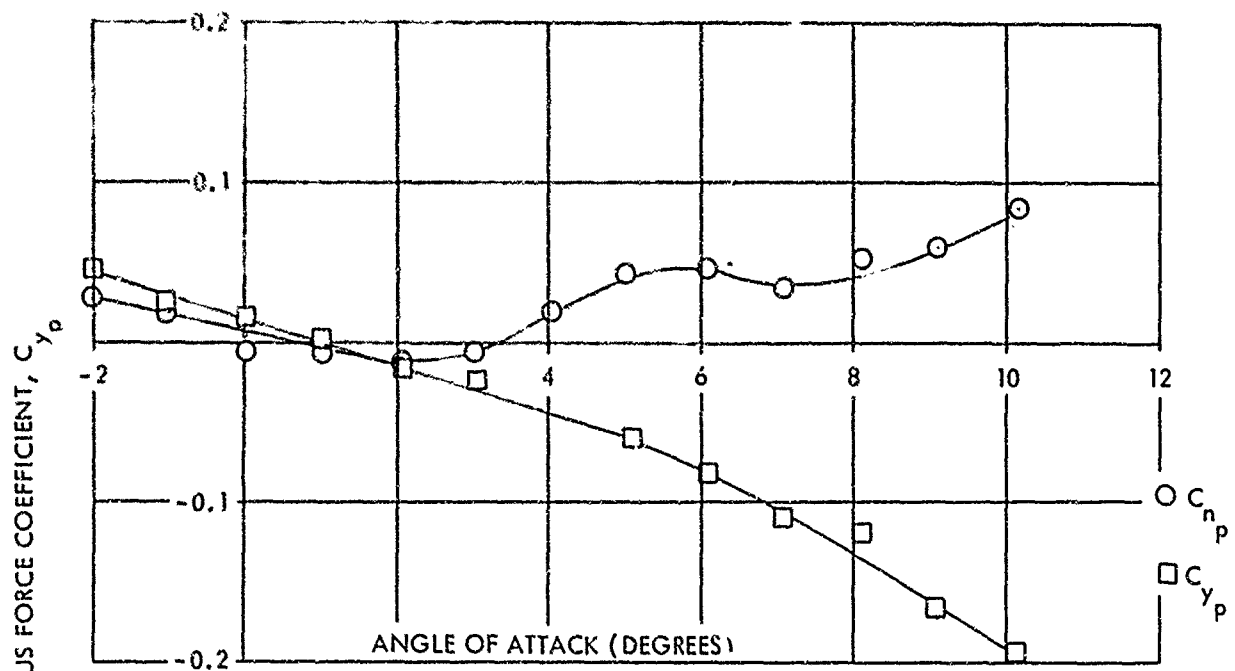MEASUREMENTS FOR THE BASIC CONFIGURATION

75

FIG. 36 MAGNUS FORCE AND MOMENT COEFFICIENTS VERSUS ANGLE OF ATTACK
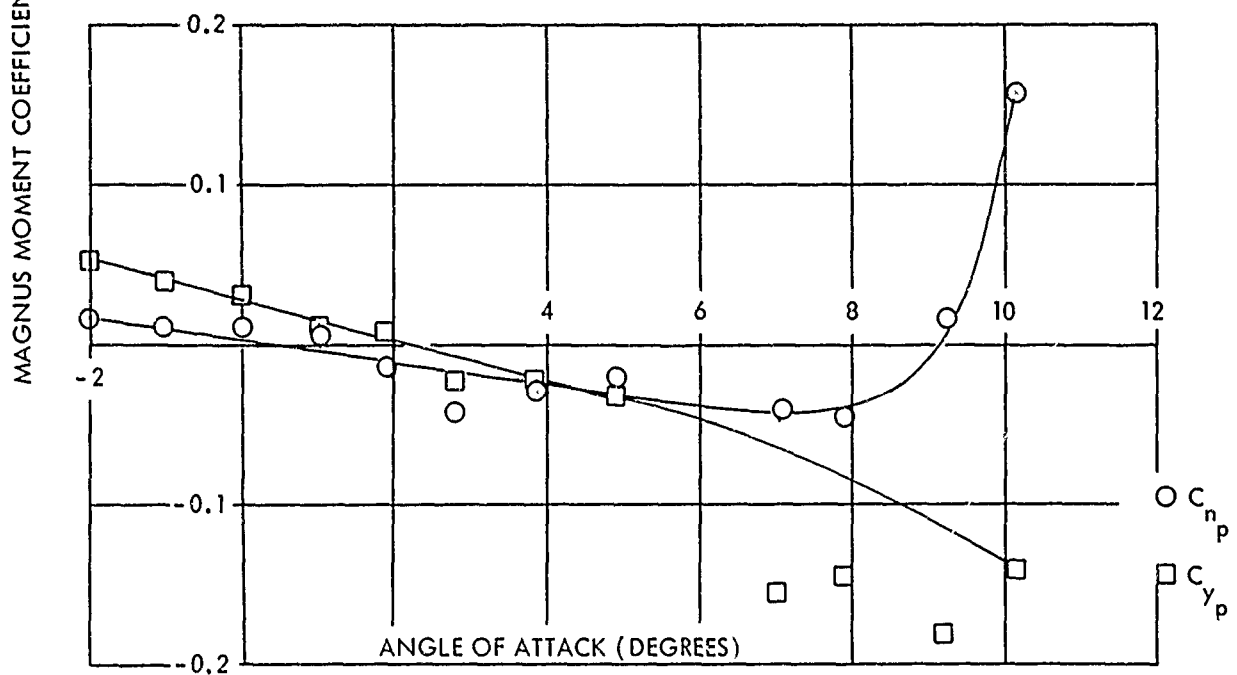AT A MACH NUMBER OF 0.8 FOR THE BASIC CONFIGURATION

FIG. 37 MAGNUS FORCE AND MOMENT COEFFICIENTS VERSUS ANGLE OF ATTACK
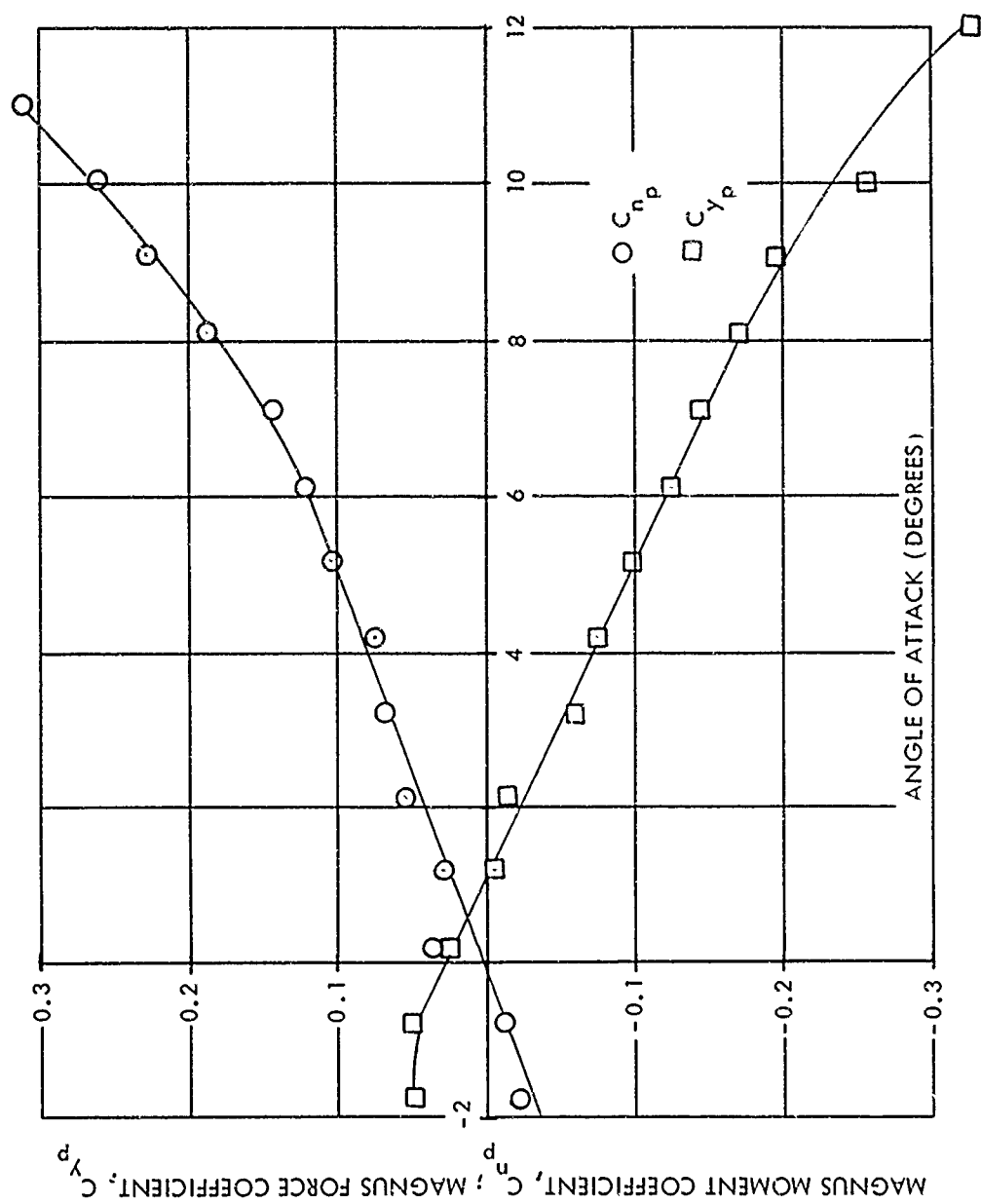AT A MACH NUMBER OF 0.9 FOR THE BASIC CONFIGURATION

FIG. 38 MAGNUS FORCE AND MOMENT COEFFICIENTS VERSUS ANGLE OF ATTACK AT A MACH NUMBER OF 1.76 FOR THE BASIC CONFIGURATION
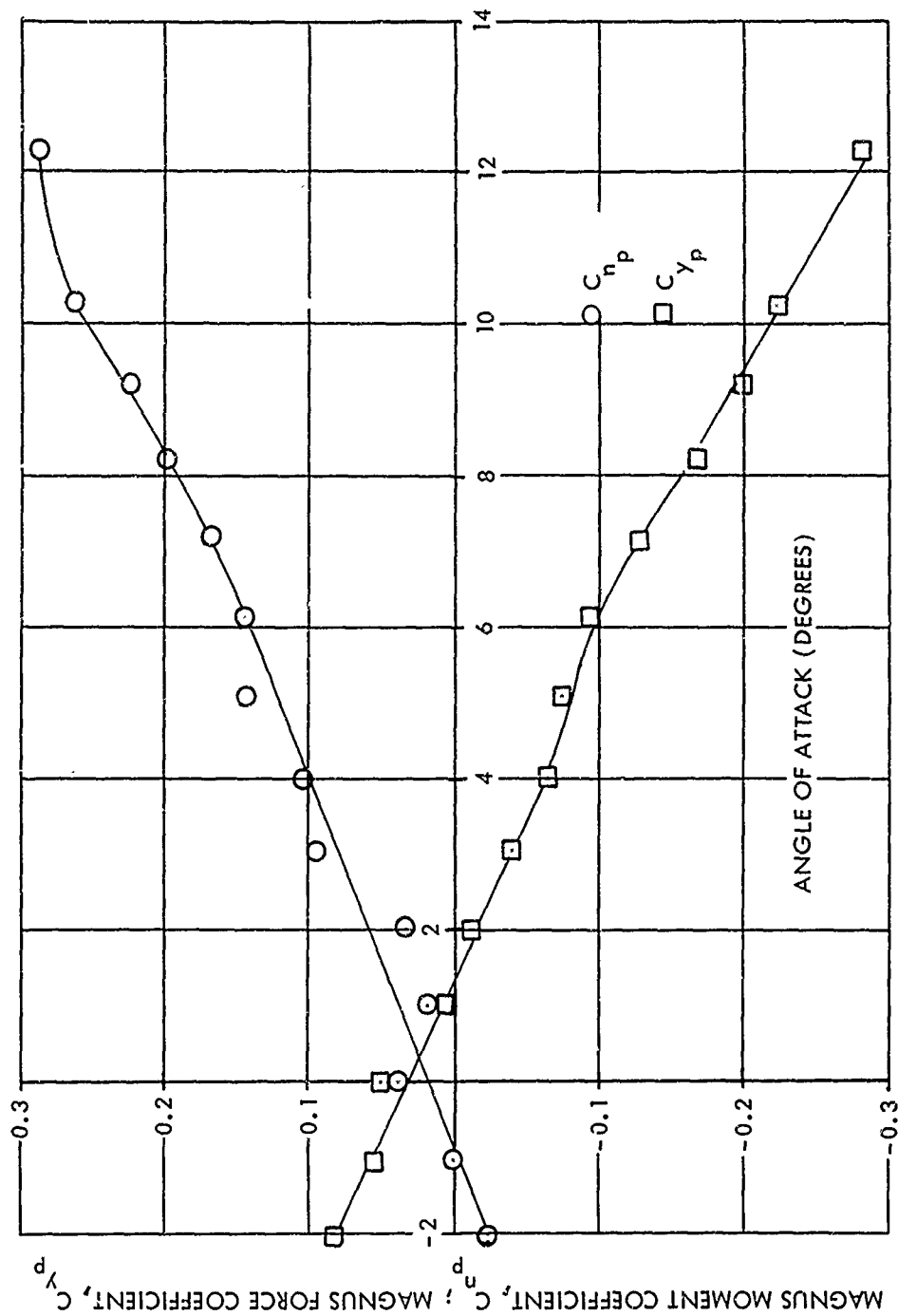
FIG. 39 MAGNUS FORCE AND MOMENT COEFFICIENTS VERSUS ANGLE OF ATTACK AT A MACH NUMBER OF 2.0 FOR THE BASIC CONFIGURATION
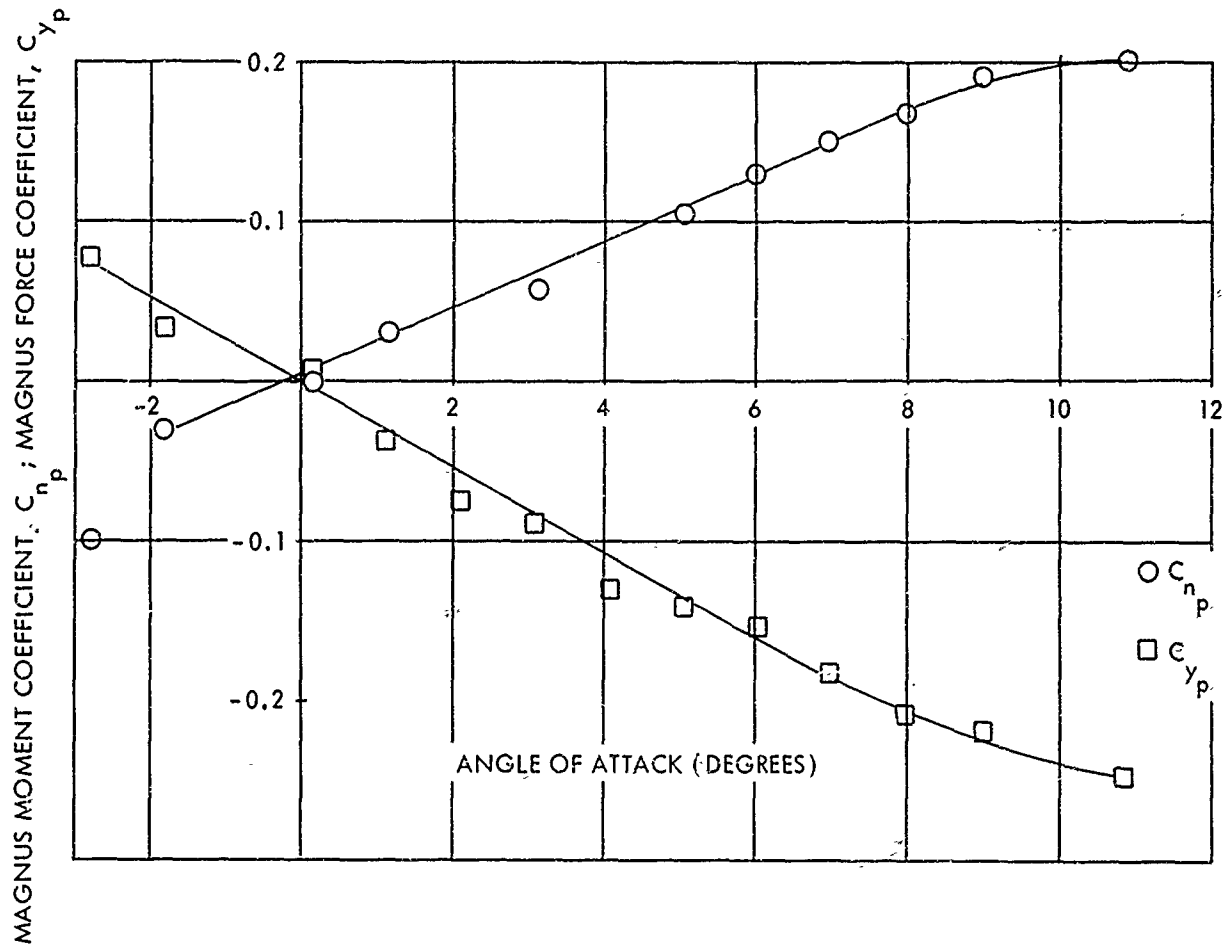
FIG. 40 MAGNUS FORCE AND MOMENT COEFFICIENTS VERSUS ANGLE OF ATTACK
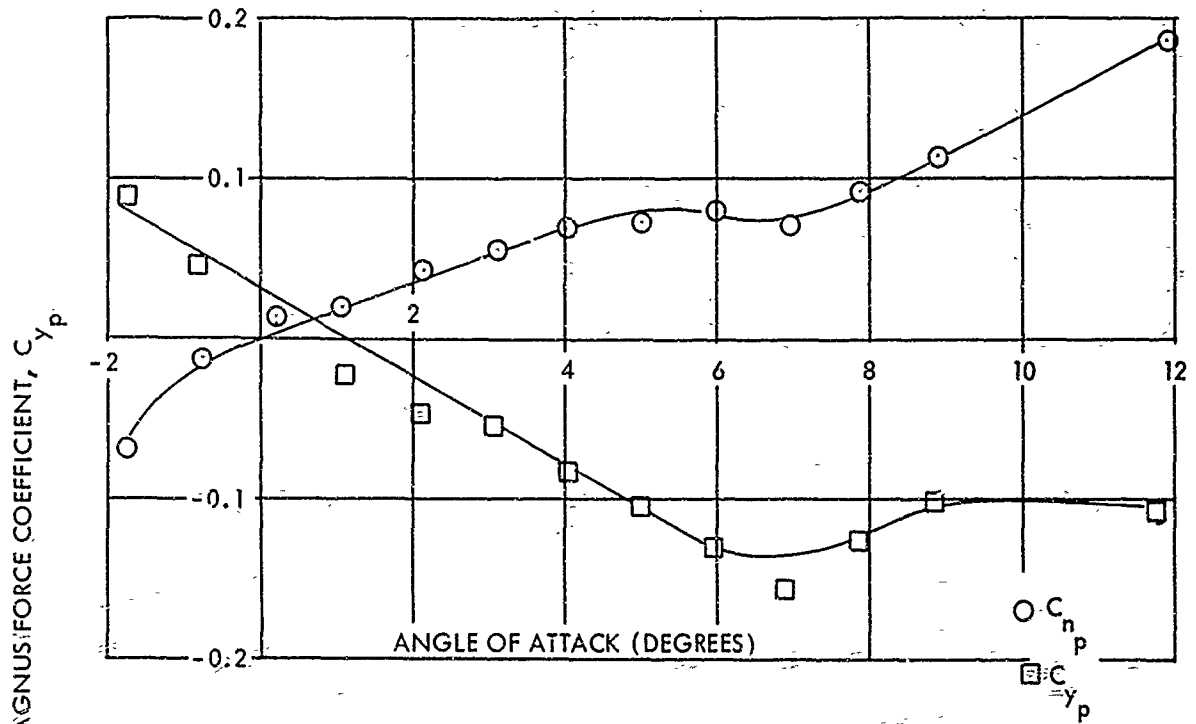AT A MACH NUMBER OF 2.5 FOR THE BASIC CONFIGURATION

79

FIG. 41 MAGNUS FORCE AND MOMENT COEFFICIENTS VERSUS ANGLE OF ATTACK
AT A MACH NUMBER OF 3.00 FOR THE BASIC CONFIGURATION

FIG. 42 MAGNUS FORCE AND MOMENT COEFFICIENTS VERSUS ANGLE OF ATTACK
AT A MACH NUMBER OF 0.80 FOR THE SMOOTH CONFIGURATION

FIG. 43 MAGNUS FORCE AND MOMENT COEFFICIENTS VERSUS ANGLE OF ATTACK
AT A MACH NUMBER OF 0.93 FOR THE SMOOTH CONFIGURATION

FIG. 44 MAGNUS FORCE AND MOMENT COEFFICIENTS VERSUS ANGLE OF ATTACK AT A MACH NUMBER OF 1.76 FOR THE SMOOTH CONFIGURATION
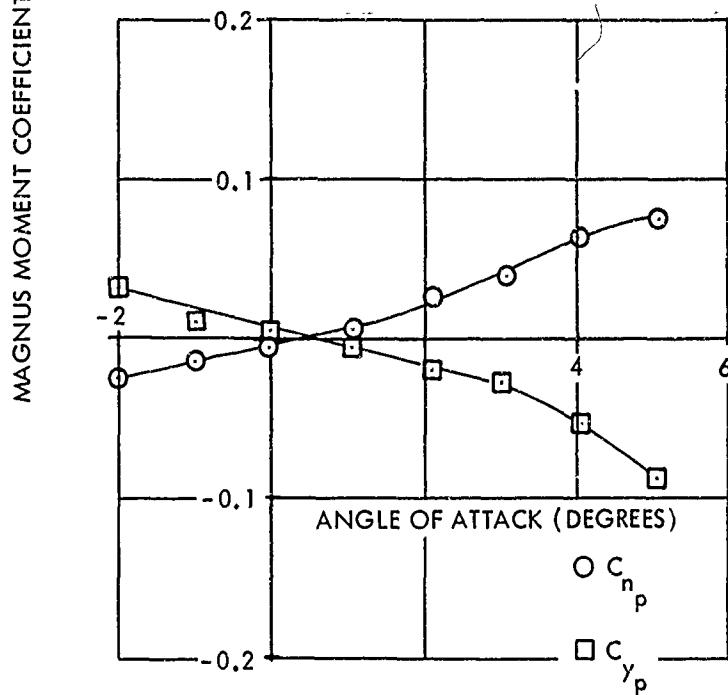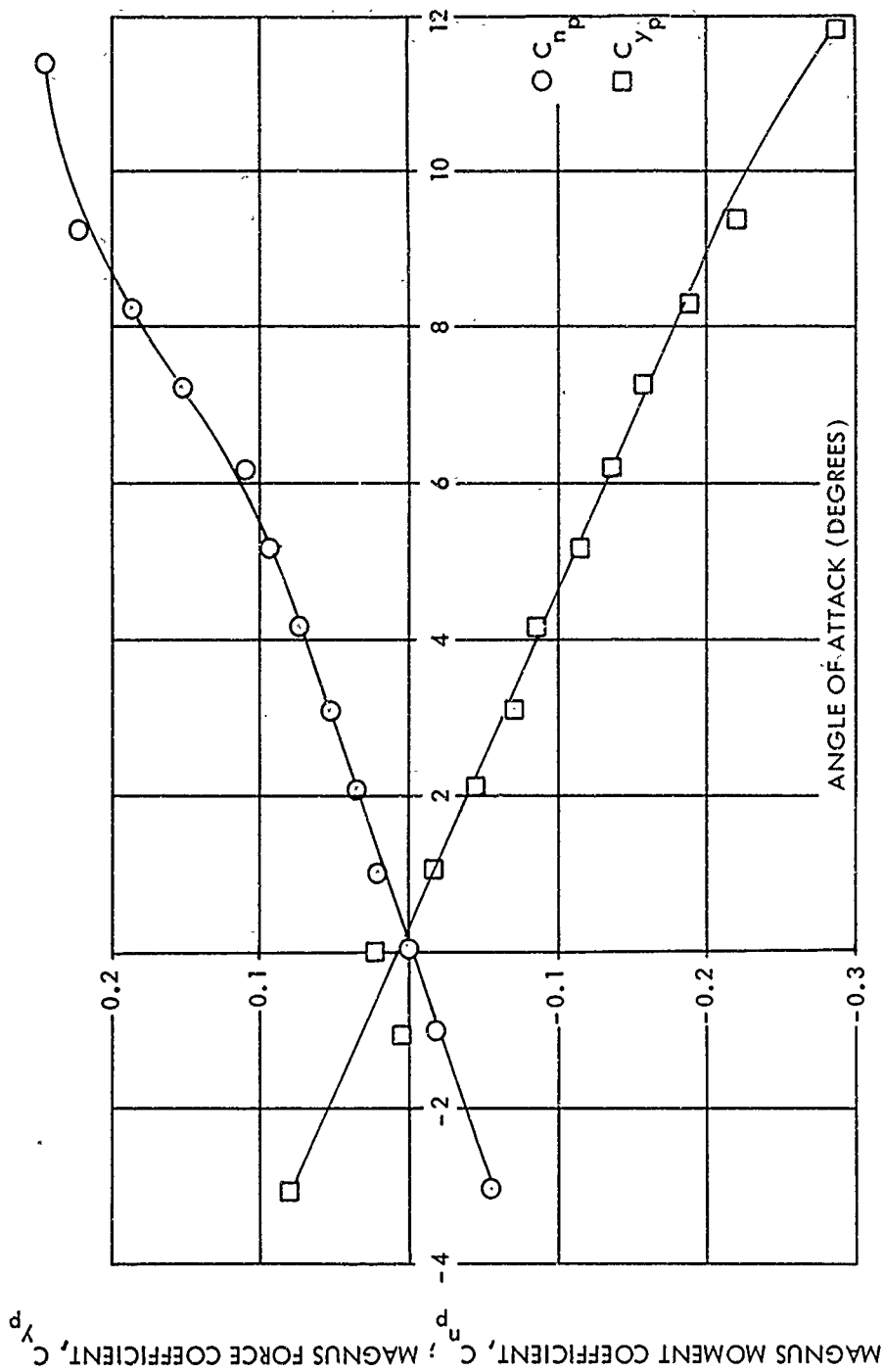
FIG. 45 MAGNUS FORCE AND MOMENT COEFFICIENTS VERSUS ANGLE OF ATTACK AT A MACH NUMBER OF 2.0 FOR THE SMOOTH CONFIGURATION
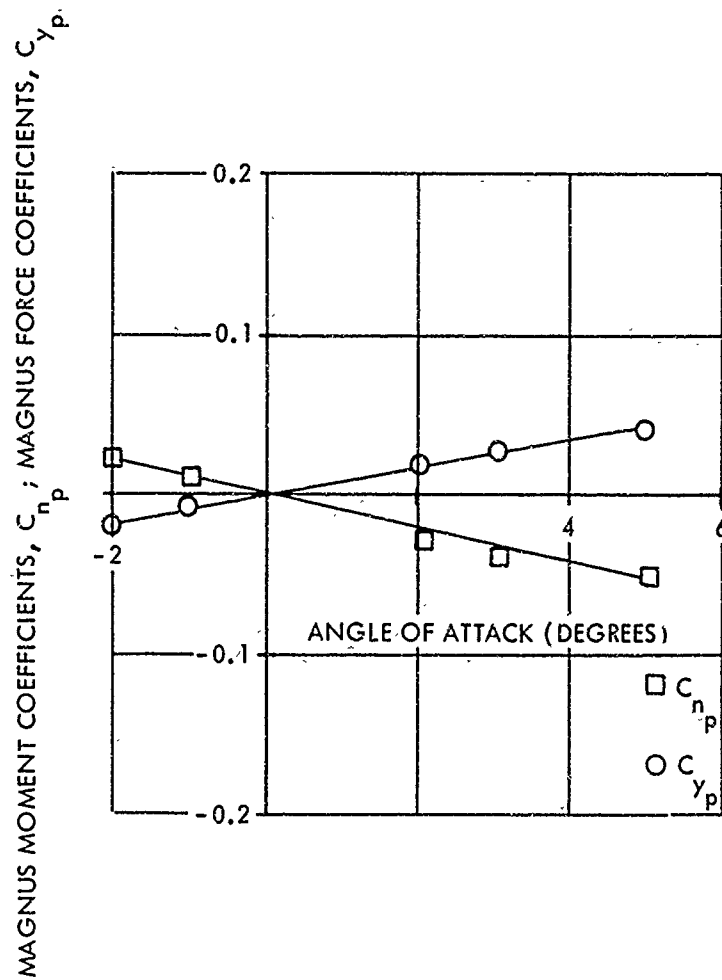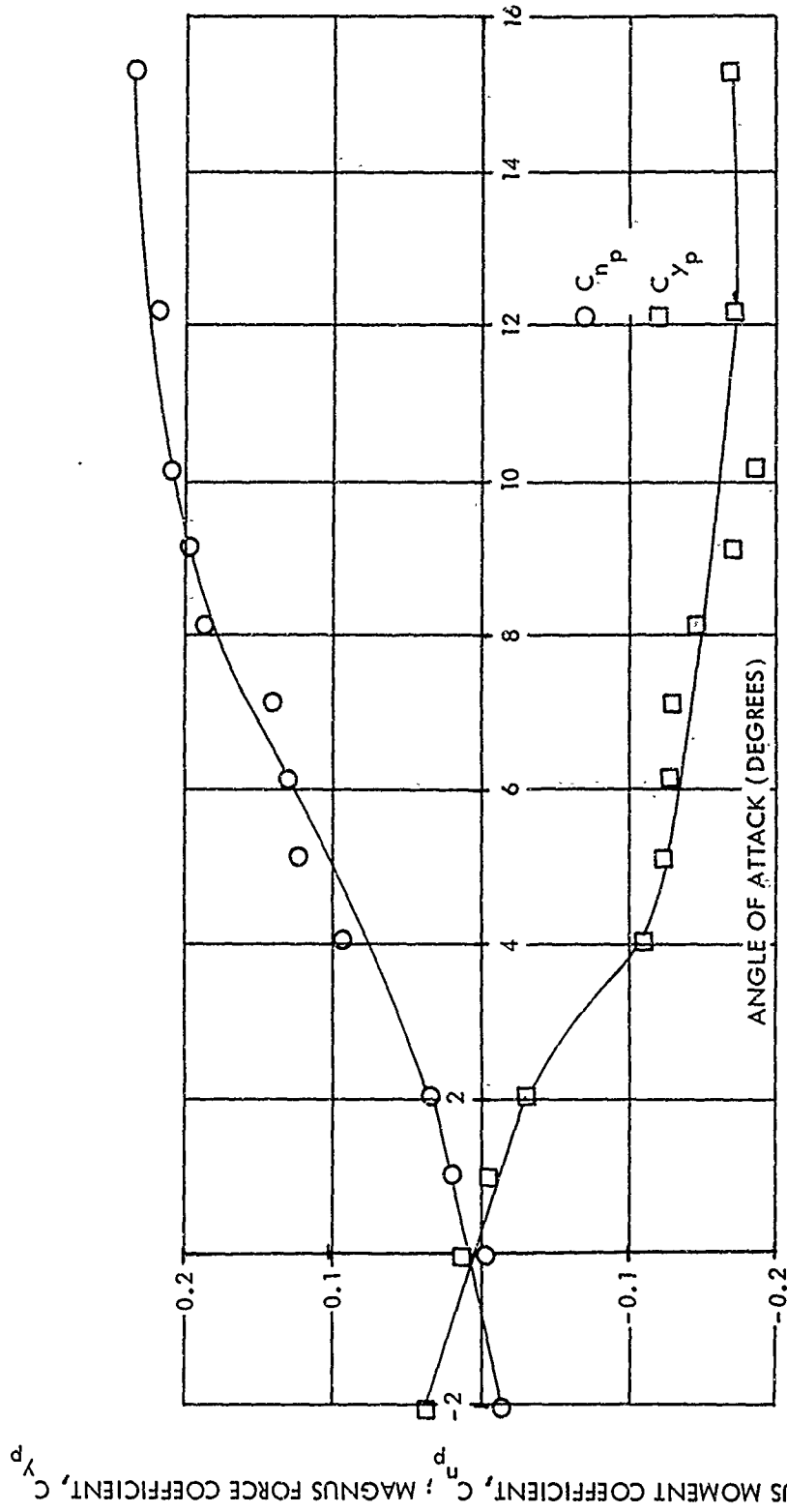
FIG. 46 MAGNUS FORCE AND MOMENT COEFFICIENTS VERSUS ANGLE OF ATTACK
AT A MACH NUMBER OF 2.5 FOR THE SMOOTH CONFIGURATION
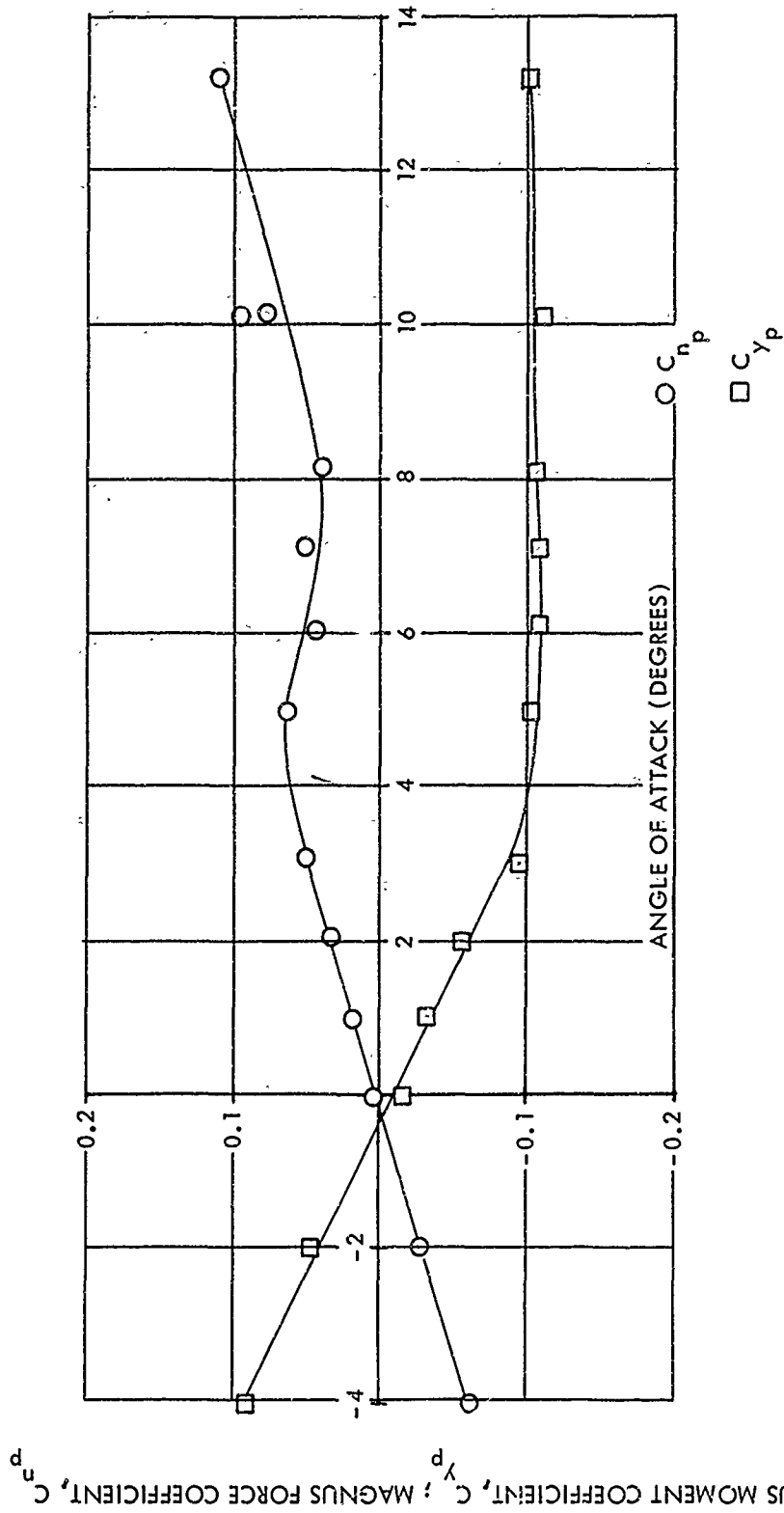
FIG. 47 MAGNUS FORCE AND MOMENT COEFFICIENTS VERSUS ANGLE OF ATTACK
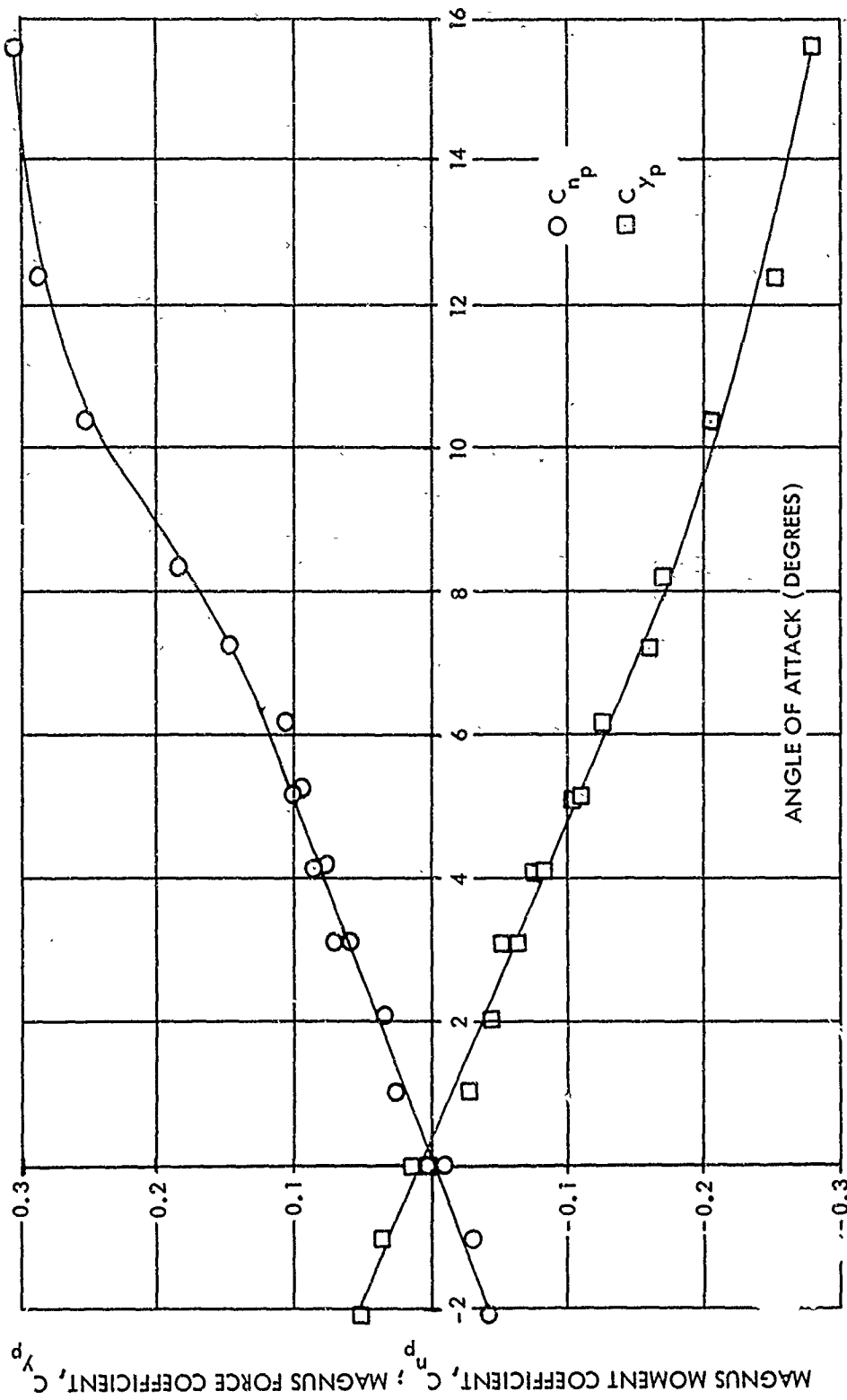AT A MACH NUMBER OF 3.0 FOR THE SMOOTH CONFIGURATION

FIG. 48 MAGNUS FORCE AND MOMENT DERIVATIVE VERSUS MACH NUMBER
FOR THE BASIC CONFIGURATION FROM WIND TUNNEL MEASUREMENTS
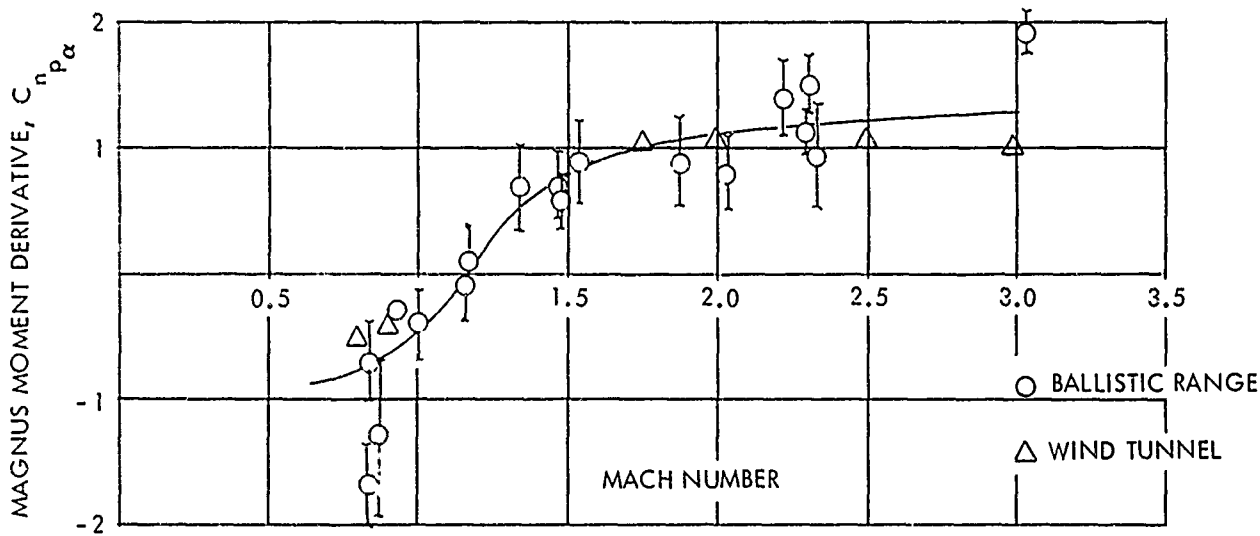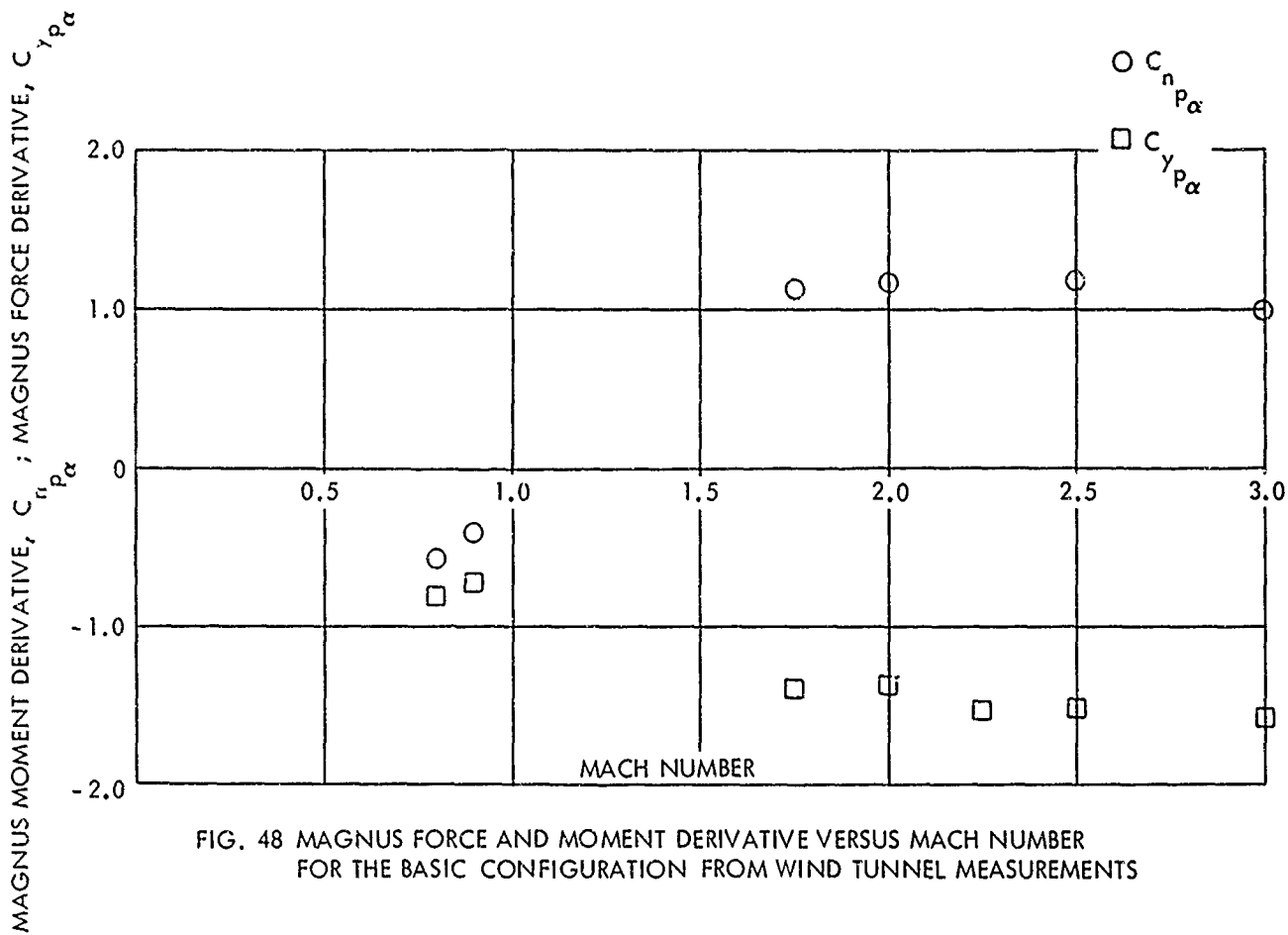
FIG. 49 MAGNUS MOMENT DERIVATIVE VERSUS MACH NUMBER FROM BALLISTIC RANGE
AND WIND TUNNEL MEASUREMENTS FOR THE BASIC CONFIGURATION
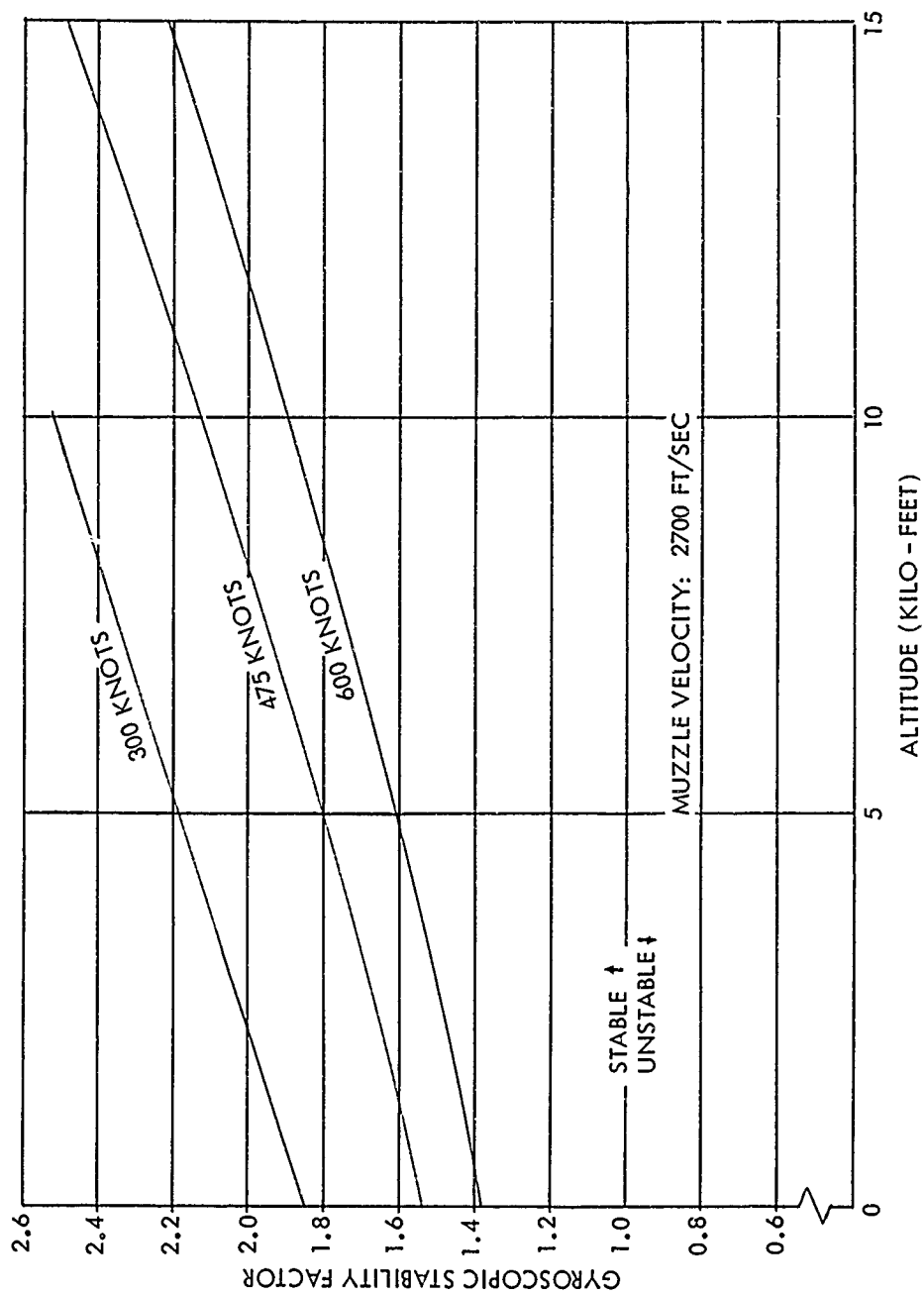
FIG. 50 GYROSCOPIC STABILITY FACTOR VERSUS ALTITUDE FOR AIR TEMPERATURE OF −65° FARENHEIT AND FOR AIRCRAFT SPEEDS OF 300, 475 AND 600 KNOTS
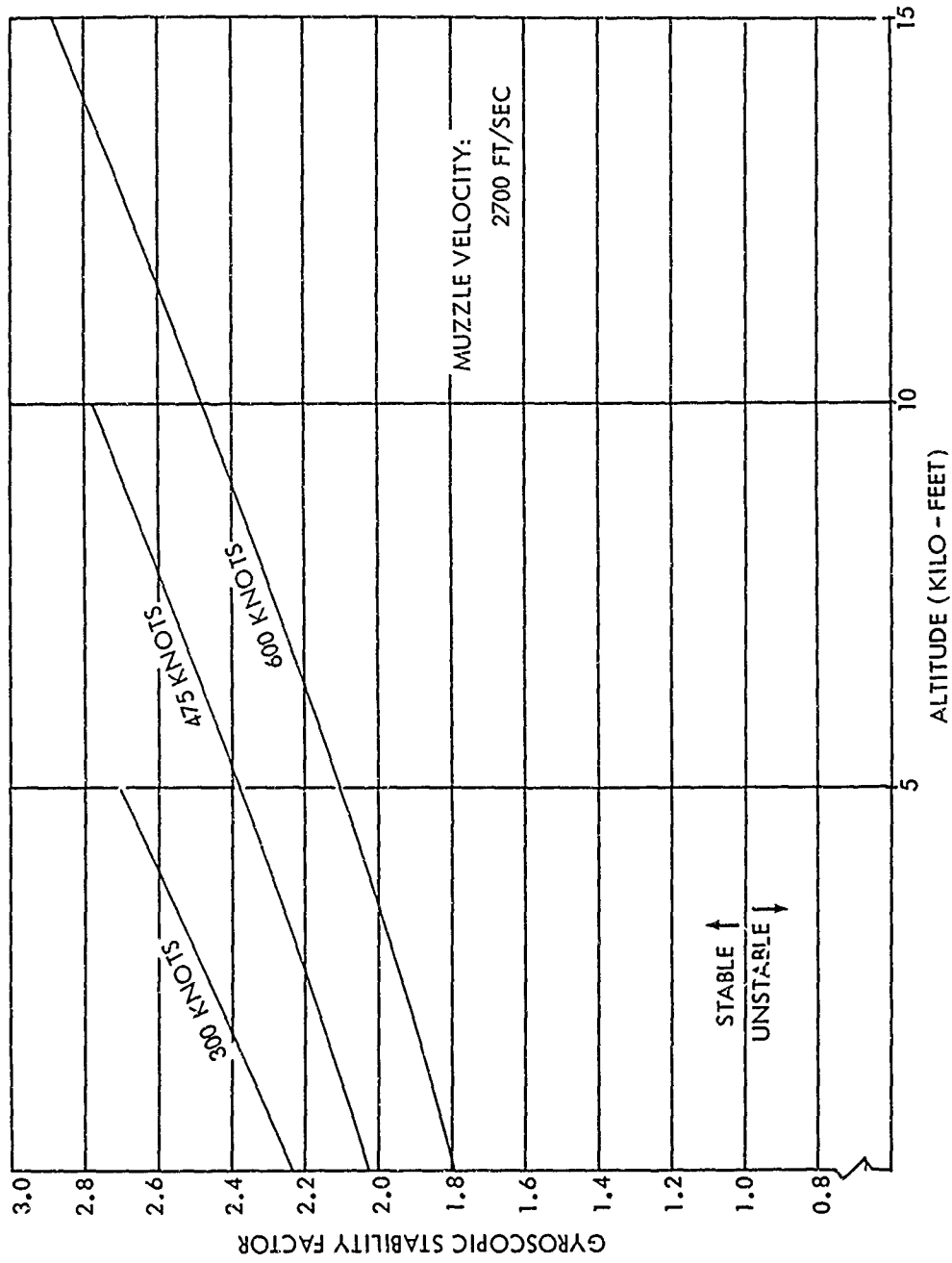
FIG. 51 GYROSCOPIC STABILITY FACTOR VERSUS ALTITUDE FOR AIR TEMPERATURE OF 59° FARENHEIT AND AIRCRAFT SPEEDS OF 300, 475, AND 600 KNOTS

| PT	T (SEC)	X (FT)	Y (FT)	V (FT/SEC)	M
A	0	0	15,000	3710	3.5
B	1	3290	14,985	2926	2.8
C	2	5917	14,944	2350	2.2
D	3	8029	14,882	1893	1.8
E	4	9737	14,803	1543	1.4
F	5	11,143	14,709	1288	1.2
G	6	12,339	14,600	1106	1.04
H	7	13,366	14,474	990	0.93
I	8	14,304	14,329	913	0.86
J	12	17,485	13,544	747	0.70

NOTE: (a) STANDARD DAY
(b) MUZZLE VELOCITY: 2700 FT,'SEC

STATIC INSTABILITY
DYNAMIC INSTABILITY

STATIC INSTABILITY
DYNAMIC STABILITY

DAMPING STABILITY FACTOR, S_d

RECIPROCAL OF GYROSCOPIC STABILITY FACTOR, $1/S_g$

FIG. 52 $1/S_g$ VERSUS S_d FOR THE BASIC BODY LAUNCHED HORIZONTALLY FROM AN AIRCRAFT FLYING AT 600 KNOTS AIRSPEED AND 15,000 FEET ALTITUDE

89

PT	T (SEC)	X (FT)	Y (FT)	V (FT/SEC)	M
A	0	0	10,000	3710	3.45
B	1	3227	9985	2810	2.61
C	2	5700	9945	2165	2.0
D	3	7612	9886	1684	1.56
E	4	9114	9811	1346	1.25
F	5	10,336	9721	1120	1.04
G	6	11,378	9614	986	0.92
H	7	12,310	8487	901	0.84
I	12	16,088	8545	687	0.64

FIG. 53 1/Sg VERSUS S_d FOR THE BASIC BOCY LAUNCHED HORIZONTALLY FROM AN AIRCRAFT FLYING AT 600 KNOTS AIRSPEED AND 10,000 FEET ALTITUDE

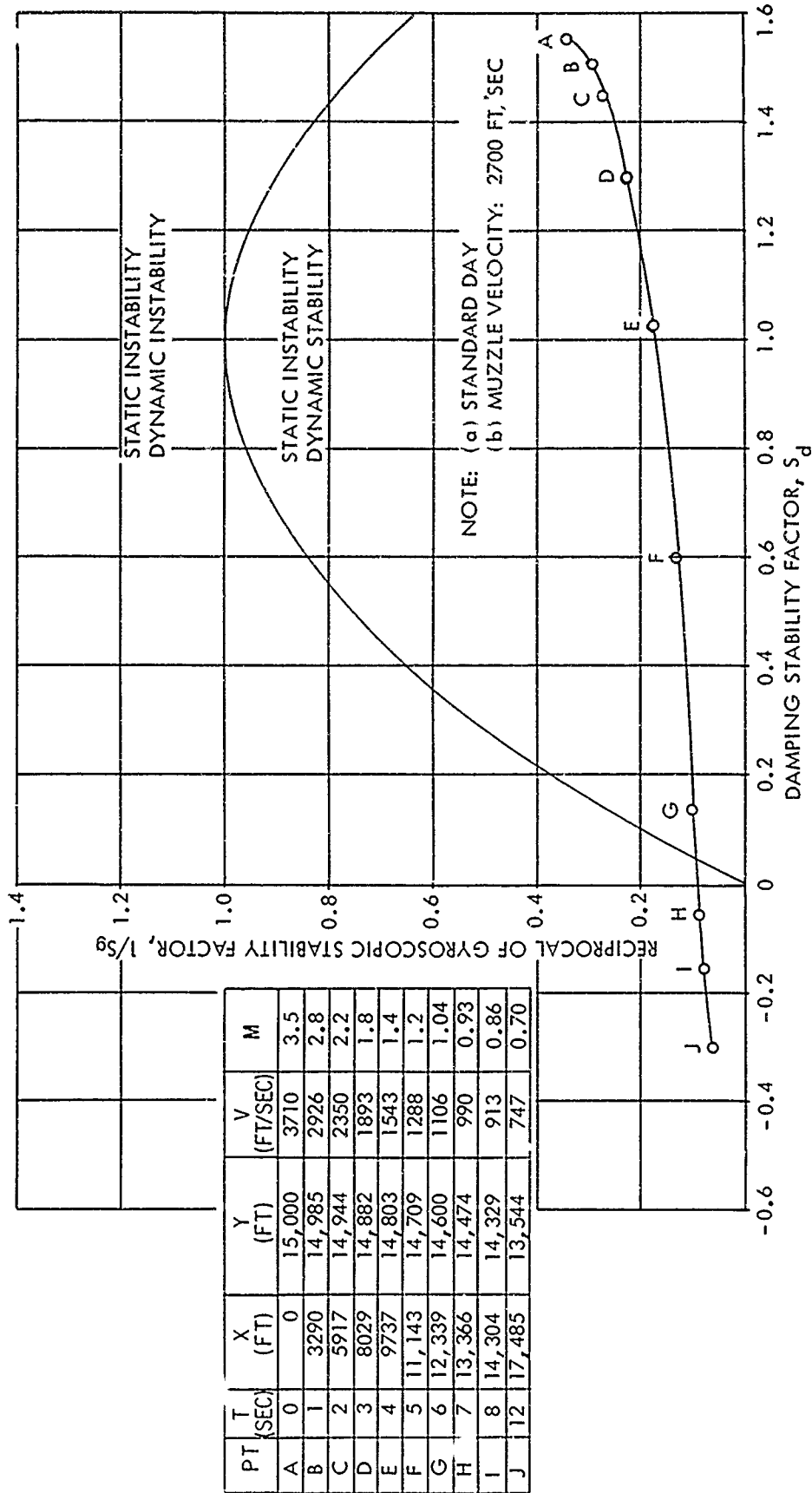| PT	T (SEC)	X (FT)	Y (FT)	V (FT/SEC)	M
A	0	0	5000	3710	3.38
B	1	3153	4985	2679	2.44
C	2	5456	4947	1966	1.79
D	3	7160	4891	1479	1.35
E	4	8470	4819	1171	1.07
F	5	9543	4731	1000	0.91
G	6	10,485	4623	901	0.82
H	8	12,131	4344	777	0.71
I	12	14,794	3547	630	0.57

FIG. 54 1/Sg VERSUS S_d FOR THE BASIC BODY LAUNCHED HORIZONTALLY FROM AN AIRCRAFT FLYING

AT 600 KNOTS AIRSPEED AND 5000 FEET ALTITUDE

91

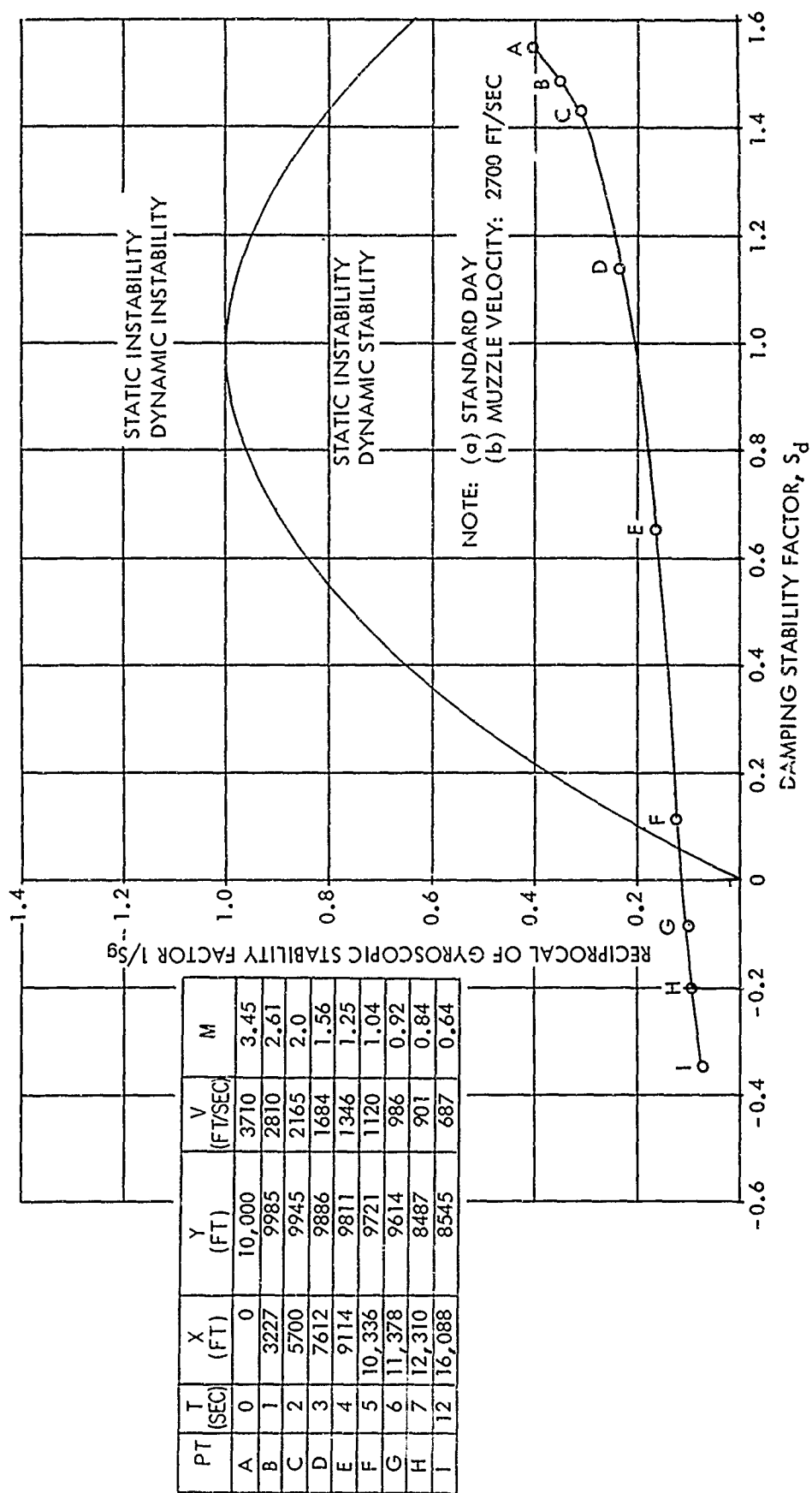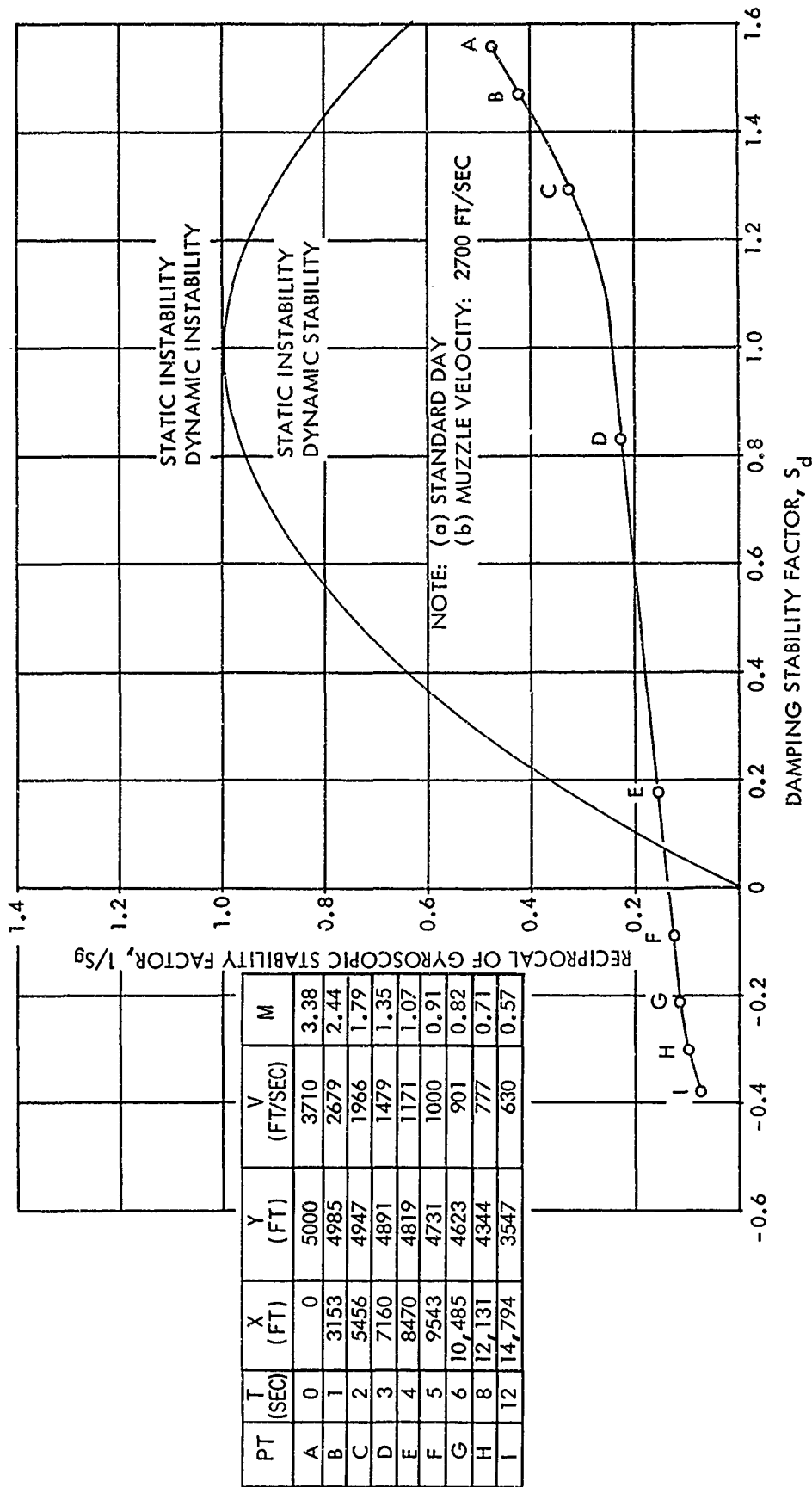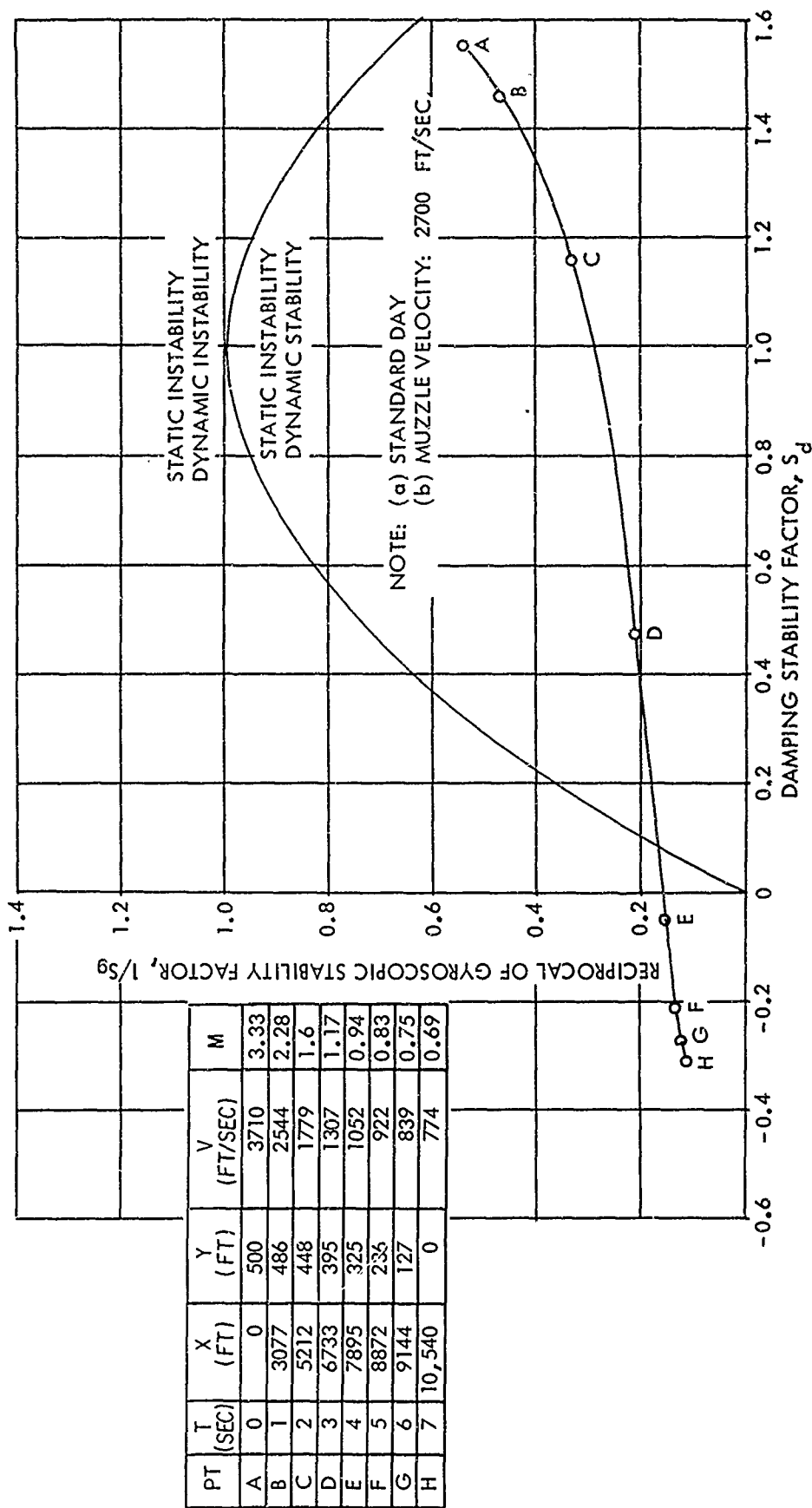| PT	T (SEC)	X (FT)	Y (FT)	V (FT/SEC)	M
A	0	0	500	3710	3.33
B	1	3077	486	2544	2.28
C	2	5212	448	1779	1.6
D	3	6733	395	1307	1.17
E	4	7895	325	1052	0.94
F	5	8872	235	922	0.83
G	6	9144	127	839	0.75
H	7	10,540	0	774	0.69

FIG. 55 $1/S_g$ VERSUS S_d FOR THE BASIC BODY LAUNCHED HORIZONTALLY FROM AN AIRCRAFT FLYING AT AN AIRSPEED OF 600 KNOTS AND 500 FEET ALTITUDE

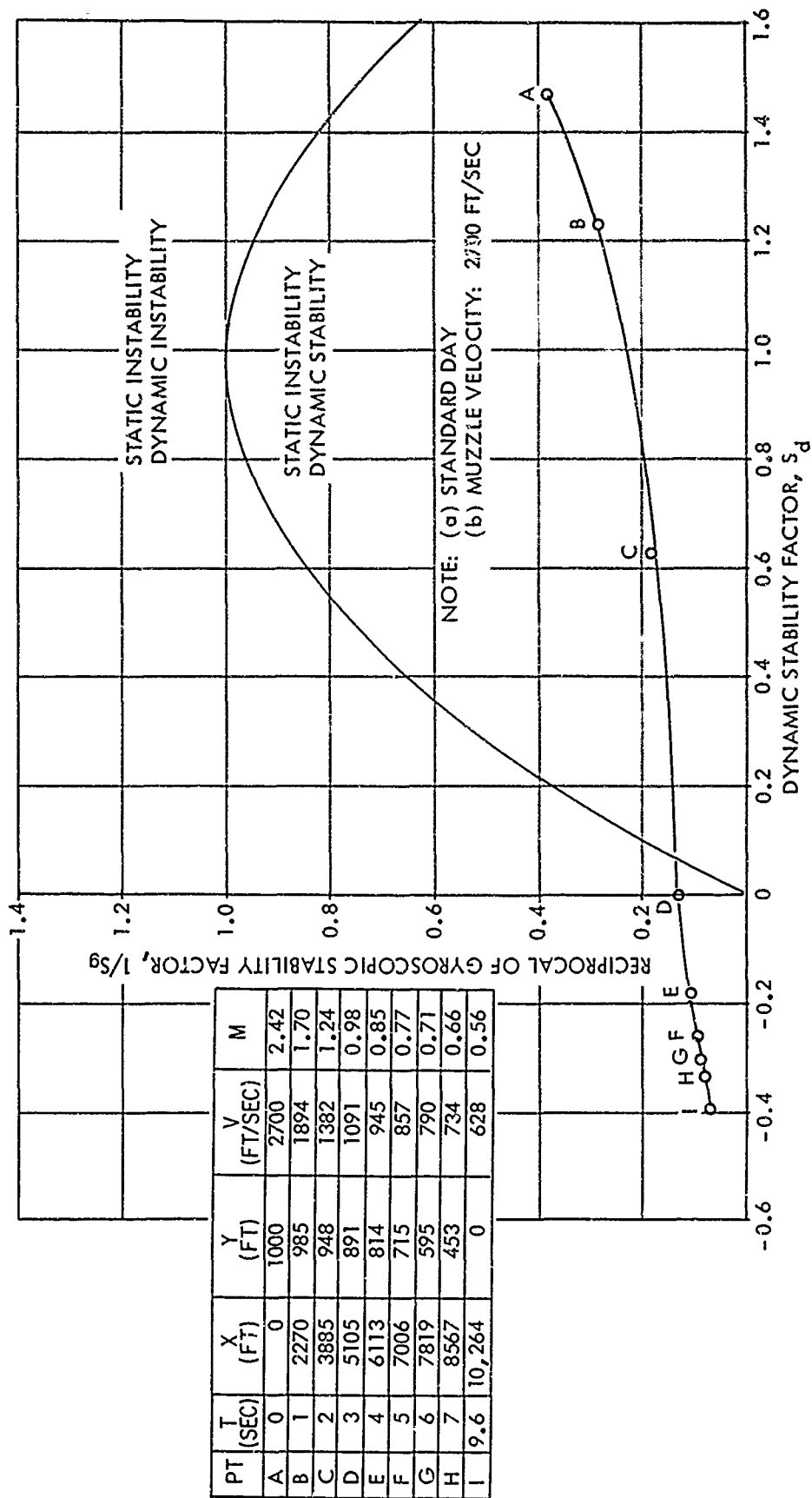| PT	T (SEC)	X (FT)	Y (FT)	V (FT/SEC)	M
A	0	0	1000	2700	2.42
B	1	2270	985	1894	1.70
C	2	3885	948	1382	1.24
D	3	5105	891	1091	0.98
E	4	6113	814	945	0.85
F	5	7006	715	857	0.77
G	6	7819	595	790	0.71
H	7	8567	453	734	0.66
I	9.6	10,264	0	628	0.56

FIG. 56 $1/S_g$ VERSUS S_d FOR THE BASIC BOCY LAUNCHED HORIZONTALLY FROM A STATIONARY PLATFORM AT 1000 FEET ALTITUDE
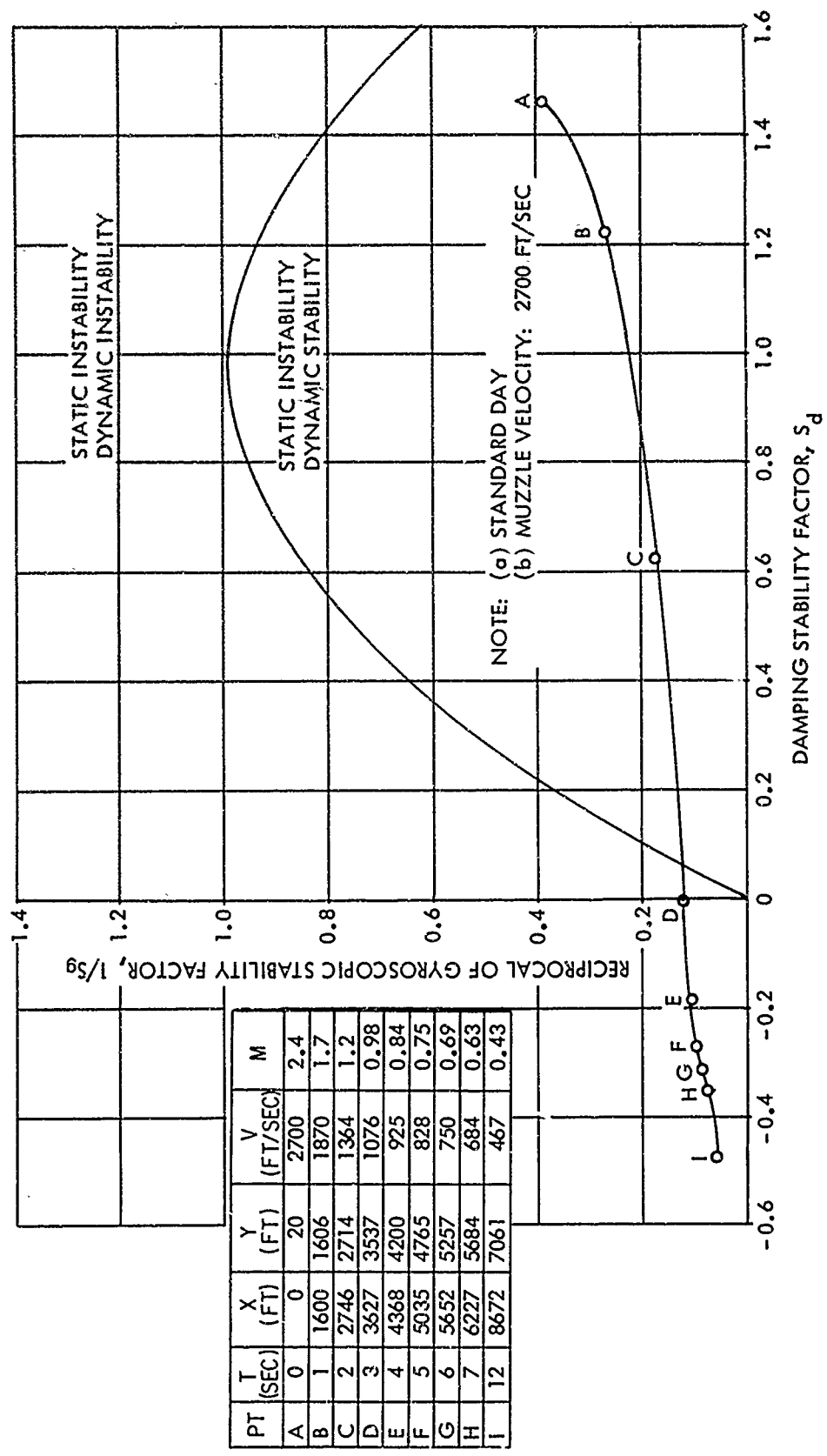
93

FIG. 57 1/Sg VERSUS S_d FOR BASIC BODY LAUNCHED AT GROUND LEVEL AT 45 DEGREE ANGLE

94